DENSITY AND RECHARGE EFFECTS DURING THE CAPE COD NATURAL-GRADIENT TRACER TEST

by

Denis R. LeBlanc

B.S., Hydrology
University of New Hampshire

Submitted to the Department of Civil and Environmental Engineering
in Partial Fulfillment of the Requirements for the Degree of

Master of Science in Civil and Environmental Engineering

at the

Massachusetts Institute of Technology

June 2001

Signature of the Author: _____
Department of Civil and Environmental Engineering
May 11, 2001

Certified by: _____
Michael A. Celia
Professor of Civil and Environmental Engineering, Princeton University
Thesis Co-Supervisor

Certified by: _____
Charles F. Harvey
Assistant Professor of Civil and Environmental Engineering
Thesis Supervisor

Accepted by: _____
Oral Buyukozturk
Chairman, Departmental Committee on Graduate Studies

DENSITY AND RECHARGE EFFECTS DURING THE CAPE COD NATURAL-GRADIENT TRACER TEST

by

Denis R. LeBlanc

Submitted to the Department of Civil and Environmental Engineering
on May 11, 2001
in Partial Fulfillment of the Requirements for the Degree of
Master of Science
in Civil and Environmental Engineering

ABSTRACT

Analytical and numerical modeling was used to show that a density difference of 0.1 percent between the ambient ground water and the tracer solution caused part of the downward movement of the tracer cloud during the 1985-88 Cape Cod natural-gradient tracer test. The modeling also showed that recharge from precipitation caused part of the downward movement.

The center of mass of the observed bromide tracer cloud moved downward about 3.2 m and laterally about 100 m during the first 237 days of the test. Analytical models over-predicted the amount of downward movement as compared to the observed movement because the models do not consider the dilution and spreading of the tracer cloud caused by dispersion. A numerical simulation of the field-scale experiment predicted only 2.2 m of downward movement during the 237-day period. Density-induced sinking caused about 1 m of the simulated downward movement, most of which took place during the first 38 days, when the density difference was greatest. The remainder of the downward movement was caused by the accretion of recharge water above the sinking tracer cloud. The under-prediction by the numerical model may be due partly to the use of a two-dimensional model to simulate the three-dimensional flow around the sinking tracer cloud. The under-prediction may also be due partly to the representation of the water table as a no-flow boundary in the numerical simulations and to an underestimate of the amount of recharge during the test period.

Analytical and numerical modeling was used to show that the amount of downward movement caused by density differences is particularly sensitive to the shape and orientation of the initial tracer cloud. Density-induced sinking is also significantly reduced as the dispersivity and the anisotropy of the permeability increase. Accurate simulation of the Cape Cod tracer test required the used of an increasing dispersivity with travel distance, as was observed during the field experiment.

Thesis Supervisor: Charles F. Harvey
Title: Assistant Professor of Civil and Environmental Engineering

Thesis Co-Supervisor: Michael A. Celia
Title: Professor of Civil and Environmental Engineering, Princeton University

ACKNOWLEDGMENTS

This thesis would not have been possible without the unfailing support of Mike Celia. I will forever be grateful to him for his patience, advice, and extraordinary instruction. The support of Lynn Gelhar, who was the inspiration for the Cape Cod tracer test, was also invaluable.

The generous assistance of a Parsons Graduate Fellowship and the U.S. Geological Survey Graduate School Program made it possible for me to attend MIT and pursue this degree.

The support of the Toxic Substances Hydrology Program of the U.S. Geological Survey is also gratefully acknowledged. The program gave us the funding and intellectual freedom to pursue our ideas and take the risks that underlie many successful scientific endeavors.

A particular thanks is due to my exceptional colleagues at the U.S. Geological Survey. Steve Garabedian, Kathy Hess, and Chip Quadri were true partners and friends as we worked as a team to carry out the field experiment. Without their help, this world-renowned tracer test never could have happened.

Finally, none of this would have been possible without the support of Denise, Jeff, Jocelyn, and Sarah. They encouraged me during those first weeks of despair when the coursework seemed impossible, and they never complained about the dozens of overnights I spent on the Cape during the field test. This achievement is truly theirs as much as it is mine.

Denis LeBlanc
May 2001

TABLE OF CONTENTS

FIGURES

TABLES

CHAPTER 1

INTRODUCTION

Many ground-water contamination problems involve dilute plumes of dissolved contaminants in shallow, granular aquifers. In these aquifers, ground water flows at rates of several feet per day, and the flow is mostly in the horizontal direction. The contaminated ground water is carried along by the flowing ground water and, therefore, the plumes extend for significant distances from their sources in the direction of ground-water flow. Although the plumes are diluted gradually by dispersion, the movement of the dissolved substances is dominated by advective transport with the regional, or ambient, flow. These systems, sometimes referred to as forced-convection flow systems, are characterized by a lack of feedback between solute concentrations and flow velocities. In other words, the density of the ground water is, for all practical purposes, a constant value in space and time.

Hydrologists commonly infer plume movement in advection-dominated, shallow ground-water systems from a map of hydraulic head, in many cases a water-table map. They assume that vertical movement is small and that the direction of flow and, therefore, plume movement, is in the same direction as the water-table gradient. This assumption is useful in many field situations, particularly when a reasonable estimate of the plume's path from water-level measurements is one of the few predictions that can be made easily with commonly available field data. The literature contains many examples of the application of this approach to plume analysis.

Field and Laboratory Studies of Vertical Movement

Even in aquifers with mostly horizontal flow, dilute plumes are observed to sink below the water table with travel distance from the source. This downward movement often reflects the influence of areal recharge from precipitation. The recharge causes a component of vertical flow that may be transient and small compared to lateral flow in the aquifer. The result is downward movement of the plume relative to the water table, and the formation of a zone of "clean" ground water above the plume. This phenomenon has been observed in many detailed studies of contaminant plumes in shallow aquifers that receive areally distributed recharge (Kimmel and Braids, 1980; MacFarlane and others, 1983; LeBlanc, 1984; Ryan and Kipp, 1997). LeBlanc (1984) reported that the zone of clean ground water above a 3-kilometer-long sewage plume in the Cape Cod aquifer is 6 to 15 m thick. The aquifer receives about 50 cm/year of recharge.

In all of the cases cited above, the plume trajectories were the primary field evidence for the downward displacement caused by recharge; vertical hydraulic-head gradients were transient or too small to measure using standard water-level measurement methods. However, the effect of areal recharge has been demonstrated in ground-water modeling studies that simulate flow paths in the aquifer. The vertical trajectory of the Cape Cod sewage plume, for example, is simulated accurately in a three-dimensional ground-water flow model that includes areally distributed recharge from precipitation (Masterson and others, 1997b).

There is also evidence from the detailed study of contaminant plumes in shallow aquifers that density may play a role in the downward movement of plumes. Kimmel and Braids (1980), in their classic report on the Babylon and Islip landfills on Long Island, New York, observed that

the highest concentrations of dissolved contaminants were near the base of the upper glacial sand and gravel aquifer. They hypothesized that dense packets of leachate generated by precipitation passing through the landfill were sinking down through the ambient ground-water flow because of density effects. Landfill leachate can have solute concentrations as high as 50,000 mg/L (Freeze and Cherry, 1979). MacFarlane and others (1979) made similar observations at the Base Borden landfill in Ontario, where the plume has moved about 20 m downward below the water table to the base of the sandy aquifer. They noted that the density-induced vertical head gradients were on the same order as the ambient vertical gradients during all but periods of recharge during the late spring and early summer. Van der Mollen and van Ommen (1988) concluded that density effects might have contributed to the downward movement of a number of landfill plumes in the Netherlands. LeBlanc (1984) suggested that density may have affected the downward movement of the sewage plume on Cape Cod, although the hydraulic loading at the sewage-disposal site and the significant areal recharge probably account for most of the observed downward movement of this dilute plume.

Bear (1972, p. 653-655) explained that, when the fluid density in a layer of stationary water in a porous medium is greater than the density of an underlying layer, even a small disturbance may result in convective flow, sometimes referred to as free convection, in which the less dense fluid tends to rise and the more dense fluid tends to sink. The forcing function is directly related to the density difference between the two fluids, $\Delta\rho/\rho_o$, where $\Delta\rho$ is the density difference between the two fluids and ρ_O is the density of the ambient fluid. Darcy's Law for a fluid of density, ρ_O, can be written as (Bear, 1972, Equation 10.7.34):

$$V_i^* = -\frac{k_{ij}}{n\mu}\left(\frac{\partial p}{\partial x_j} + \rho_o g \frac{\partial z}{\partial x_j}\right), \qquad (1.1)$$

where:

V_i^* = ground-water velocity (L/T),

k_{ij} = permeability tensor (L^2),

n = effective porosity (dimensionless),

μ = dynamic viscosity (M/(L·T),

p = fluid pressure (M/(L·T^2),

ρ_0 = ambient fluid density (M/L^3),

g = gravitational acceleration (L/T^2), and

x, z = horizontal and vertical coordinate directions.

Darcy's Law can be rewritten in the form (Bear, 1972, Equation 10.7.45):

$$V_i^* = -\frac{k_{ij}\rho_o g}{n\mu}\frac{\partial}{\partial x_j}\left(z + \frac{p}{\rho_o g}\right) - \frac{k_{ij} g(\rho_t - \rho_o)}{n\mu}\frac{\partial z}{\partial x_j}, \qquad (1.2)$$

where ρ_t is density of the tracer fluid.

Bear (1972, p. 654) noted that the motion can be interpreted as being caused by two driving forces shown by the two terms on the right side of Equation (1.2). One results from the piezometric head differences, where the head ($z + p/\rho_o g$) is defined with respect to the reference fluid. The other results from the buoyancy force, directed vertically upward or downward, acting on the fluid of density ρ_t imbedded in a fluid of density ρ_O. The relative importance of the forced convection and the buoyancy force can be related to the ratio of the hydraulic-head gradient ($\Delta h/L$) and the density-related gradient ($\Delta\rho/\rho_o$). When $\Delta\rho/\rho_o >> \Delta h/L$, the flow is determined mainly by the buoyancy force. Therefore, the larger the

density difference between the ambient ground water and the contaminant solution, the greater the likelihood of density-induced sinking.

Most shallow ground-water systems in granular aquifers are advection dominated. Therefore, the effects of density-induced downward movement are difficult to distinguish because of the large component of lateral movement and the significant areal recharge. Field evidence for density-induced downward movement has come mostly from landfill studies because of the high concentrations of dissolved substances and, therefore, the elevated density of landfill leachate. Field tracer tests, however, have provided additional evidence of density-induced downward movement for tracer solutions that are considerably less dense than leachate.

In one of the first detailed natural-gradient tracer experiments reported in the literature, Sudicky and others (1983) observed a downward trajectory of a chloride tracer cloud injected into the Borden aquifer. The tracer solution was added as a 700-liter pulse injected just below the water table. They attributed part of the downward movement to a density contrast ($\Delta p/\rho_o$) of about 10^{-3}g/cm^3 (0.1 percent) between the tracer solution and the ambient ground water. Mackay and others (1986) and Freyberg (1986) reported a similar downward trajectory in the now famous large-scale tracer test at the Borden site. The tracer cloud was injected as a 12,000-liter pulse with chloride and bromide concentrations of 892 and 324 mg/L, respectively, and the cloud was tracked through an array of multilevel samplers as it moved more than 80 m laterally during a 1,038-day period. The center of mass of the tracer cloud moved downward about 2.7 m during this period. The downward movement was most rapid, however, in the early part of the test, when the cloud moved downward 1.0 m in only 111 days. The vertical trajectory of the cloud was concave upward, which may have been an indication of the diminishing influence of density

because of dilution of the tracer cloud with time. Freyberg (1986, p. 2040) attributed the observed downward movement to a small vertical component of the regional velocity field, the density contrast between the tracer cloud and the native ground water, and to local infiltration and recharge above the sinking cloud.

The large-scale natural-gradient tracer test at the Cape Cod site in 1985-88 (LeBlanc and others, 1991; Garabedian and others, 1988, 1991) provides additional evidence for downward movement because of density and recharge. This test is described in detail in the next chapter. The bromide tracer cloud moved downward about 3.2 m during the first 237 days of the field experiment, and a distinct zone of tracer-free ground water formed above the cloud. The trajectory was concave upward, which is similar to the trajectory reported by Freyberg (1986). LeBlanc and others (1991, p. 905) attributed about 1.5 m of the downward movement to areal recharge during this period. Based on a preliminary application of the analytical models of Hubbert (1953) and Yih (1965), they attributed the remainder of the downward movement to the density difference (about 0.1 percent) between the tracer solution and the ambient ground water.

Davis and others (2000) conducted a second large-scale tracer test at the Cape Cod site in 1993-95. About 10,000 liters of tracer solution, including bromide and various reactive metals, were injected into the aquifer about 50 m downgradient from the injection location of the 1985-88 test. The center of mass of the bromide cloud moved downward about 1.9 m and laterally about 52 m during the first 111 days of the experiment. The water-level hydrograph suggests that there was little recharge to the aquifer during this period. The vertical trajectory had the same concave-upward shape reported by LeBlanc and others (1991) and Freyberg (1986). Davis

and others (2000) attributed part of the downward movement to density-induced sinking, although they did not estimate the amount of recharge that occurred during the test.

The Cape Cod and Borden natural-gradient tracer tests were run in relatively homogeneous glacial outwash aquifers. Boggs and others (1992) and Adams and Gelhar (1992) reported on a natural-gradient test that was run in a heterogeneous alluvial aquifer at Columbus Air Force Base in Mississippi. The test involved the injection of 10,000 liters of ground water containing several tracers, including bromide at a concentration of 2,500 mg/L. The density contrast between the tracer solution and the ambient ground water was estimated to be about 0.4 percent. Because of significant upward hydraulic gradients near the injection site, the center of mass of the tracer cloud rose in elevation during the test. Boggs and others (1992, p. 3287) noted, however, that a downward spreading of the plume near the source, in spite of the upward gradient, was probably evidence of density-induced sinking of the tracer cloud.

Jensen and others (1993) reported on two natural-gradient tracer tests that were conducted in glacial outwash in Denmark. One tracer cloud included tritium and had an estimated density that was similar to that of the ambient ground water; the second tracer cloud included chloride and was estimated to have a density contrast of about 0.7 percent. The tritium cloud showed no downward movement relative to the water table, but the chloride cloud moved rapidly downward to the base of the aquifer. Jensen and others (1993) attributed the downward movement to the density difference between the tracer solution and the ambient ground water.

In all of the tracer tests described above, the tracer solution was injected as a pulse into the aquifer, and the cloud was observed by collection of water samples as it passed through an array of multilevel wells. Rivett and others (1994) conducted a tracer test with organic solvents

at the Borden site by creating a plume that emanated continuously from an emplaced semi-permanent source. The total concentration of the three organic compounds exceeded 2,000 mg/L in ground water collected near the source volume. Rivett and others (1994, p. 35) observed high levels of contamination in the aquifer layers immediately below the base elevation of the source. They ascribed the downward expansion of the plume near the source to the density difference between the tracer solution and the ambient ground water.

A number of researchers have investigated the factors that affect density-induced downward movement of dense solutions by use of laboratory "sand tank" experiments. Most of the experiments reported in the literature involved the creation of a contaminant plume from a continuous source rather than the pulsed injections used in most field-scale tracer tests. Paschke and Hoopes (1984) conducted a set of 11 experiments in which the tracer solutions had relative densities ($\Delta\rho/\rho_o$) of 0.03 to 0.20. They observed that the amount of downward movement increased as the density difference increased and as the rate of ambient lateral flow across the model decreased.

A focus of most other laboratory experiments reported in the literature was the development of instabilities during density-induced sinking. These instabilities develop as the unstable density stratification leads to free convection in the porous medium, in which fingers develop in the flow that result in the rapid and erratic redistribution of solutes. The rapid flow causes the fluids to mix to achieve a stable density gradient (Shincariol and Schwartz, 1990). Although Pashchke and Hoopes (1984) used a density contrast that should have led to intense instability and strong free convection, they do not report on the nature of the flow system during their experiments.

Shincariol and Schwartz (1990) ran several sets of experiments in which tracer solutions were introduced along the upstream side of a sand tank that had a steady ambient horizontal flow and various configurations of homogeneous, uniformly layered, and lenticular media. They varied the relative density and ambient flow rate during the experiments. In the homogeneous medium, density effects were apparent with small ambient flows even at modest density contrasts. The instabilities in the flow became noticeable for the particular configuration of the tests at concentrations as low as 1,000 mg/L. In the layered media, the denser tracer solution tended to accumulate at the boundaries between high-permeability and low-permeability layers, much like dense nonaqueous liquids (DNAPLs) are reported to accumulate on low-permeability lenses and layers beneath spill sites. Shincariol and Schwartz (1990) noted that the accumulation occurred because the downward-moving dense fluid arrived at the interface at a greater flux rate than the rate at which it could move into the lower permeability unit below. A similar phenomenon was observed in the lenticular media, in which complex flow patterns occurred at large density contrasts. The heterogeneity tended to increase the stability of the flow system and reduce the amount of downward movement for a given density contrast. In the lenticular media, flow tended to remain stable even at concentrations as high as 2,000 mg/L. Schincariol and Schwartz (1990) concluded that the "realization that dense plumes should sink to some extent in a homogeneous and isotropic medium is inherent in the physical laws of groundwater flow." Once a density difference exists, there is a component of downward velocity. Whether it is significant or not depends on other factors, such as the scale of the problem, the initial density difference, and the rate of ambient lateral flow.

Oostrom and others (1992) also conducted sand-tank experiments, but with a line source at the top of the tank to represent the input of dense leachate from a landfill. The porous media

were all homogeneous and isotropic, and they varied the ambient flow, leachate inflow rate, and density contrast for the various experiments. The results they obtained were similar to those reported by Shincariol and Schwartz (1990) for a homogeneous medium. They showed that large values of permeability and relative density favored the development of instabilities, and high values for the ambient horizontal flow, effective porosity, and dispersion coefficient favored the maintenance of stable flow. Oostrom and others (1992) noted that no single criterion was found to predict the flow stability, but that density-induced sinking was observed even with modest density differences.

Istok and Humphrey (1993) conducted sand-tank experiments at relatively low solute concentrations (40 to 1,000 mg/L). Few details are provided in the short abstract. They reported that buoyancy-induced vertical flow occurred at all tracer concentrations investigated, and the amount of vertical movement could be predicted from the ratio of the relative density to the lateral hydraulic gradient. They concluded that buoyancy-induced flow might be a more widespread phenomenon than had been previously recognized.

Analytical and Numerical Models

Analytical models can provide insight into the factors that affect the rate of downward movement of a dense plume within an ambient flow field at low relative densities, when the flow field remains stable. Hubbert (1953) developed analytical expressions for the relative movement of two fluids of different densities when one of the fluids dominates the ambient flow field. Hubbert's method, developed to explain the migration and entrapment of petroleum in reservoir rocks, assumes that both fluids can occupy any point in the aquifer and that the fluids do not mix.

The analytical expressions relate the potential field of the tracer fluid to the potential field of the ambient fluid by the relative density ($\Delta\rho/\rho_o$) described by Bear (1972). The amount of downward movement predicted by the Hubbert method is dependent on this vertically oriented density driving force.

Analytical models developed by Yih (1963, 1965) predict the downward movement of fluid bodies of various shapes in an arbitrarily oriented, unidirectional ambient flow field. The Yih method computes the components of velocity of a three-dimensional body by solving the Laplace equation with appropriate pressure and continuity conditions at the boundary between the two fluids. The method assumes that the aquifer is homogeneous, isotropic, and infinite in extent; and that the fluid body, although it displaces the ambient fluid as it sinks, does not deform or become diluted by dispersion. The relative density determines the rate of downward movement of the fluid body. Yih (1963) showed that the shape of the fluid body and its orientation relative to the ambient flow direction and the direction of the gravitational force all affect the computed rate of downward movement. For example, for a given density difference, an elliptical body sinks more rapidly with its major axis oriented vertically than with its major axis oriented horizontally. A comparison of predicted rates of downward movement of a spherical body and an infinitely long circular cylinder suggests that the predicted sinking rate of similarly shaped bodies is smaller for two-dimensional models than for three-dimensional models. The Hubbert (1953) and Yih (1963) models are discussed further in Chapter 3 of this report.

The analytical analysis of Paschke and Hoopes (1984) addressed the downward movement of a dense plume from a source at the top of a horizontal ambient flow system. Their

model predicts the trajectory, concentration, and boundary of a density-influenced ground-water plume, similar to a leachate plume from a landfill. The model includes two regions, one near the source, where vertical flow caused by density dominates, and one far from the source, where the plume is influenced primarily by the ambient flow. The models assume that the pressure distribution is hydrostatic within the plume and that the viscosity is constant in the flow domain. In the region near the source, the rate of downward displacement is proportional to the relative density and inversely proportional to the cumulative downward displacement, the latter because of the diluting effect of dispersion with vertical travel distance. Perhaps most interestingly, the cumulative downward displacement (i.e., the vertical position relative to the initial position) is proportional to the square root of the horizontal displacement. This relationship is consistent with the concave-upward shape of the trajectories observed during the Cape Cod and Borden tracer tests. In the region far from the source, the cumulative downward displacement is proportional to the cube root of the horizontal displacement. This relationship indicates that, although the effects of density diminish as the plume moves far from the source, a component of vertical movement persists as long as there is a density contrast between the two fluids. Paschke and Hoopes (1984, p. 1185) presented a characteristic length scale for the plume, which indicates that the relative importance of the buoyancy-induced flow increases with increasing permeability, source flux, and density contrast, and decreases with increasing porosity, ambient flow rate, and dispersion coefficients.

Jalbert and others (2000) used an analytical analysis to demonstrate that density effects should be considered when using tracer-test breakthrough curves to estimate aquifer properties, such as dispersivity and hydraulic conductivity. They developed equations describing the change in a sloping front between two fluids with different densities as the front advances along a layer

of the aquifer. The smearing of the arrival of the denser tracer fluid at a given observation point can provide inaccurate values for the apparent hydraulic conductivity and dispersivity from fitting of the advection-dispersion model to the average breakthrough data. Jalbert and others (2000) concluded that density-induced flow must be considered in the interpretation of tracer-test data, even at relatively low concentrations where no feedback between concentrations and flow is typically assumed.

Numerical models provide increased flexibility in the simulation of density-induced sinking by allowing incorporation of variable aquifer properties, irregular aquifer boundaries, and various configurations of the source of the dense fluid. A number of computer codes have been developed to simulate density-dependent ground-water flow and solute transport with conservative and non-conservative, reactive chemical species. These codes include those described by Frind (1982), Voss (1984), Sanford and Konikow (1985), Kipp (1987), van Walsun (1987), Mendoza and Frind (1990a,b), Zhang and others (1994), and Zhang (1995). It is beyond the scope of this report to evaluate and compare these models.

Frind (1982) used a two-dimensional finite-element model to simulate a hypothetical landfill plume. Little density-induced downward movement was simulated because a large value of transverse dispersivity (α_T = 1 m) rapidly diluted the simulated plume. Frind (1982) concluded that the vertical dispersivity would have to be decreased by at least an order of magnitude in order for the effect of density to become noticeable.

The vertical trajectory of the tracer cloud during the large-scale natural-gradient tracer test at the Borden site (Mackay and others, 1986) was simulated by van Walsun (1987) using a two-dimensional alternating-direction Galerkin finite-element model. The model assumed an

isotropic hydraulic conductivity and a small constant regional vertical gradient across the model domain. A lateral ambient flow was imposed by use of a specified-flux upgradient boundary condition and specified-pressure downgradient boundary condition. The source was assumed to appear instantaneously in the aquifer at the start of the simulation; it was not injected into place. Initial simulations with a relative density difference of 0.1 percent and a longitudinal dispersivity of 0.45 m significantly under-predicted the observed downward movement during the experiment. Better agreement was obtained by increasing the regional vertical gradient to represent a greater rate of recharge from precipitation. An increase in the initial density of the tracer cloud also increased the simulated rate of downward movement. Van Walsun (1987) also simulated an increasing dispersivity with travel distance to represent the scale-dependence of the dispersion process. In several simulations, the value was increased nonlinearly to an asymptotic value of 0.45 m over various time intervals since the start of the tracer test. The results demonstrated that a constant value of dispersivity at its asymptotic, late-time value generated too much spreading and dilution at early times and decreased the influence of the density-dependent forces too rapidly.

Koch and Zhang (1992) used the computer code MOCDENSE (Sanford and Konikow, 1985) to simulate two-dimensional density-dependent transport of a conservative solute representing a typical landfill plume. Their simulation setup was similar to that of van Walsun (1987), except that there was no ambient vertical gradient and the source area was a patch along the top boundary of the model. The aquifer was assumed to be homogeneous, and a value of 5 m was used for longitudinal dispersivity. An anisotropic hydraulic conductivity and a uniform rate of recharge along the top boundary of the model were used for some simulations. The various simulations showed that a relative density of about 0.3 percent caused discernable downward

movement of the plume. The downward movement was small, however, compared to the lateral movement. Koch and Zhang (1992) noted that considerable travel distance might be needed for the downward movement to become discernable in a field situation. The rate of sinking was proportional to the horizontal hydraulic conductivity and the relative density difference. Additional simulations indicated that increases in dispersivity and the anisotropy of hydraulic conductivity decreased the amount of simulated downward movement.

Most contaminant plumes consist of many chemical species that may interact chemically with one another and with the aquifer matrix. Zhang and Schwartz (1995) used an optimized and modified version of the computer code VapourT (Mendoza and Frind, 1990a, b) to simulate two-dimensional density-dependent flow and transport of two species in a typical landfill plume based loosely on the Babylon landfill (Kimmel and Braids, 1980). The conservative species was assumed to incorporate all the density-determining properties, while transport of the second species could be retarded relative to transport of the first species. Both intermittent and continuous input of the leachate was simulated. For the particular set of simulation parameters, density effects were important when the leachate concentration exceeded about 2,000 mg/L. Important factors that influenced the development of the plumes included the temporal pattern of loading, the initial concentration of the density-determining species, and the extent of retardation of the sorbing species. Zhang and Schwartz (1995) noted that the ambient flow field encountered by a sinking plume also affects the plume development. They suggested that the relative change in the horizontal and vertical positions of the concentration distributions of various species in a plume is a good indicator of whether density effects or ambient flow dominate transport.

Purpose and Scope

The purpose of this report is to examine the hypothesis of LeBlanc and others (1991) that density effects and recharge from precipitation caused the observed downward movement of the bromide tracer cloud during the first 237 days of the 1985-88 Cape Cod tracer experiment. Analytical and numerical modeling is used to examine the hydraulic factors and model-design considerations that affect the simulated rate of downward movement. The models are then applied to the specific parameters for the Cape Cod test to test the hypothesis.

Preliminary results of this work have been reported in several proceedings papers and a journal article. LeBlanc and Celia (1991) used the analytical models of Hubbert (1953) and Yih (1965) to examine the factors that affect the rate of downward movement. They also used SUTRA (Voss, 1984) to simulate density-dependent flow and transport for a simplified representation of the first several days of a tracer test. LeBlanc and Celia (1996) reported on the field-scale simulation of the Cape Cod tracer test. This thesis presents the details of the work described in these two reports.

Zhang and others (1998) used the results reported by LeBlanc and Celia (1991, 1996), and additional concepts described by Zhang and Schwartz (1995), to simulate the variable-density flow and transport of bromide and lithium during the Cape Cod experiment. They simulated bromide as a conservative species and lithium as a sorbing, slightly retarded species, based on the results of Garabedian and others (1988) and Wood and others (1990). They modified a vectorized finite-element model (Mendoza and Frind, 1990a,b; Zhang and others, 1994) to simulate two-dimensional coupled ground-water flow and mass transport with a kinetic adsorption model in a variable-density system. A finite-volume code (Zhang, 1995) was used to

simulate flow and transport in three-dimensions for a small subsection of the aquifer for comparison to the two-dimensional results. The boundaries for the models are the same as those used in LeBlanc and Celia (1996), and the test parameters were taken from the various Cape Cod tracer-test papers described in Chapter 2 of this thesis. A major difference from the earlier modeling is that aquifer heterogeneity was incorporated explicitly in the model and, therefore, only a small value of local longitudinal dispersivity (α_L = 0.1 m) was used in the simulations.

Zhang and others (1998) confirmed the results of LeBlanc and Celia (1996), which demonstrated that the amount of downward movement was dependent on the initial density difference between the tracer cloud and the ambient ground water, and that recharge from precipitation contributed significantly to the vertical displacement of the tracer cloud. The three-dimensional simulations confirmed the findings of LeBlanc and Celia (1991, 1996) that the size of the initial cloud affected the rate of downward movement. The three-dimensional simulations also demonstrated that the amount of downward movement was less in a two-dimensional simulation than in a three-dimensional simulation. LeBlanc and Celia (1991) had inferred this relationship by comparing the Yih (1963) analytical solutions for a sphere and an infinitely long circular cylinder.

Zhang and others (1998) extended the work of LeBlanc and Celia (1991, 1996) by incorporating a deterministic trend in hydraulic conductivity in the two-dimensional simulations. LeBlanc and others (1991) had hypothesized that the asymmetrical shape of the bromide cloud was caused by a zone of high hydraulic conductivity near the water table. By incorporating this trend into the heterogeneous conductivity field, Zhang and others (1998) were able to better simulate the observed asymmetrical shape of the tracer cloud. They also were able to simulate the general trajectory, shape, and retarded velocity of the lithium tracer cloud.

As mentioned above, this report documents the detailed analysis that is summarized in the preliminary reports by LeBlanc and Celia (1991, 1996). Chapter 2 is a brief description of the 1985-88 Cape Cod tracer test. In Chapter 3, analytical models are used to examine the factors that affect density-induced sinking, and the models are applied to the Cape Cod tracer test. The numerical model SUTRA (Voss, 1984) is used in Chapter 4 to further examine the factors that affect downward movement, including various issues related to model design. Chapter 5 describes the application of SUTRA to simulate the first 237 days of the Cape Cod test, when density was most responsible for the observed downward movement. The results of the analysis are discussed in Chapter 6.

The work presented in this thesis began in about 1990 and was completed only recently. During this time, there have been many advances in computing technology and analytical methods. Some of the methods that were used to circumvent computing limitations would no longer be necessary. However, the principles of flow and transport remain the same, and this work focused on an examination of those principles for density-induced flow and solute transport.

CHAPTER 2

CAPE COD NATURAL-GRADIENT TRACER TEST

The purpose of this chapter is to present a brief summary of the 1985-88 natural-gradient tracer test at the Cape Cod site. This experiment was conducted to measure the field-scale dispersion of solutes and to obtain data with sufficient detail to test various stochastic theories that relate aquifer heterogeneity to the dispersive process (Gelhar and Axness, 1983; Dagan, 1982, 1984; Neuman and others, 1987). Detailed descriptions of the tracer test and hydrology of the test area have been reported by LeBlanc and others (1991), Garabedian and others (1988, 1991), Hess and others (1992), Wood and others (1990), and Stollenwerk (1995). The information given below, which is drawn from these sources, describes the features of the test that are relevant to the problem of density-induced downward movement of the tracer cloud.

Site Description and Aquifer Characteristics

The tracer test was conducted in an abandoned gravel pit on western Cape Cod near the Massachusetts Military Reservation (Figure 2-1). The test site is located above a plume of sewage-contaminated ground water that was formed by more than 60 years of land disposal of treated sewage at the base (LeBlanc, 1984; LeBlanc and others, 1999).

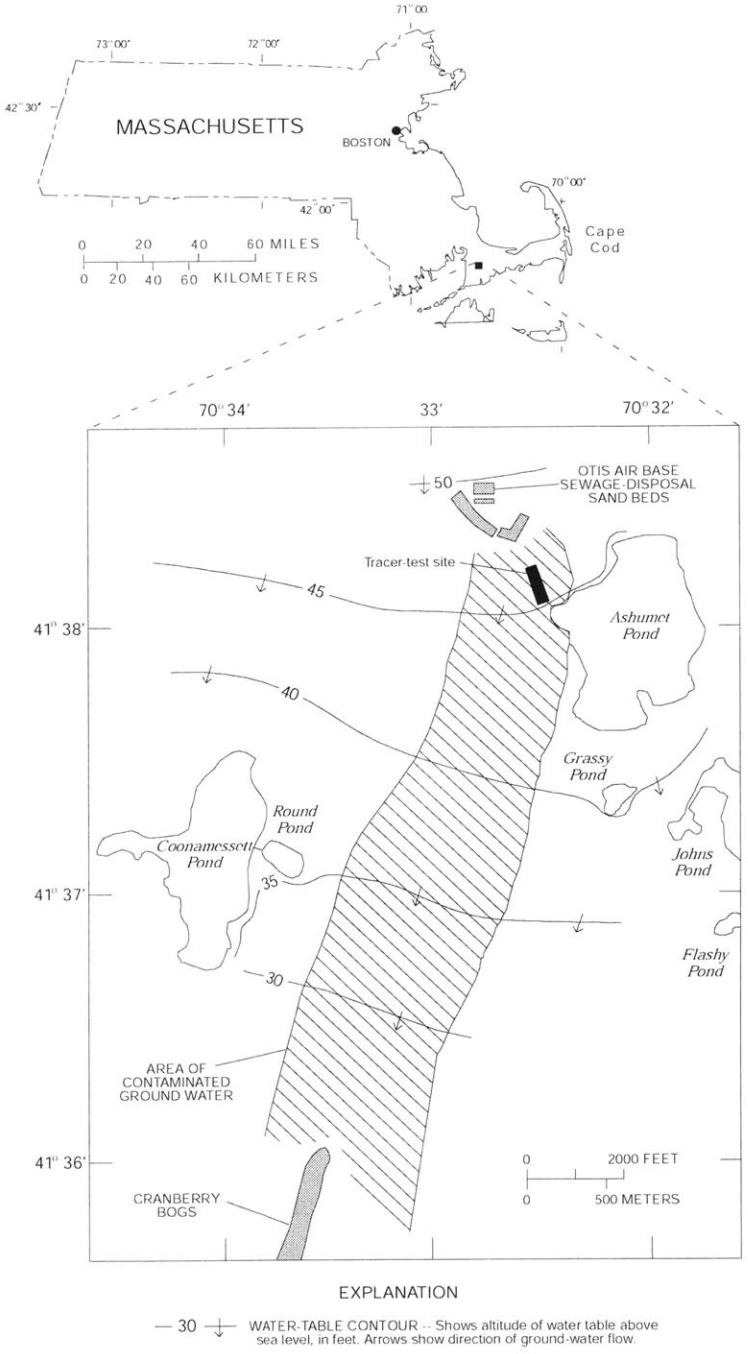

Figure 2-1. Location of the study area, showing the sewage plume and the tracer-test site [adapted from LeBlanc and others, 1991, Figure 1].

Hydrogeologic Characteristics

The aquifer at the test site is composed of about 100 m of unconsolidated sediments that overlie crystalline bedrock. The upper 30 m of the aquifer consists of stratified sand and gravel glacial outwash. The estimated average hydraulic conductivity of the sand and gravel is 110 m/d. Hydraulic tests made with a borehole flowmeter and permeameter tests made on cores (Hess and others, 1992; Wolf and others, 1991) indicate that the hydraulic conductivity varies about one order of magnitude. This results from the interbedded lenses and layers of the sand and gravel. Hess and others (1992) used a variogram analysis to estimate an anisotropy of 1.2:1 for horizontal to vertical hydraulic conductivity. The effective porosity of the sand and gravel was estimated from the results of the tracer test to be about 0.39 (Garabedian and others, 1991).

There is some evidence that the average hydraulic conductivity decreases with depth at the test site. Borehole flowmeter measurements and permeameter analysis of cores at a site about 15 m west of the tracer-test array (Wolf, 1988; Hess, 1989) detected a zone near the water table in which hydraulic conductivity is as great as 260 m/d. It is not known if a similar zone of high hydraulic conductivity is present in the path of the tracer cloud. But a trend of decreasing grain size with depth is a common characteristic of glacial outwash, sand and gravel deposits on western Cape Cod (Masterson and others, 1997a).

Hydrologic Characteristics

The water table at the test site is generally between 3 and 7 m below land surface and slopes to the south at about 0.15 m per 100 m (Figure 2-2). The water-table altitude typically fluctuates about 1 m annually because of seasonal variations in precipitation and recharge (LeBlanc and others, 1986) and the direction of the hydraulic gradient can vary by as much as 15

degrees (Walter and others, 1996). However, during the first 17 months of the tracer test (July 1985 to December 1986), the water table fluctuated only about 0.3 m and the direction of the hydraulic gradient varied by about 8 degrees (Figure 2-3).

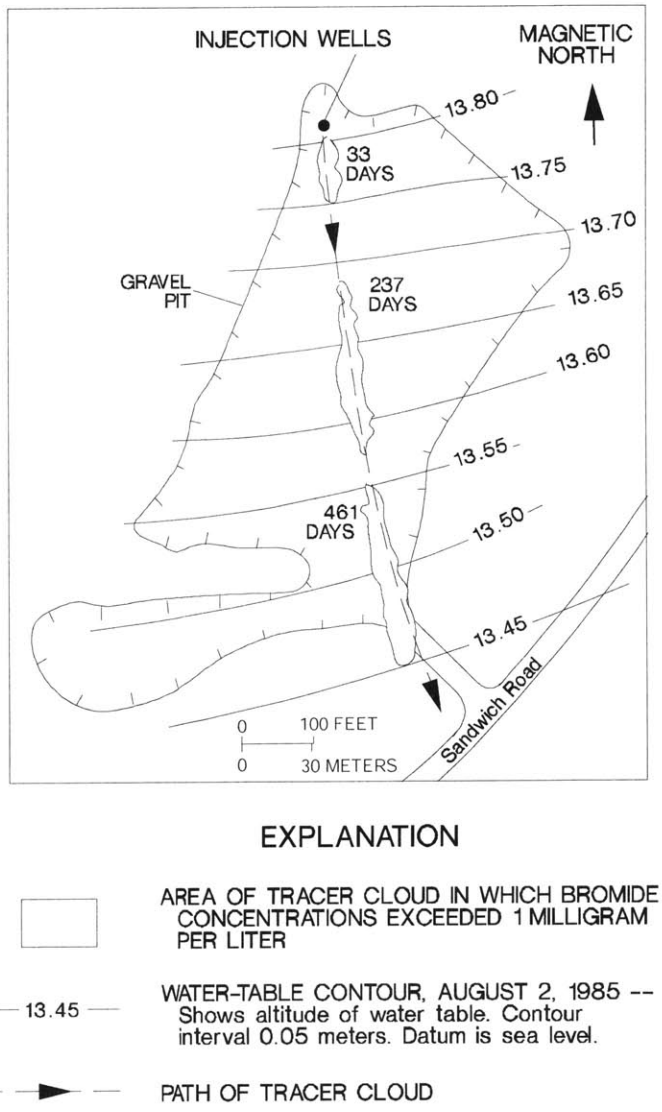

Figure 2-2. Tracer-test site, showing area of abandoned gravel pit, the water table, and the predicted and observed path of the bromide tracer cloud [adapted from LeBlanc and others, 1991, Figure 4].

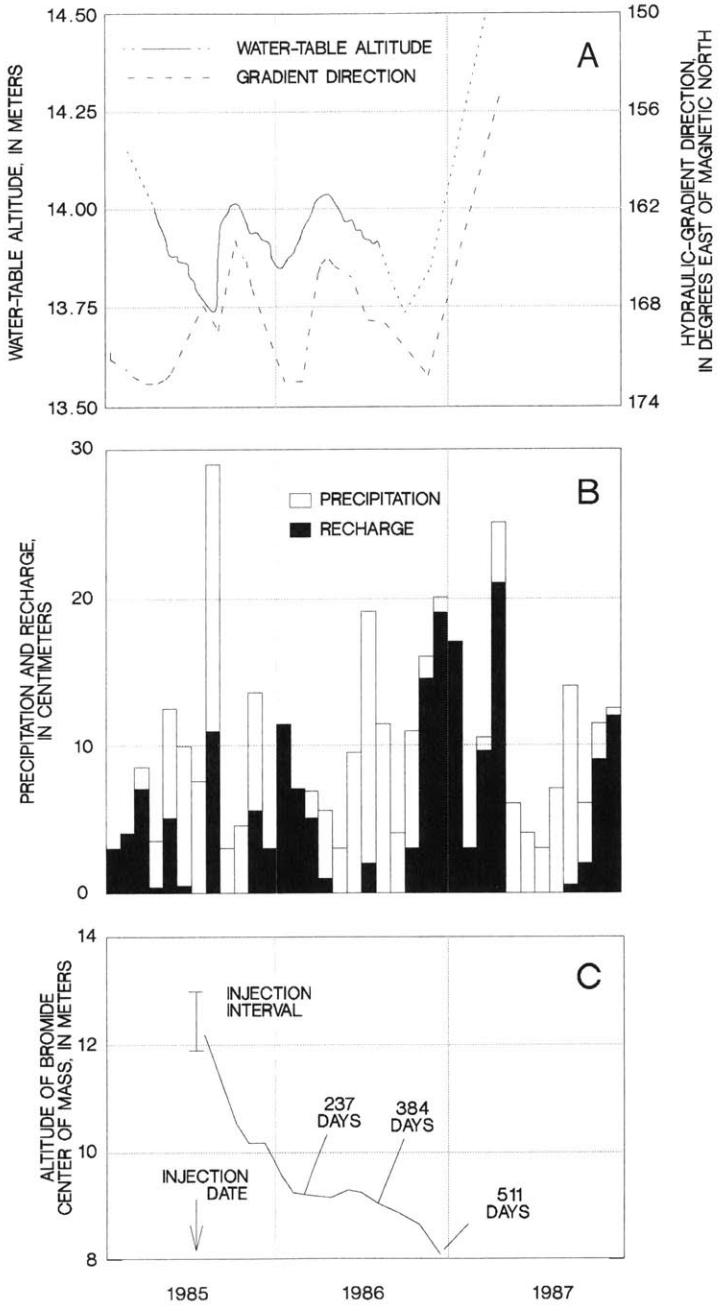

Figure 2-3. Graphs showing (A) altitude of the water table and direction of the hydraulic gradient, (B) monthly estimated recharge and precipitation, and (C) vertical position of the center of mass of the bromide cloud during 1985-1987 [from LeBlanc and others, 1991, Figure 5].

The estimated average ground-water velocity is about 0.4 m/d, which is based on the values of hydraulic gradient, hydraulic conductivity, and effective porosity given above. The ambient flow is nearly horizontal. Although there must be a vertical component of flow because of recharge from precipitation, vertical hydraulic gradients are too small to measure in the clusters of monitoring wells at the test site.

The source of water to the aquifer is recharge from precipitation. At the time of the study, it was estimated that about 45 percent of the total average annual precipitation on Cape Cod, or about 50 cm/year, recharges the ground-water system (LeBlanc and others, 1986). A recent study by Masterson and others (1998) suggested that the percentage of precipitation that becomes recharge may be as high as 55 percent. During the tracer experiment, there were several periods in which recharge is estimated to have occurred (Figure 2-3). Most of the recharge occurred during the fall and winter, when there is little evapotranspiration. Several intense storms in August 1995, shortly after the tracer test began, are believed to have resulted in unusual summertime recharge to the aquifer.

Tracer-Test Design

The tracer test began in July 1985 with the injection of 7.6 m^3 of tracer solution into the aquifer. Movement of the tracer cloud was then monitored by collection of water samples from an array of 656 multilevel samplers. The water samples were collected in 16 synoptic sampling events between July 1985 and December 1986 to monitor the movement of the bromide tracer cloud.

Tracer Characteristics

Four tracers were added as salts to 7.6 m^3 (2,015 gallons) of ambient ground water that had been obtained from a shallow well at the site. The tracers are shown in Table 2-1. A total mass of 6.48 Kg of tracer was added to the solution. The initial concentration of bromide, the conservative tracer, was 640 mg/L. The densities of the ambient ground water and the tracer solution were not measured, but the densities were estimated from the concentrations of dissolved solids in the two fluids (see discussion in Chapter 4). The estimated density of the tracer solution was about 0.1 percent greater than the density of the ambient ground water. Because the solution was stored for about one day above ground during the preparation of the solution and the subsequent injection, the tracer solution was about 3° C warmer than the ambient ground water when it was injected into the aquifer (16° C versus 13° C).

Table 2-1. Characteristics of the tracers injected on July 18-19, 1985, at the Cape Cod site [adapted from LeBlanc and others, 1991, Table 2].

Tracer	**Injected mass (g)**	**Injected concentration (mg/L)**
Bromide (Br^-)	4,900	640
Lithium (Li^+)	590	78
Molybdate (MoO_4^{2-} as Mo)	610	80
Fluoride (F^-)	380	50

Injection of the Tracers

The tracers were injected into three 2-inch-diameter (5.08-cm) wells during a 17-hour period beginning on July 18, 1985, and ending on July 19, 1985. Each injection well had a polyvinyl chloride (PVC) slotted screen set at an altitude of 11.9-13.1 m above sea level, or

about 1.2-2.4 m below the water table. The three wells were located 0.9 m apart along a line perpendicular to the flow of ground water.

The tracer solution was injected at a total rate of 7.6 L/min, or 2.5 L/min in each well. The initial volume of aquifer occupied by the tracer solution, assuming a porosity of 0.39 and no mixing with the ambient ground water, was about 19.5 m^3, which is equivalent to a box around the wells with dimensions of 1.2 x 4 x 4 m. The actual solute distribution immediately after injection was not determined. Because of local aquifer heterogeneity at the injection site, the tracer cloud probably had a complex shape that was quite different from a rectangular volume.

Monitoring of the Tracer Cloud

The location and distribution of solutes within the tracer cloud was monitored by collection of water samples from an array of 656 multilevel samplers (see LeBlanc and others, 1991, Figures 7 and 8). Each sampler consisted of 15 sampling ports set at various intervals in the vertical direction. Therefore, the sampling network consisted of about 9,840 individual sampling locations that allowed a three-dimensional characterization of the tracer distributions with time.

Water samples were collected from subsets of the multilevel samplers at about monthly intervals, beginning 13 days after the injection, to obtain snapshot views of the three-dimensional distributions of tracer concentrations. A total of 19 rounds of sampling were completed between July 1985 and June 1988, although the complete bromide cloud was captured only for the first 16 rounds. Each sampling round involved the collection of samples from 40 to 290 multilevel samplers and was generally completed in 2-3 days. LeBlanc and others (1991, Table 3) present a complete tabulation of the sampling rounds.

samplers and was generally completed in 2-3 days. LeBlanc and others (1991, Table 3) present a complete tabulation of the sampling rounds.

The final database for the period from July 1985 to June 1988 includes about 30,000 bromide analyses, 33,000 lithium analyses, and 38,000 molybdate analyses. Graphical and statistical methods were used to interpret the characteristics of the tracer cloud from this large database.

Observed Tracer Movement

The movement of the tracer cloud was tracked during the test by preparing maps and cross sections of the concentration data. Although LeBlanc and others (1991) report on the movement of bromide, lithium, and molybdate, only the bromide cloud was considered for the density analysis in this paper because it accounted for about 75 percent of the total injected mass of tracers.

Horizontal Movement

During the tracer test, the bromide cloud moved in a southerly direction along a path that matched the path predicted from the water-table gradient (Figure 2-2). The average rate of movement of the cloud was 0.42 m/d (Garabedian and others, 1991), which matches the ground-water velocity that was predicted from Darcy's Law.

The average rate of movement was accompanied by significant longitudinal spreading of the bromide cloud in the direction of flow (Figure 2-4). The cloud spread much less in the direction transverse to flow. At 237 days, the bromide cloud, as defined by concentrations

greater than 1 mg/L (or a relative concentration compared to the initial concentration of 0.0016), was about 75 m long, but only about 11 m wide. The maximum observed concentration at 237 days was 65.2 mg/L (Table 2-2), or a relative concentration of about 0.1.

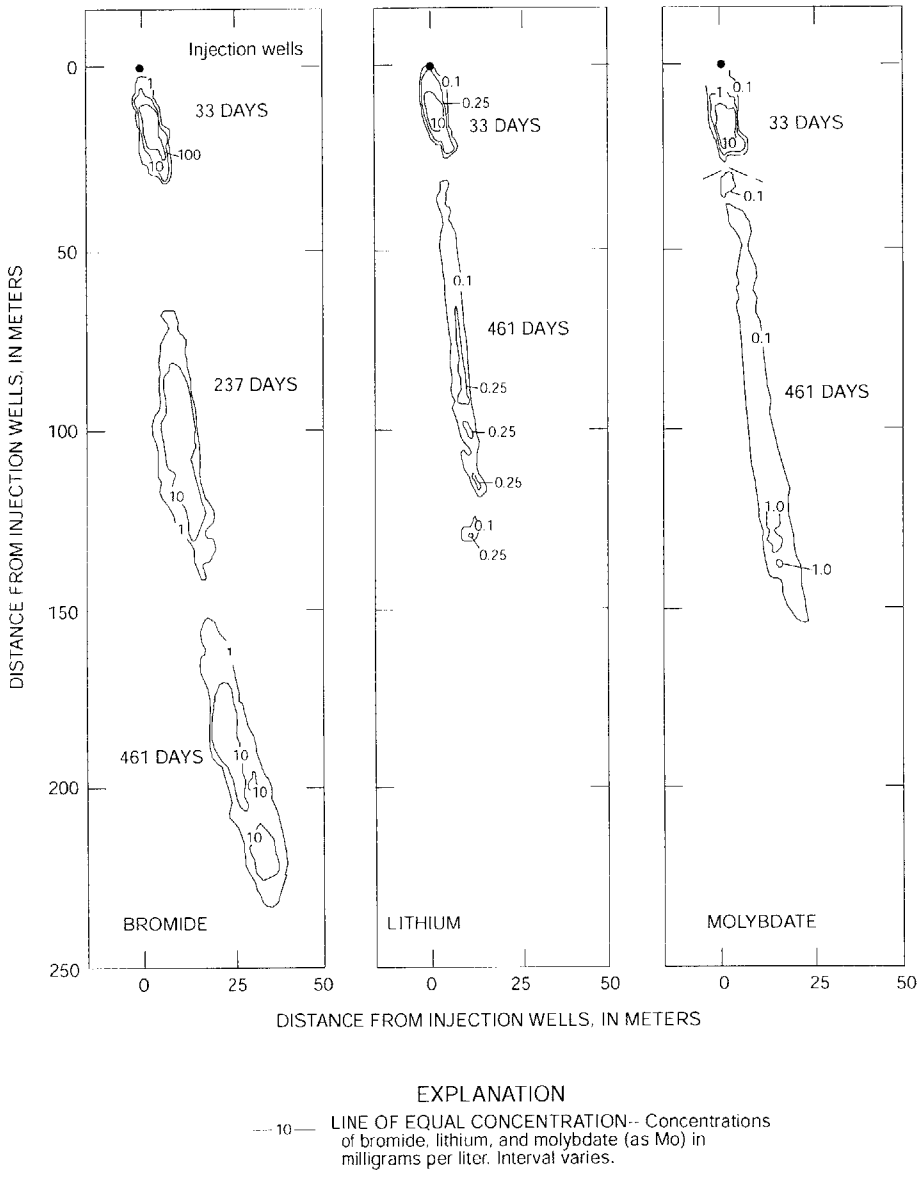

Figure 2-4. Areal distribution of maximum concentrations of bromide, lithium, and molybdate at 33, 237, and 461 days after injection [from LeBlanc and others, 1991, Figure 10].

Vertical Movement

The bromide cloud also moved downward vertically during the tracer test, and a zone of ground water that did not contain the tracers formed above the cloud (Figure 2-5). An analysis of the spatial moments of the bromide cloud (Garabedian and others, 1991) showed that the center of mass of the bromide cloud moved downward about 3.2 m during the first 237 days of the tracer test (Figure 2-3 and Table 2-2).

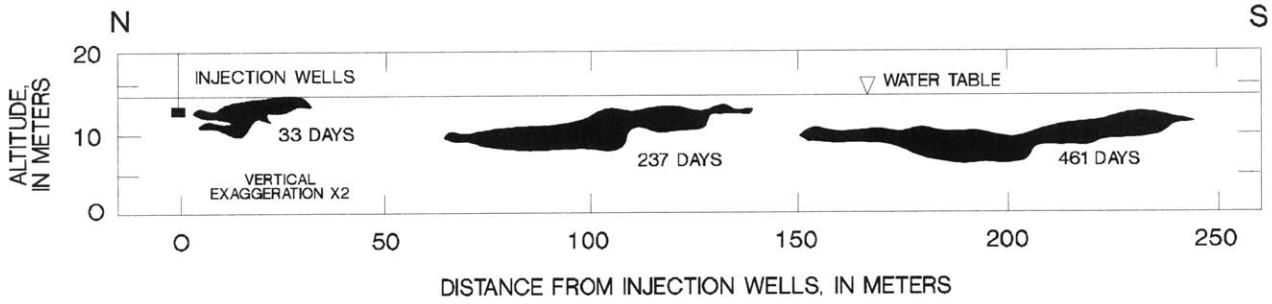

Figure 2-5. Vertical location of the bromide tracer cloud at 33, 237, and 461 days after injection. Cloud locations defined by zones in which the bromide concentration exceeded 1 mg/L [from LeBlanc and others, 1991, Figure 11].

LeBlanc and others (1991) hypothesized that two processes contributed to the downward movement observed during the tracer test: (1) vertical components of flow associated with areal recharge, and (2) sinking of the denser tracer cloud into the native ground water. Both of these processes were probably important during the first 237 days after injection, when about 75 percent of the total vertical displacement of the bromide cloud observed during the entire test occurred. LeBlanc and others (1991) estimated that about 60 cm of recharge occurred during the first 237 days of the test, which is equivalent to about 1.5 m of water in the aquifer (given a porosity of 0.39). This represents slightly less than half of the vertical movement observed

during this period. The zone of tracer-free water above the tracer cloud was formed partly by this influx of recharge at the water table and partly by the ambient ground water that moved up and around the sinking tracer cloud. The density difference between the tracer solution and the ambient ground water was the presumed cause of the remainder of the observed downward movement.

Table 2-2. Selected statistics and spatial moments for the bromide tracer cloud during the first 237 days of the Cape Cod tracer test [from LeBlanc and others, 1991, Table 3; Garabedian and others, 1991, Table 1. Coordinates, x-direction is positive east from magnetic north, y-direction is positive north from magnetic north, z-direction is altitude above sea level. Flow direction generally in negative y-direction].

Days after injection	**Maximum observed bromide concentration (mg/L)**	**Center of mass (m)**			**Principal components of variance (m^2)**		
		$\bar{x}$	$\bar{y}$	$\bar{z}$	$s_{x'}^2$	$s_{y'}^2$	$s_{z'}^2$
0	640	0	0	12.5	--	--	--
13	576	0.8	-7.4	12.3	1.5	6.5	0.37
33	429	2.7	-16.9	11.7	1.8	20.2	0.46
55	311	3.0	-25.9	11.1	1.9	34.8	0.50
83	124	5.6	-38.9	10.6	2.5	52.4	0.72
111	132	8.1	-50.9	10.3	3.1	85.6	0.73
139	76.6	10.2	-64.7	10.4	3.4	118	0.74
174	76.6	11.1	-77.5	9.6	4.3	134	1.03
203	61.5	11.4	-88.8	9.4	3.9	162	1.02
237	65.2	11.9	-100.1	9.3	5.2	189	1.06

As the tracer cloud moved downward, it spread little in the vertical direction and remained about 4 to 6 m thick as it moved through the aquifer (Figure 2-5). The bromide cloud

developed two zones of elevated concentration, one near the leading edge of the cloud and just below the water table, and another near the center of the cloud and deeper in the aquifer, which gave the cloud its asymmetrical shape. LeBlanc and others (1991) hypothesized that part of the injection solution may have moved rapidly outward from the injection wells in a very permeable layer near the water table, while the remainder of the cloud began sinking into the aquifer under the driving force of the density difference. Although both factors may have been influential for only a short period, the asymmetrical shape remained imprinted on the cloud because vertical mixing is limited.

Spatial Moments of the Bromide Distribution

Garabedian and others (1991) used a spatial-moments analysis of the bromide concentrations to calculate the bromide mass, velocity, and dispersivity during the tracer test. The method involved linear, trapezoidal interpolation of the concentration data vertically along the multilevel-sampler ports and planar triangulation methods for areal integration. A summary of selected moments values reported by Garabedian and others (1991) is given in Table 2-2.

Total Mass and Position of the Center of Mass

The calculated mass for the 16 bromide sampling rounds varied from 85 to 105 percent of the injected mass. The porosity used in the mass calculation (0.39) was obtained by fitting the average calculated mass from the moments analysis to the known total injected mass of bromide. The good agreement between the known and calculated total mass for bromide indicates that the sampling network was sufficiently dense to capture the characteristics of the tracer cloud.

The center of mass of the bromide cloud moved horizontally at a nearly constant rate of 0.42 m/d. The horizontal trajectory of the tracer cloud closely matched the temporal changes in hydraulic gradient at the site (Figure 2-3). The center of mass, as was mentioned above, moved vertically downward about 3.2 m during the first 237 days of the test (Figure 2-3). About half of this downward displacement took place during the first 83 days of the test. The average angle of downward movement during the 83-day period was about 2.5 degrees below the horizontal (1.7 m in 39.3 m). During the entire 511 days in which the bromide cloud was monitored, the total vertical displacement was 4.2 m, and the horizontal movement was about 217 m.

Variance and Dispersivity

The longitudinal variance of the bromide concentrations changed linearly with travel distance. Because of the strongly linear trend, Garabedian and others (1991) calculated the longitudinal dispersivity as one half the slope of the change in variance with respect to the travel distance of the center of mass. The resultant longitudinal dispersivity is 0.96 m. Similar calculations yielded a transverse horizontal dispersivity of 0.018 m (1.8 cm) and a transverse vertical dispersivity of about 0.0015 m (1.5 mm). The much smaller transverse dispersivities as compared to the longitudinal dispersivity are consistent with the observed spreading of the bromide cloud, which occurred mostly in the longitudinal direction (Figure 2-2).

Garabedian and others (1991) noted that the longitudinal variance deviated from the linear trend with travel distance in the first 26 m of distance traveled by the bromide cloud. The variance increased nonlinearly during this period, which was about 60 days long, indicating an increasing dispersivity with travel distance until the asymptotic value of 0.96 m was reached. The estimated incremental values of dispersivity were at most 0.44 m during 0-13 days, 0.71 m

during 13-33 days, and 0.81 during 33-55 days (Garabedian and others, 1991, p. 918). These field observations agree with the theoretical results of Gelhar and others (1979) and Dagan (1984), which predict an early period when the dispersivity should increase with time (or travel distance).

Hydraulic Conductivity and Estimated Macrodispersivity

Hess and others (1992) and Wolf and others (1991) made nearly 1,500 measurements of hydraulic conductivity at the tracer-test site using borehole flowmeter measurements in 16 long-screened wells and permeameter tests of cores from 16 boreholes. The measurement sites were 70 to 115 m downgradient from the tracer injection wells and about 15 m to the west of the multilevel-sampler array.

The geometric mean hydraulic conductivity for the flowmeter data was 95 m/d (0.11 cm/s), while the geometric mean for the permeameter data was only 30 m/d (0.035 cm/s). Hess and others (1992) attributed the lower mean for the permeameter values to compaction of the sediments during collection of the cores. The variance of ln K (K in cm/s) for the flowmeter data was 0.24, and the flowmeter values ranged over about one order of magnitude. The small value of variance as compared to reported values for other aquifers (see Hess and others, 1992, Table 2) indicates that the Cape Cod sand and gravel, at least in a statistical sense, is a relatively homogeneous porous medium with respect to hydraulic conductivity.

The spatial variability of the hydraulic conductivity was characterized using a variogram analysis. Estimated correlation scales range from 2.9 to 8 m in the horizontal direction and 0.18 to 0.38 m in the vertical direction. The relative magnitude of these scales is consistent with the

stratified lenses and layers of sand and gravel observed in surface exposures of the aquifer at the test site. The stochastic theory of Gelhar and Axness (1983) was used with the correlation scales to estimate a value of 1.2 for the ratio of horizontal to vertical hydraulic conductivity in the aquifer.

Hess and others (1992) used the stochastic models of Gelhar and Axness (1983) to estimate the components of macrodispersion from the statistical description of the hydraulic-conductivity variability. The predicted values of 0.35 to 0.78 m for longitudinal dispersivity are similar in magnitude to the value of 0.96 m that was obtained from the spatial moments analysis of the bromide concentrations. This finding supports the hypothesis that the macroscale dispersion of contaminant plumes is the result of spatial variability of hydraulic conductivity in the aquifer.

CHAPTER 3

ANALYTICAL MODELS OF DENSITY-INDUCED DOWNWARD MOVEMENT

The vertical displacement of a tracer cloud because of density differences involves the movement of a fluid body with elevated solute concentrations within a flow field that is dominated by the ambient ground water. This problem has been examined analytically by several researchers. Although the analytical models address simplified systems, they provide insight into the process of density-induced sinking. In this chapter, the analytical models described by Hubbert (1953) and Yih (1963, 1965) are used to examine the factors that may affect downward movement of fluid bodies that are not diluted by mixing with the ambient fluid. A model suggested by Gelhar (written communication, 1983) is used to estimate the effect of dispersion on the rate of downward movement. The analytical models are used to evaluate the likelihood that density was a factor in causing the downward movement observed during the Cape Cod tracer test.

Hubbert (1953) Model

Hubbert (1953), in his classic paper on the entrapment of petroleum under hydrodynamic conditions, examined the migration of oil in a dispersed state in a normally water-saturated environment. He developed relationships between the potential field of the water and the oil to explain how oil, which is lighter than water, can migrate into geologic traps and accumulate into exploitable petroleum bodies. The relationships he developed can be used to examine the

migration of a tracer cloud, which would be denser than the water because of the increased concentration of dissolved substances in the tracer solution.

Description of Hubbert Analytical Model

Hubbert (1953) assumed that the two fluids occupy the same space, but they do not mix or dilute one another, although, for this analysis, the fluids were assumed to be miscible and capillary forces were ignored. Each fluid migrates in the porous medium in response to its own potential field. In an isotropic medium, the flow of each fluid is in the direction of the gradient of its potential field. Hubbert also assumed that the ambient fluid, in this case the water in the aquifer, dominates the flow, and presence of the tracer fluid does not affect the ambient flow field. In essence, the tracer fluid is assumed to be dispersed evenly within the ambient fluid. The hydraulic gradient of the tracer fluid can then be expressed in terms of the gradient of the ambient fluid.

The potential of ambient ground water, Φ_w, is given by the relationship:

$$\Phi_w = gz + \frac{p}{\rho_w}, \tag{3.1}$$

where

g = gravitational constant (L/T^2),

z = height above an arbitrary datum (L),

p = fluid pressure ($M/(L \cdot T^2)$), and

ρ_w = density of the fluid (M/L^3).

Similarly, the potential of the tracer solution is given by

$$\Phi_s = gz + \frac{p}{\rho_s}. \tag{3.2}.$$

Solving Equation (3.2) for p, substituting into Equation (3.1), and rearranging yields:

$$\Phi_s = \frac{\rho_w}{\rho_s}\Phi_w - \frac{(\rho_w - \rho_s)}{\rho_s} gz \,. \tag{3.3}$$

Therefore, a family of equipotentials for the tracer solution can be mapped by knowing the potential field of the ambient ground water and the densities of the two fluids. The negative gradient of the potential field gives the force vector acting on the respective fluid.

The relationship shown in Equation (3.3) can also be expressed in terms of the hydraulic head of each fluid. Given that $\Phi_w = gh_w$ and $\Phi_s = gh_s$, the following relationship holds:

$$h_s = \frac{\rho_w}{\rho_s} h_w - \frac{(\rho_w - \rho_s)}{\rho_s} z \,, \tag{3.4}$$

where h_s = hydraulic head of the tracer solution (L) and h_w = hydraulic head of the ambient ground water (L). This expression can be used to map the hydraulic head for both fluids in a given problem domain. This procedure is shown schematically in Figure 3-1 for a simplified

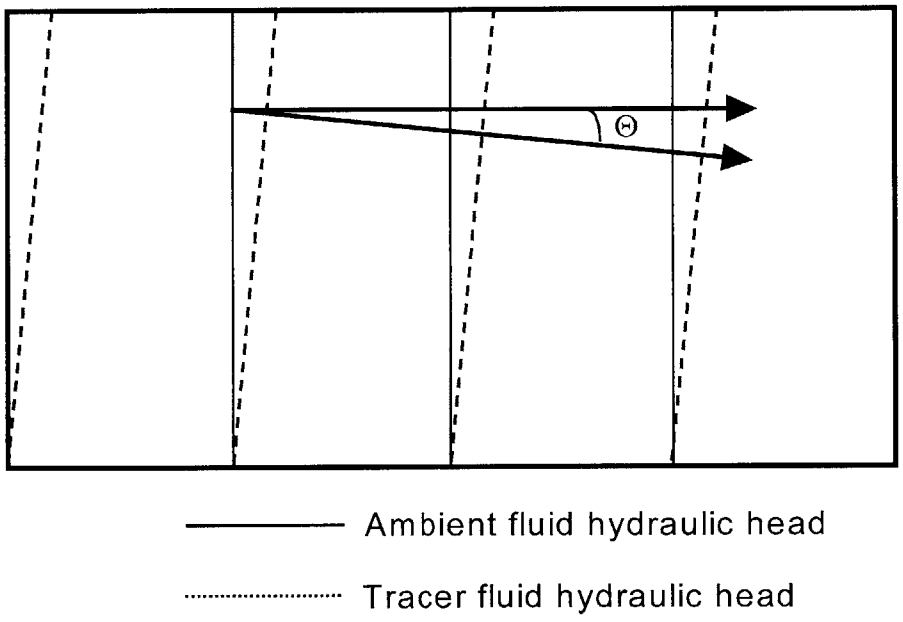

Figure 3-1. Hydraulic-head distribution for the ambient fluid and a denser tracer solution in the simple case where the ambient flow is horizontal.

example in which the ambient flow is horizontal and the lines of equal hydraulic head of the ambient fluid are vertical. Because $\rho_s > \rho_w$, the lines of equal hydraulic head for the tracer solution indicate a downward component of flow.

The components of the hydraulic-head gradient can be used to determine the direction below the horizontal of the negative head gradient for the tracer solution:

$$\Theta = \tan^{-1}\left[\frac{\partial h_s / \partial z}{\partial h_s / \partial x}\right]. \tag{3.5}$$

Taking the appropriate derivatives of Equation (3.4) and substituting into Equation (3.5) gives:

$$\Theta = \tan^{-1}\left[\frac{\frac{\rho_w}{\rho_s}\frac{\partial h_w}{\partial z} - \frac{(\rho_w - \rho_s)}{\rho_s}}{\frac{\rho_w}{\rho_s}\frac{\partial h_w}{\partial x}}\right]. \tag{3.6}$$

For an ambient flow field that is horizontal, which is a reasonable approximation to conditions at the Cape Cod site, $\partial h_w / \partial z = 0$. In this case, Equation (3.6) would simplify to:

$$\Theta = \tan^{-1}\left[\frac{\frac{\rho_s - \rho_w}{\rho_w}}{\partial h_w / \partial x}\right]. \tag{3.7}$$

Equation (3.7) shows that the angle of downward movement is zero when there is no density difference, and the angle is 90 degrees when there is no ambient flow. The angle of downward movement increases nonlinearly, but at a decreasing rate, as the density difference increases because the angle is a function of the tangent of the density difference.

Hubbert (1953) derived the same relationships by considering the energy force vectors. The force acting on a fluid acts perpendicularly to the potential gradient. The energy force

vectors acting on the ambient ground water and the tracer solution are given by:

$$\overline{\mathrm{E}}_w = \overline{\mathrm{g}} - \left(\frac{1}{\rho_w}\right)\overline{\nabla}\mathrm{p} \tag{3.8}$$

$$\overline{\mathrm{E}}_s = \overline{\mathrm{g}} - \left(\frac{1}{\rho_s}\right)\overline{\nabla}\mathrm{p}, \tag{3.9}$$

where $\overline{\mathrm{g}}$ is the gravitational vector, the subscripts w and s refer to the ambient ground water and the tracer solution, and vectors are denoted by the overbar. Because the pressure must be the same for both fluids at a given point, and capillary forces are assumed to be zero because the fluids are miscible, Equation (3.8) can be solved for $\overline{\nabla}\mathrm{p}$ and substituted into Equation (3.9), yielding:

$$\overline{\mathrm{E}}_s = \overline{\mathrm{g}} + \frac{\rho_w}{\rho_s}\left(\overline{\mathrm{E}}_w - \overline{\mathrm{g}}\right). \tag{3.10}$$

Figure 3-2 illustrates this vector relationship for the simple case of horizontal ambient ground-water flow. The tracer cloud is carried along with the ambient flow. In the case where the tracer solution is denser than the ambient ground water ($\rho_w/\rho_s < 1$), the density difference adds a downward component to the flow of the tracer solution.

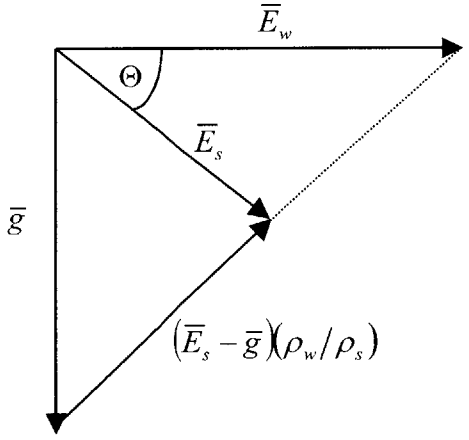

Figure 3-2. Vector diagram with energy force vectors for the ambient fluid and the denser tracer solution.

Direction of Movement of Tracer Cloud

In an isotropic porous medium, the hydraulic conductivity is independent of direction, and the direction of flow is coincident with the direction of the negative hydraulic gradient. Therefore, the direction of movement of the tracer cloud will coincide with the direction indicated by Equations (3.6) and (3.7).

In an anisotropic medium, however, the hydraulic conductivity varies with direction, and flow is biased toward the direction of maximum conductivity. The angle of flow can be calculated from the angle of the hydraulic gradient and the ratio of the horizontal and vertical hydraulic conductivity. Assume that the principal directions of hydraulic conductivity are aligned with the principal coordinate axes, as shown in Figure 3-3. The hydraulic-gradient vector is given by:

$$\bar{J} = -\frac{\partial h}{\partial x} - \frac{\partial h}{\partial z}. \tag{3.11}$$

The tangent of the angle Θ is given by:

$$\tan\Theta = \frac{\partial h / \partial z}{\partial h / \partial x}. \tag{3.12}$$

The seepage-velocity vector, $\bar{q}$, is given by Darcy's Law:

$$\bar{q} = -K_{xx}\frac{\partial h}{\partial x} - K_{zz}\frac{\partial h}{\partial z}. \tag{3.13}$$

The tangent of the angle β is given by:

$$\tan\beta = \frac{-K_{zz}\dfrac{\partial h}{\partial z}}{-K_{xx}\dfrac{\partial h}{\partial x}}. \tag{3.14}$$

Taking the ratio of Equations (3.12) and (3.14) and simplifying yields:

$$\tan\beta = \frac{K_{zz}}{K_{xx}}\tan\Theta . \qquad (3.15)$$

Therefore, Equation (3.15) can be used to correct the angle of downward movement caused by the density difference (Equation 3.7) for the additional effect of anisotropic hydraulic conductivity. Because most aquifers are more permeable in the horizontal direction than in the vertical direction, the ratio K_{zz}/K_{xx} is less than one, and anisotropy decreases the amount of downward movement for a given density difference.

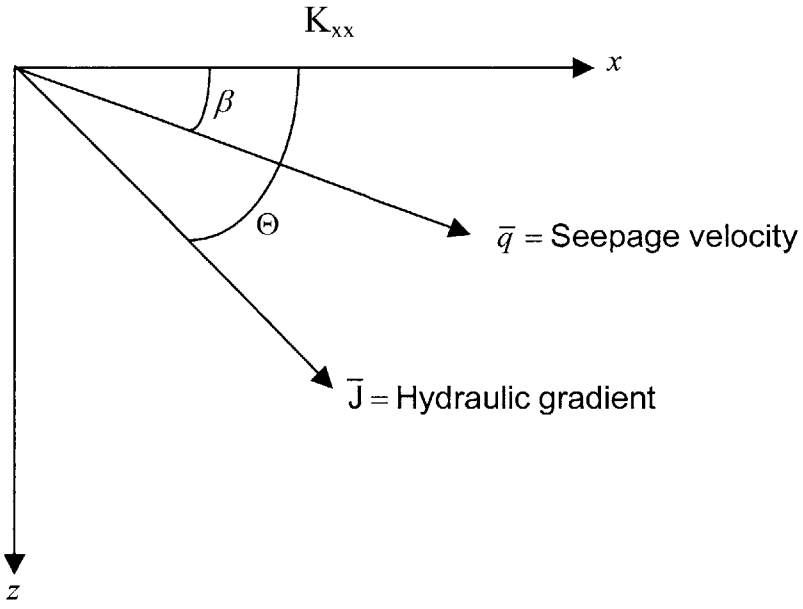

Figure 3-3. Relationship of the direction of the negative hydraulic gradient to the direction of flow for an anisotropic porous medium.

Application of Hubbert Model to Cape Cod Tracer Test

The Hubbert model was used to predict the initial angle of downward movement for a tracer solution under hydrologic conditions that are similar to those during the Cape Cod tracer

Table 3-1. Predicted angles of downward movement of a tracer solution for various values of tracer-solution density using the Hubbert (1953) model. Angles predicted using Equations (3.7) and (3.15). [Conditions for all predictions: Ambient ground-water vertical gradient, $\partial h_w/\partial z = 0$; ambient ground-water horizontal hydraulic gradient, $\partial h_w/\partial x$ = -0.0015 m/m; ambient ground-water density, ρ_w = 999.4091 Kg/m^3. ρ_s, tracer-solution density; $[C_o]/[C_o^C]$, ratio of total initial solute concentration to total initial solute concentration for Cape Cod tracer test.]

ρ_s (Kg/m^3)	$\frac{[C_o]}{[C_o^C]}$	$\frac{\rho_s - \rho_w}{\rho_w}$ (%)	**Angle of Downward Movement, Θ**				
			Ratio of horizontal to vertical hydraulic conductivity (K_{xx}/K_{zz})				
			1.0	**1.2**	**2**	**5**	**10**
1003.3491	4.0	0.39	69.2	65.5	52.7	27.7	14.7
1001.2731	2.0	.19	51.2	46.0	31.9	14.0	7.1
1000.8671	1.5	.15	44.2	39.0	25.9	11.0	5.6
1000.4691	1.1	.11	35.3	30.5	19.5	8.0	4.0
1000.3701	1.0	.096	32.7	28.1	17.8	7.3	3.7
1000.3101	.94	.090	31.0	26.6	16.7	6.9	3.4
1000.2711	.90	.086	29.9	25.6	16.0	6.6	3.3
1000.0421	.67	.063	22.9	19.4	11.9	4.8	2.4
999.8741	.50	.046	17.2	14.5	8.8	3.5	1.8
999.6251	.25	.022	8.2	6.8	4.1	1.7	0.8

test. The ambient flow was assumed to be horizontal, so $\partial h_w/\partial z = 0$. The horizontal hydraulic gradient was $\partial h_w/\partial x$ = -0.0015 m/m, and the density of the ambient ground water was 999.4091 Kg/m^3.

Table 3-1 shows the predicted angles of downward movement for several values of tracer-solution density and anisotropy of hydraulic conductivity. The estimated initial tracer-solution density and the estimated anisotropy for the Cape Cod test are 1000.3701 Kg/m^3 and

K_{xx}/K_{zz} = 1.2, respectively (see next chapter). The predicted angle of initial downward movement for these values is about 33 degrees. This angle is much greater than the angle of about 3 degrees observed during the first 83 days of the field experiment (LeBlanc and others, 1991).

Figure 3-4 shows selected results from Table 3-1 as a family of curves relating the predicted angle of downward movement to the density difference and anisotropy. The lines represent the various density differences; adjacent lines have density differences that differ by about a factor of 2. The nonlinear response of downward movement to both density difference and anisotropy of hydraulic conductivity is evident. The effect of anisotropy is particularly significant as the system begins to deviate from an isotropic medium. The angle of downward movement is reduced by about 75 percent when the anisotropy is increased from a ratio of 1:1 to a ratio of 5:1.

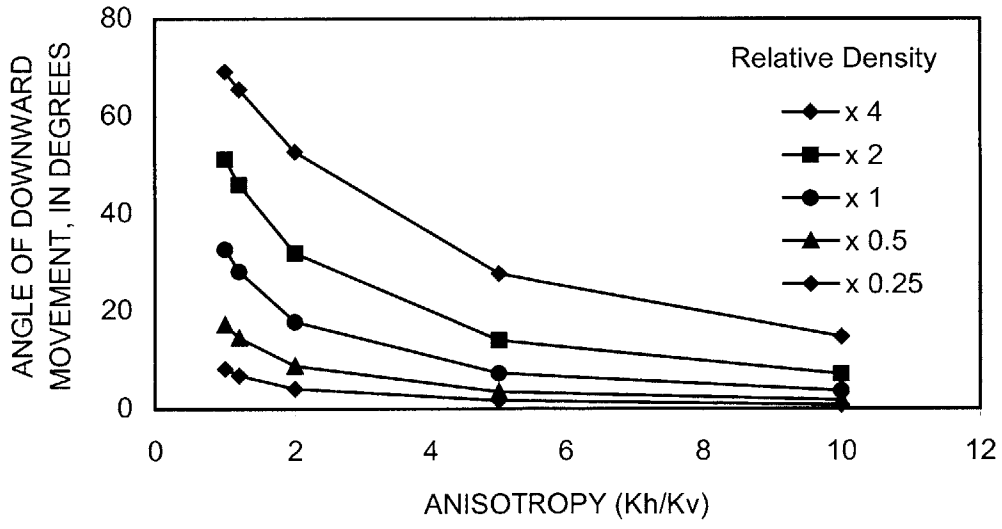

Figure 3-4. Predicted angle of downward movement of tracer solution from the Hubbert (1953) model as a function of density difference and anisotropy of hydraulic conductivity.

Yih (1963) Models

The Hubbert model addresses the movement of a diffuse tracer solution within a flow field dominated by the ambient ground water. A tracer cloud, however, is a distinct fluid body with a particular initial shape and a different density than that of the ambient fluid. Yih (1963) examined the movement of regularly shaped three-dimensional fluid bodies in a uniform, ambient flow field. His work was done to address the problem of water removal from felt, a problem encountered in the papermaking industry. His results provide insight into the factors that affect the rate of downward movement of tracer clouds in ground water because of density differences.

Description of Yih Analytical Models

Yih (1963) examined the seepage-velocity components of a three-dimensional body having various shapes in an ambient ground-water flow field. He developed equations for the velocity of the fluid body with respect to the ambient fluid flow and the gravitational vector for the condition in which the density and the viscosity of the two fluids are different. The fluid bodies he considered include a sphere, an ellipsoid, an infinitely long circular cylinder, and an infinitely long elliptical cylinder.

The Yih analytical models assume that the aquifer is homogeneous, isotropic, and infinite in extent. Therefore, fluid flow is described by the Laplace equation:

$$\left(\frac{\partial^2}{\partial x^2}+\frac{\partial^2}{\partial y^2}+\frac{\partial^2}{\partial z^2}\right)\Phi = 0\,. \qquad (3.16)$$

The ambient flow is steady, and the flow is uniform and unidirectional, except near the fluid body. The solutions are obtained by solving the Laplace equation in the frame of reference of the

moving fluid body, with appropriate pressure and continuity conditions at the boundary between the two fluids. In particular, the pressure is continuous, so pressure at the boundary and the velocity component normal to the boundary must be the same for both fluids.

A critical assumption of the Yih models is that the fluid body moves as a solid body that does not change shape or disperse as it moves within the ambient flow field. Therefore, the volume of the body does not change, and the density and viscosity of the two fluids remain constant. Yih (1963, p. 1407) notes that the stable fluid motion corresponding to his solutions may not apply when the fluid body becomes too large or has particular shapes, such as a large flat mass that is moving broadside. The effect of dispersion is examined at the end of this chapter.

Yih (1963) obtained his solutions by using a coordinate system that is fixed relative to the geometry of the fluid body, which can have any orientation in space. Therefore, the general solutions presented in Yih (1963) include factors for the direction cosines of the ambient fluid flow and the gravitational force relative to the fluid body's coordinate axes. The direction cosines are designated α, β, and γ for the x, y, and z direction cosines of the gravitational force, and α', β', and γ' for the x, y, and z direction cosines of the ambient fluid flow.

In this report, the equations are simplified by aligning the body's coordinate axes so that Yih's arbitrary coordinates are aligned with the standard (x, y, z) coordinate system, in which the vertical direction is coincident with the gravitational vector. The result is that the direction cosines have values of either 0 or 1. Furthermore, the notation used by Yih is modified so that the x-direction in the equations presented below refers to the horizontal direction of ambient flow and the z-direction is aligned with the gravitational vector.

Three-Dimensional Sphere

The three-dimensional sphere is a reasonable representation of the initial tracer cloud during the Cape Cod tracer test. Yih (1963, Equation 27) presented the general equations for the seepage-velocity of the sphere relative to its arbitrary coordinate system. If the ambient flow is assumed to align with the x-coordinate and the gravitational force is aligned with the z-coordinate (Figure 3-5), Yih's solution is simplified to the following equations:

$$q_x^s = \frac{3\mu_w}{2\mu_s + \mu_w} q_x^w \tag{3.17}$$

$$q_y^s = q_y^w = 0$$

$$q_z^s = \frac{2kg(\rho_w - \rho_s)}{2\mu_s + \mu_w},$$

where

q_x, q_y, and q_z = seepage velocity in the x, y, and z directions (L/T)

μ = dynamic viscosity (M/(L·T), and

ρ = fluid density (M/L^3),

and the subscripts s and w refer to the solute cloud and the ambient ground-water, respectively.

If the viscosities of the two fluids are assumed to be equal (see later discussion), Equation (3.17) can be simplified to:

$$q_x^s = q_x^w \tag{3.18}$$

$$q_y^s = q_y^w = 0$$

$$q_z^s = \frac{2kg(\rho_w - \rho_s)}{3\mu}.$$

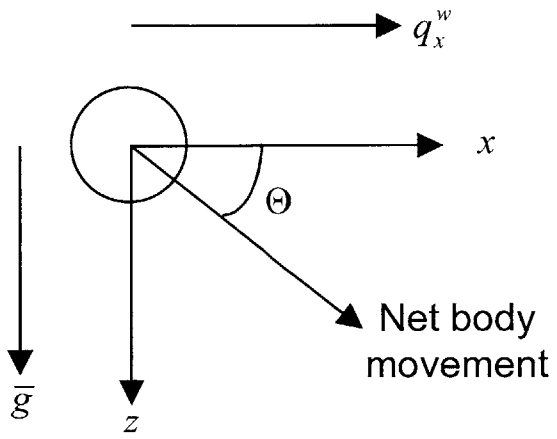

Figure 3-5. Spherical fluid body, coordinate system, and orientations of the ambient flow direction and the gravitational force.

The direction of movement of the tracer fluid body can be obtained from the horizontal and vertical components of the seepage velocity:

$$\Theta = \tan^{-1}\left[\frac{q_z^s}{q_x^w}\right] = \tan^{-1}\left[\frac{2kg(\rho_w - \rho_s)}{3\mu} \Big/ q_x^w\right]. \qquad (3.18)$$

Because the viscosities are assumed to be equal, the fluid body is carried along horizontally with the ambient flow. The additional downward component of seepage velocity causes the net motion of the fluid body to be at an oblique angle to the horizontal.

Three-Dimensional Infinitely Long Circular Cylinder

Yih (1963) also considered the movement of an infinitely long circular cylinder in a uniform, ambient flow field. The axis of the cylinder (Figure 3-6) can be oriented arbitrarily with respect to the gravitational vector and the direction of ambient fluid flow. Yih (1963,

Equations 6, 16, and 17) presented the general equations for the seepage velocity of the cylindrical fluid body with respect to its coordinate system. Yih's equations can be simplified if the axis of the cylinder is assumed to be oriented either horizontally or vertically with respect to the gravitational force (Figure 3-6). The additional assumption is made that the viscosities of the two fluids are equal.

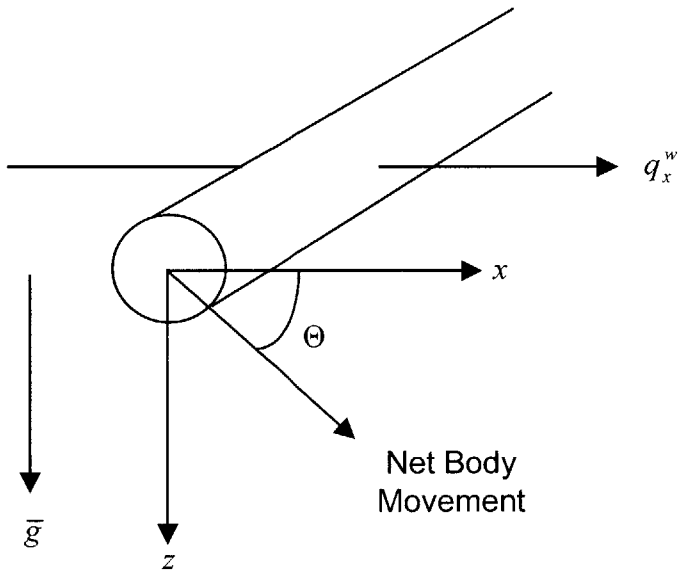

Figure 3-6. Cylindrical fluid body with circular cross section, coordinate system, and orientations of the ambient flow direction and the gravitational force.

If the cylinder is oriented horizontally and its long axis is aligned with the y-direction (Figure 3-6), transverse to the direction of ambient fluid flow, Yih's solutions can be simplified to the following equations:

$$q_x^s = q_x^w \tag{3.19}$$
$$q_y^s = q_y^w = 0$$

$$q_z^s = \frac{kg(\rho_w - \rho_s)}{2\mu}.$$

If the cylinder is oriented vertically, its long axis is coincident with the direction of gravity (z-direction). The ambient flow remains in the x-direction. Yih's solution can be simplified for this situation to the following equations:

$$q_x^s = q_x^w \tag{3.20}$$
$$q_y^s = q_y^w = 0$$
$$q_z^s = \frac{kg(\rho_w - \rho_s)}{\mu}.$$

Three-Dimensional Infinitely Long Elliptical Cylinder

The circular cylinder is a special case of a cylinder with a cross section in the shape of an ellipse. Yih (1963, Equations 6, 14, and 15) presents the general solution for a cylinder with an elliptical cross section in which the axis of the cylinder and the major and minor axes of the elliptical cross section are oriented arbitrarily with respect to the direction of ambient flow and the gravitational vector. The shape of the elliptical cross section is given by:

$$\frac{y^2}{a^2} + \frac{z^2}{b^2} = 1, \tag{3.21}$$

where the a and b are the major and minor axes of the ellipse, respectively, and $a > b$. A circular cross section is the special case in which $a = b$. Yih's solutions can be simplified if the infinitely long axis of the cylinder is assumed to be oriented horizontally with respect to the gravitational force and transverse to the ambient horizontal flow (Figure 3-7). Again, the viscosities of the two fluids are assumed to be equal.

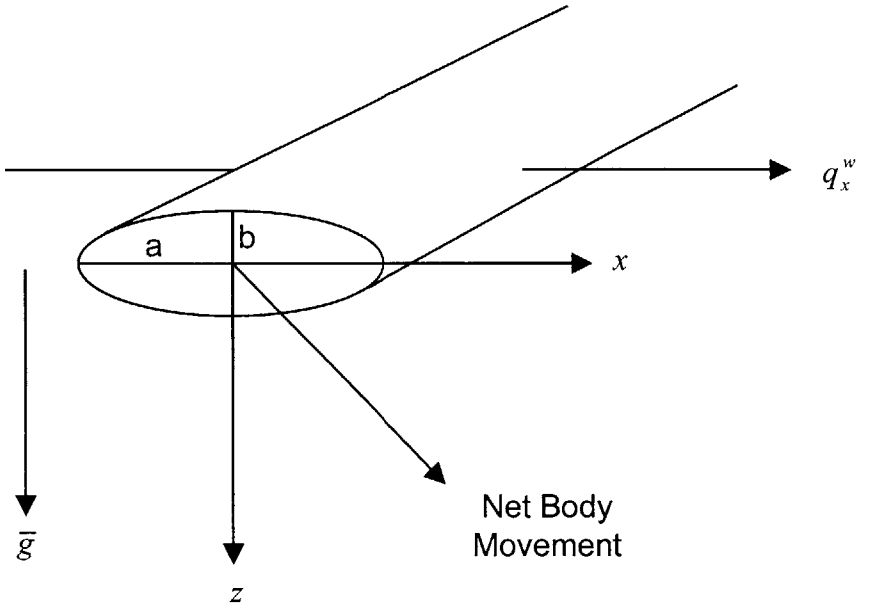

Figure 3-7. Cylindrical fluid body with elliptical cross section, coordinate system, and orientations of the ambient flow direction and the gravitational force.

If the major axis of the elliptical cross section is horizontal and aligned with the direction of ambient flow, Yih's solution becomes:

$$q_x^s = q_x^w \tag{3.22}$$
$$q_y^s = q_y^w = 0$$
$$q_z^s = \left[\frac{b}{a+b}\right]\frac{kg(\rho_w - \rho_s)}{\mu}.$$

If the major axis of the elliptical cross section is vertical and is coincident with the gravitational vector, Yih's solution becomes:

$$q_x^s = q_x^w \tag{3.23}$$
$$q_y^s = q_y^w = 0$$

$$q_z^s = \left[\frac{a}{a+b}\right]\frac{kg(\rho_w - \rho_s)}{\mu}.$$

Factors Affecting Rate of Downward Movement

The analytical models can be used to examine the relative influence of several factors on the predicted amount of downward movement of a tracer cloud. It is interesting to note that the solutions obtained by Yih (1963) are independent of the size of the fluid body, which is not the case in numerical simulations, in which the tracer cloud changes shape and size as it moves through the aquifer (see next chapter). The amount of downward movement is dependent, however, on the dimensionality of the model and the shape and orientation of the fluid body.

Dimensionality

In Equation (3.19), the axis of a horizontal, infinitely long circular cylinder is oriented perpendicular to the direction of ambient flow. The cylinder moves laterally under the influence of the ambient fluid flow and downward because of the density difference, but no flow takes place in the direction of the axis of the cylinder. The problem is one essentially of a two-dimensional circular body sinking in two-dimensional flow field. In Equation (3.18), on the other hand, the fluid body is a sphere in a three-dimensional flow field. Flow in both fluids can take place in all directions.

Because the solutions presented by Yih (1963) are independent of the size of the fluid body, Equations (3.18) and (3.19) can be used to examine the difference between the two-dimensional and three-dimensional analysis of a circular fluid body. The horizontal component of seepage velocity is the same for both problems. Assume that the ambient ground-water flow is quiescent. Then the movement of the fluid body in both cases is vertically downward. The

ratio of the vertical seepage velocities is:

$$\frac{q_x^s\ (sphere)}{q_x^s\ (cylinder)} = \frac{\left[\dfrac{2kg(\rho_w - \rho_s)}{3\mu}\right]}{\left[\dfrac{kg(\rho_w - \rho_s)}{2\mu}\right]} = \frac{4}{3} \tag{3.24}$$

Therefore, the downward component of seepage velocity for the three-dimensional model is 33 percent larger than the downward component for the two-dimensional model. In the three-dimensional representation, the ambient fluid can move up and around the sinking fluid body in all directions. In the two-dimensional representation, however, the ambient fluid is restricted to movement in the two-dimensional plane and impedes the rate of downward movement relative to the three-dimensional case.

Shape and Orientation of the Fluid Body

The analysis of a horizontal cylinder with its long axis oriented perpendicular to the ambient flow provides additional insight into the effect of the shape of the fluid body on downward movement. Equation (3.19) describes the movement of a cylinder with a circular cross section, while Equations (3.22) and (3.23) describe the movement of a cylinder with an elliptical cross section. As noted above, the seepage velocities are independent of the size of the bodies, and the predicted rates of downward movement can be compared directly. Assume that there is no ambient flow. Then all three bodies move vertically downward at different rates given by the expressions in Table 3-2. Furthermore, the relative rates of downward movement can be obtained by dividing the expressions through by $kg(\rho_w - \rho_s)/\mu$.

Table 3-2. Downward seepage velocity and relative rate of downward movement for a horizontal cylinder with cylindrical and elliptical cross sections.

Shape of cross section	**Orientation of major axis of the ellipse**	**Downward seepage velocity**	**Relative rate of downward movement**
Circular	Not applicable	$q_z^s = \left[\frac{1}{2}\right]\frac{kg(\rho_w - \rho_s)}{\mu}$	$\frac{1}{2}$
Elliptical	Horizontal	$q_z^s = \left[\frac{b}{a+b}\right]\frac{kg(\rho_w - \rho_s)}{\mu}$	$\frac{b}{a+b}$
Elliptical	Vertical	$q_z^s = \left[\frac{a}{a+b}\right]\frac{kg(\rho_w - \rho_s)}{\mu}$	$\frac{a}{a+b}$

Table 3-2 shows that the rate of downward movement is greatest for the elliptical body with its long axis oriented in the vertical direction and smallest for the elliptical body with its long axis oriented in the horizontal direction. The body that presents the smallest relative horizontal cross section to downward flow sinks at the greatest rate because the ambient ground water can move up and around the sinking body more easily. As the body becomes increasingly elliptical in shape $(a >> b)$, the orientation of the long axis becomes increasingly important.

Yih (1963) presented solutions for cases in which the axes of the ellipse for a cylindrical body and a 3-dimensional ellipsoid (similar in shape to a football) are oriented obliquely to the horizontal. These solutions indicate that an obliquely oriented ellipsoidal body in quiescent ambient flow will move not only in the vertical direction, but also will drift downward at an oblique angle in such a way as to favor the axes of the body in the order of their length. In a system with ambient flow, the seepage-velocity components that arise from density differences can result in movement of the body laterally at a greater or slower rate than the ambient fluid, depending on the orientation of the body.

The horizontally and vertically oriented circular cylinders provide additional evidence of the effect of orientation on the rate of downward movement. The relative vertical seepage velocities from Equations (3.19) and (3.20) are:

$$\frac{q_z^s\ (horizontal\ cylinder)}{q_z^s\ (vertical\ cylinder)} = \frac{\left[\dfrac{kg(\rho_w - \rho_s)}{2\mu}\right]}{\left[\dfrac{kg(\rho_w - \rho_s)}{\mu}\right]} = \frac{1}{2}. \qquad (3.25)$$

A vertically oriented circular cylinder moves downward at twice the rate of a horizontally oriented cylinder. This relationship is independent of the diameter of the cylinder. Because the cylinder is infinitely long, the ambient fluid is not displaced by the downward-moving, vertically oriented cylinder; however, the ambient fluid is displaced by the downward-moving, horizontally oriented cylinder.

Viscosity

Because the focus of this analysis is density-induced downward movement, the viscosity of the two fluids was assumed to be equal to simplify the general solutions obtained by Yih (1963). The concentration of solutes has a much larger effect on the density of the fluids than on the viscosity. However, the viscosity appears in the Yih (1963) solutions and has an effect on seepage velocities. The case of the three-dimensional sphere is used to examine the possible additional effects of viscosity on downward movement.

The most likely factor that would affect viscosity during a tracer experiment is temperature. During the Cape Cod tracer experiment, which was started in July, the temperature of the tracer solution was 16°C, while the temperature of the ambient ground water was about 13°C. The viscosity of water at 13°C and 16°C are 1.2069 x 10^{-3} Kg/(m·s) and 1.1168 x 10^{-3}

Kg/(m·s), respectively. Therefore, the tracer solution was about 7 percent less viscous than the ambient ground water as it was injected into the ground.

The effect of viscosity can be examined using the solution for movement of a sphere (Equation 3.17). Let $\mu_s = a\mu_w$. Then the components of the seepage velocity are given by:

$$q_x^s = \frac{3\mu_w}{2a\mu_w + \mu_w} q_x^w \tag{3.26}$$

$$q_z^s = \frac{2kg(\rho_w - \rho_s)}{2a\mu_w + \mu_w},$$

which can be simplified to:

$$q_x^s = \left[\frac{3}{2a+1}\right] q_x^w \tag{3.27}$$

$$q_z^s = \left[\frac{2}{2a+1}\right] \frac{kg(\rho_w - \rho_s)}{\mu_w}.$$

The scaling factors for several values of a are shown in Table 3-3. A 7 percent decrease in viscosity ($a = 0.93$) results in about a 5 percent increase for both the horizontal and vertical seepage velocities. Therefore, the tracer body moves slightly faster laterally than the ambient fluid, and its rate of downward movement also increases. The net effect is that the angle of downward movement below the horizontal does not change significantly.

With a small difference in viscosity, the effect on the angle of downward movement is small for the case of a sphere. The speed of the solute body changes appreciably, however. The viscosity change inferred for the Cape Cod tracer test was caused by the warming of the tracer solution when it was stored above ground prior to injection. Once in the ground, the temperature difference probably diminished rapidly and the viscosities of the two fluids became essentially equal.

Table 3-3. Change in coefficients for the horizontal and vertical seepage velocity shown in Equation (3.27) for selected ratios of the viscosity of the tracer fluid to the viscosity of the ambient ground water [q_x^s, horizontal seepage velocity of tracer fluid; q_z^s, vertical seepage velocity of tracer solution, μ_w, viscosity of ambient ground water; μ_s, viscosity of tracer solution].

Velocity component	**Coefficient**	a $(\mu_s = a\mu_w)$				
		0.90	**0.93**	**1.00**	**1.07**	**1.10**
q_x^s	$\frac{3}{2a+1}$	1.07	1.05	1.00	0.96	0.94
q_z^s	$\frac{2}{2a+1}$	0.71	0.70	0.67	0.64	0.62

Application of Yih Model to the Cape Cod Tracer Test

The Yih (1963) models were used to predict the initial angle of the downward trajectory of a tracer cloud for hydrologic conditions that are similar those during the Cape Cod tracer test. The angles of downward movement were predicted for a sphere, a horizontally oriented circular cylinder, and a horizontally oriented elliptical cylinder for several values of density of the tracer solution. The major axis of the elliptical cross section (a) was assumed to be horizontally oriented. As noted above, the horizontally oriented cylinders behave as two-dimensional bodies in a vertical plane that is aligned with the direction of ambient ground-water flow.

The velocity components were calculated using Equations (3.18), (3.19), and (3.22). The downward angles of movement were obtained from the following equations:

Sphere $$\Theta = \tan^{-1}\left[\frac{2kg(\rho_w - \rho_s)}{3\mu} \Big/ q_x^w\right] \qquad (3.28)$$

Horizontal circular cylinder $$\Theta = \tan^{-1}\left[\frac{kg(\rho_w - \rho_s)}{2\mu} \Big/ q_x^w\right]$$

Horizontal elliptical cylinder $\Theta = \tan^{-1}\left[\left(\frac{b}{a+b}\right)\frac{kg(\rho_w - \rho_s)}{\mu}\Big/ q_x^w\right]$.

The values of the parameters used in the calculations are shown in Table 3-4. The source of these values is described in the next chapter. The calculations assume that the horizontal ambient ground-water seepage velocity was $q_x^w = 0.1638$ m/d. Note that the Yih models refer to seepage velocity, not average linear velocity, $\bar{v}_x^w$. The two velocities are related by the equation $\bar{v}_x^w = q_x^w / n$, where n is the effective porosity. Calculations were done for two elliptical shapes with different length proportions of the major and minor axes of the ellipse.

Table 3-4. Parameters used to calculate the downward angles of movement for various tracer clouds using the analytical models of Yih (1963). Source of values given in Table 4-2.

Parameter	Symbol	Value	Units
Permeability	k	1.514×10^{-10}	m^2
Gravitational acceleration	g	9.8066	m/s^2
Viscosity	μ	1.2069×10^{-3}	Kg/(m·s)
Density of ambient ground water	ρ_w	999.4091	Kg/m^3
Ambient horizontal seepage velocity	q_x^w	1.8958×10^{-6}	m/s

Table 3-5 shows the predicted angles of downward movement for several values of tracer-solution density. The estimated density of the solution injected during the Cape Cod test was 1000.3701 Kg/m^3. The predicted angle of downward movement for this tracer-solution density ranges from about 23 degrees for a spherical tracer cloud to about 7 degrees for a two-dimensional ellipse with major and minor axes that are 2.4 m and 0.6 m long, respectively. LeBlanc and others (1991) reported an angle of downward movement of about 3 degrees during the first 83 days of the tracer experiment.

Table 3-5. Predicted angles of downward movement of a tracer cloud for various values of tracer-solution density using the Yih (1963) models. Angles predicted using Equation (3.28).
[Parameters common to all predictions shown in Table 3-4. ρ_w, ambient ground-water density; ρ_s, tracer-solution density; $[C_o]/[C_o^C]$, ratio of total initial solute concentration to total initial solute concentration for Cape Cod tracer test; a, major axis of elliptical cross section; b, minor axis of elliptical cross section. Major axis of ellipse horizontally oriented.]

ρ_s (Kg/m^3)	$\frac{[C_o]}{[C_o^C]}$	$\frac{\rho_s - \rho_w}{\rho_w}$ (%)	**Angle of Downward Movement**			
			Round body		Elliptical body	
			3-D	2-D	a = 1.7 b = 0.9	a = 2.4 b = 0.6
1003.3491	4.0	0.39	59.6	52.0	41.5	27.1
1001.2731	2.0	.19	38.9	31.2	22.7	13.6
1000.8671	1.5	.15	32.2	25.3	18.1	10.7
1000.4691	1.1	.11	24.6	19.0	13.4	7.8
1000.3701	1.0	.096	22.6	17.3	12.2	7.1
1000.3101	.94	.090	21.3	16.3	11.4	6.7
1000.2711	.90	.086	20.5	15.6	11.0	6.4
1000.0421	.67	.063	15.3	11.6	8.1	4.7
999.8741	.50	.046	11.4	8.6	6.0	3.5
999.6251	.25	.022	5.3	4.0	2.8	1.6

The results in Table 3-5 indicate that the angle of downward movement increases with the density difference. A tracer cloud with four times the initial total solute concentration of the Cape Cod test was predicted to move downward at about three times the angle of the actual initial cloud. The effect of the dimensionality of the analysis is also clearly evident. A two-dimensional analysis predicts a smaller angle of downward movement than a three-dimensional analysis. The most significant effect, however, is the shape and orientation of the initial cloud. The initial Cape Cod tracer cloud is estimated to have been about 3.4 m long and 1.8 m high (see discussion in Chapter 5). If this body is represented by an ellipse having major and minor axes

with these dimensions (a = 1.7 m and b = 0.9 m), and the initial density is the value estimated for the Cape Cod test (1000.3701 Kg/m^3), the angle of downward movement is predicted to be 12.2 degrees. The equivalent angle for a circular body is 17.3 degrees, almost 40 percent larger. It is interesting to note that the same elliptical body, if oriented so that the major axis of the ellipse was pointing vertically downward, would be predicted by Equation (3.23) to move downward at an angle of 23.6 degrees.

Dispersion

The analytical models of Hubbert (1953) and Yih (1963) do not include the effect of source size on the rate of downward movement. In the Hubbert model, the tracer fluid is dispersed as a continuum within the ambient flow field. In the Yih models, the tracer fluid body moves as a solid body that does not change shape or mix with the surrounding ambient fluid. However, the observations from the Cape Cod tracer test show that the tracer cloud was gradually diluted by dispersion as it moved through the aquifer. The maximum observed bromide concentration decreased from 640 mg/L in the injected solution to 65.2 mg/L at 237 days after injection (Table 2-2). The decrease in maximum concentration was accompanied by spreading of the tracer cloud, so that by 237 days the cloud was about 75 m long (LeBlanc and others, 1991, Figure 11).

The Hubbert and Yih models cannot address the effect of dispersion directly. In this section, two methods are used to estimate the effects of dispersion on downward movement caused by density differences. The Yih models for a three-dimensional sphere, a two-dimensional circular body, and a two-dimensional elliptical body are applied in a stepwise manner with a decreasing density difference with time. The density difference is estimated from

the observed change in maximum bromide concentration during the Cape Cod test. An analytical approach suggested by Lynn Gelhar (written communication, 1983) for incorporating dispersion into the Yih model is used to examine the effects of dispersion on downward movement of a circular tracer cloud.

Yih (1963) Models With Estimated Density Decrease

The density of the tracer solution and the ambient ground water was not measured during the Cape Cod experiment. The density difference was too small (less than 0.1 percent) to be measured with the methods that were available to the research team. The maximum observed bromide concentration during each sampling round (LeBlanc and others, 1991, Table 3) was used as a surrogate for the density change. Table 3-6 shows the maximum observed bromide concentration and the relative maximum bromide concentration for the nine sampling rounds that took place in the first 237 days of the field experiment. Each value was assumed to represent the maximum concentration for the time interval centered on the corresponding sampling date. The relative maximum bromide concentrations were then used to estimate tracer-cloud density for the time intervals by using the following relationship:

$$\rho_s^t = \rho_w + \left(\rho_s^o - \rho_w\right)\frac{C_{\max}^t}{C^o}, \tag{3.29}$$

where

ρ_w = density of the ambient ground water,

ρ_s^o = density of the initial tracer solution,

ρ_s^t = density of the tracer cloud at time t,

C^o = bromide concentration of the initial tracer solution, and

$C_{\max}^t$ = maximum bromide concentration of the tracer cloud at time t.

Table 3-6 shows the resulting estimated tracer-cloud densities for the time intervals associated with each sampling round. The maximum concentration decreased rapidly during the early part of the tracer test, and a corresponding rapid decrease in density of the tracer cloud is inferred from Equation (3.29). The Yih solutions are independent of cloud size and assume a constant cloud shape, so only the density was assumed to change with time.

Table 3-6. Observed maximum bromide concentration and estimated tracer-cloud density for the first 237 days of the Cape Cod tracer test.

Sampling date	**Start of time interval (days)**	**End of time interval (days)**	**Observed maximum bromide concentration (mg/L)**	**Relative maximum bromide concentration**	**Estimated tracer-cloud density (Kg/m^3)**
0	0	6.5	640	1.00	1000.3701
13	6.5	23	576	0.90	1000.2740
33	23	44	429	0.67	1000.0530
55	44	69	311	0.49	999.8800
83	69	97	124	0.28[1]	999.6782
111	97	125	132	0.21	999.6109
139	125	156	76.6	0.12	999.5244
174	156	188	76.6	0.12	999.5244
203	188	220	61.5	0.10	999.5052
237	220	237	65.2	0.10	999.5052

[1]Relative concentration was increased from 0.19 to 0.28 to insure a monotonically decreasing density.

The stepwise approximation of the density decrease with time was used in the Yih models to simulate the trajectory of the tracer cloud for several cloud geometries. The downward movement of a three-dimensional sphere was calculated using Equation (3.17). The trajectory of

a two-dimensional circular body was calculated using Equation (3.19). The trajectory of a two-dimensional elliptical body was calculated using Equation (3.22). The elliptical body was oriented so that its major axis was horizontally oriented and its longest dimension was broadside to vertical movement caused by density differences.

The same procedure was followed for each of the three body geometries. The starting position of the tracer body was assumed to be at coordinates (0,0). For each successive time increment, the appropriate density for the tracer cloud (ρ_S) was used to calculate the horizontal and vertical seepage velocities (q_x^S and q_z^S), which were then adjusted for the anisotropy of the permeability field using Equation (3.15). Next, the seepage velocities were divided by the effective porosity (n = 0.39) to obtain the ground-water velocities for the time interval ($\bar{v}_x^S$ and $\bar{v}_z^S$). The ground-water velocities were then multiplied by the length of the time interval (Δt) to obtain the horizontal and vertical distances (Δx and Δz) that were traveled in the time increment. The distances were accumulated from time interval to time interval so that the position of the tracer body (x, y) was determined through time relative to the starting point.

The values of the various parameters that were used in the calculations are shown in Table 3-4. The major axis of the elliptical tracer body was 3.4 m long (a = 1.7 m) in the x-direction, while the minor axis was 1.8 m long (b = 0.9 m) in the z-direction. The ratio of the two axes was kept constant with time. The anisotropy of the permeability was set to the value reported by Hess and others (1992) for the Cape Cod tracer test site ($k_{zz}/k_{yy} = 0.83$). The anisotropy was assumed to affect the vertical permeability ($k_{zz} = 0.83k_{xx}$, where k_{xx} is given in Table 3-4), so the effect of anisotropy was to decrease the vertical velocity by a factor of 0.83.

The results of these calculations are shown in Table 3-9, which includes the incremental and cumulative displacements of the three clouds and the angle of downward movement during

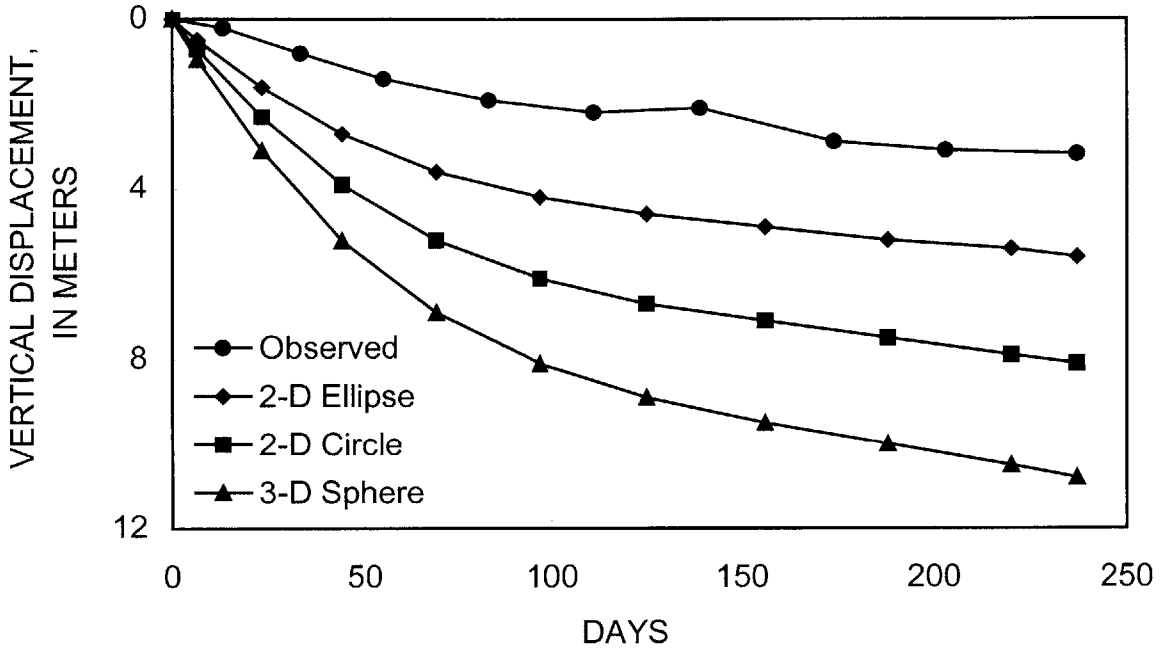

Figure 3-8. Comparison of the observed trajectory of the Cape Cod tracer cloud to trajectories for a three-dimensional sphere and two-dimensional circular and elliptical tracer bodies calculated using the Yih (1963) models and an estimated decrease in density difference with travel time because of dispersion.

each time interval. The total predicted downward movement after 237 days is about 10.8 m for the three-dimensional sphere. The downward movement for the two-dimensional elliptical body is about 50 percent less, or about 5.6 m. The observed downward movement during the same period was about 3.2 m.

Figure 3-8 shows the trajectories for the three cases and the observed trajectory during the Cape Cod tracer test. All three simulated trajectories flatten with time as dispersion dilutes the tracer cloud and decreases the density difference that causes the downward movement. The predicted rate of downward movement decreases when a two-dimensional model is used to

simulate the three-dimensional field situation. The rate decreases further when the shape of the fluid body is altered to make it less "streamlined" with respect to density-induced vertical movement. Even with the incorporation of an elliptical shape and the small additional effect of anisotropy, the predicted downward movement is significantly greater than the observed movement. This difference is discussed further at the end of this chapter.

Gelhar (1983) Model

Gelhar (written communication, 1983) suggested an analytical approach to estimate the density-induced sinking of a circular tracer cloud undergoing dilution by dispersion. He began with the solution of Yih (1963) for a circular body, given by Equation (3.19), which is presented here in a slightly different form:

$$q_z^s = \frac{1}{2}\frac{kg}{u}(\rho_w - \rho_s). \tag{3.30}$$

By letting $(\rho_w - \rho_s) = \Delta\rho$, and using the definition of hydraulic conductivity, $K = k\rho g/\mu$, one obtains:

$$q_z^s = \frac{1}{2}K\frac{\Delta\rho}{\rho}, \tag{3.31}$$

where ρ is a representative density for the system (for example, the ambient density). Dividing both sides by the effective porosity gives an expression for the vertical average linear velocity, in which the term $\Delta\rho/\rho$ is equivalent to a hydraulic gradient caused by the density difference:

$$v_z^s = v_0 = \frac{1}{2}\frac{K}{n}\frac{\Delta\rho}{\rho}. \tag{3.32}$$

Gelhar refers to this vertical component of ground-water velocity as v_o because it is the maximum rate of density-induced sinking of a circular body in a quiescent ambient flow system. The vertical displacement of the circular body after time t has elapsed would be $z(t) = v_o t$.

Table 3-7. Calculated downward movement of the tracer fluid body for a three-dimensional sphere, a two-dimensional circular body, and a two-dimensional elliptical body using the analytical models of Yih (1963) and an estimated decrease in density difference with travel time because of dispersion.

t^i	t^{i+1}	Δt	$\frac{\rho_s - \rho_w}{\rho_w}$	ρ_s	All cases		3-D sphere			2-D circular cylinder			2-D elliptical cylinder $a = 1.7$ m, $b = 0.9$ m		
					Δx	$\Sigma\Delta x$	Δz	$\Sigma\Delta z$	Θ	Δz	$\Sigma\Delta z$	Θ	Δz	$\Sigma\Delta z$	Θ
0	6.5	6.5	1.00	1000.3701	2.7	2.7	0.95	0.95	19	0.71	.71	15	0.49	0.49	10
6.5	23	16.5	.90	1000.2740	6.9	9.6	2.2	3.1	17	1.6	2.3	13	1.1	1.6	9.2
23	44	21	.67	1000.0530	8.8	18.4	2.0	5.2	13	1.5	3.9	9.9	1.1	2.7	6.9
44	69	25	.49	999.8800	10.5	28.9	1.8	6.9	9.6	1.3	5.2	7.3	.93	3.6	5.0
69	97	28	.28	999.6782	11.8	40.7	1.1	8.1	5.5	.86	6.1	4.2	.59	4.2	2.9
97	125	28	.21	999.6109	11.8	52.5	.86	8.9	4.2	.64	6.7	3.1	.44	4.6	2.2
125	156	31	.12	999.5244	13.0	65.5	.54	9.5	2.4	.41	7.1	1.8	.28	4.9	1.2
156	188	32	.12	999.5244	13.4	78.9	.56	10.0	2.4	.42	7.5	1.8	.29	5.2	1.2
188	220	32	.10	999.5052	13.4	92.3	.47	10.5	2.0	.34	7.9	1.5	.23	5.4	1.0
220	237	17	.10	999.5052	7.1	99.5	.24	10.8	2.0	.19	8.1	1.5	.13	5.6	1.0

Time in days from the start of the tracer test. Distance in meters. Initial tracer cloud at $(x, y) = (0, 0)$ m.

t^i = time at start of interval, days

t^{i+1} = time at end of interval, days

Δt = length of time interval, days

ρ_w = density of ambient ground water, Kg/m^3

ρ_s = density of tracer cloud, Kg/m^3

Δx = distance traveled by tracer body in x-direction in time Δt, m

$\Sigma\Delta x$ = cumulative distance traveled by tracer body in x-direction through end of time interval, m

Δz = distance traveled by tracer body in z-direction (positive downward) in time Δt, m

$\Sigma\Delta z$ = cumulative distance traveled by tracer body in z-direction through end of time interval, m

Θ = angle of downward movement of tracer body below the horizontal during time interval, degrees

a = major axis of ellipse, m

b = minor axis of ellipse, m.

Gelhar then considered a circular body with an initial radius equal to a. He defined two mixing lengths to describe the increase in size of the body as it was diluted by dispersion:

$$\delta_L = 2\sqrt{\alpha_L s} \tag{3.33}$$
$$\delta_T = 2\sqrt{\alpha_T s},$$

where

α_L = longitudinal dispersivity (L),

α_T = transverse dispersivity (L), and

s = distance traveled by the fluid body (L).

The ambient flow was assumed to be quiescent, so the only movement was vertically downward because of density; therefore, $s = z$. Gelhar then assumed that the decrease in the tracer-fluid density is proportional to the increase in the area of the circular body, which, in turn, was assumed to be a product of the mixing lengths, $\delta_L \delta_T = 4z\sqrt{\alpha_L \alpha_T}$. Through a derivation not shown in detail here, he obtained the following expression for the vertical movement of a circular body that is affected by dispersion:

$$z = v_o t - \frac{2\alpha z^2}{a^2}, \tag{3.34}$$

where $\alpha = \sqrt{\alpha_L \alpha_T}$ and a is the initial radius. The first term on the right side of the equation represents the downward movement without the influence of dispersion. The second term represents the reduction in the vertical displacement because of dispersion. The second term may underestimate the reduction in displacement because only vertical displacement is considered in the derivation.

An examination of Equation (3.34) shows that the displacement is particularly sensitive to the initial radius of the tracer body. A small body will be diluted more rapidly than a large

body, so the density difference that drives the downward movement will also diminish more rapidly. The displacement is also sensitive to dispersivity. A large dispersivity will cause the tracer cloud to dilute rapidly and decrease the rate of density-induced sinking accordingly.

Equation (3.34) can be rearranged into the form of a quadratic equation with z as a function of t:

$$\frac{2\alpha}{a^2} z^2 + z - v_o t = 0, \tag{3.35}$$

which can be solved for z using the quadratic formula:

$$z = \left[-1 \pm \left(1 + \frac{8\alpha\, v_o t}{a^2} \right)^{\frac{1}{2}} \right] \Bigg/ \left[\frac{4\alpha}{a^2} \right]. \tag{3.36}$$

Equations (3.32) and (3.36) were applied for various values of dispersivity and diameter of the initial cloud using parameters similar to those for the Cape Cod site (Table 3-4). The value for hydraulic conductivity was:

$$K = \frac{k\rho_w g}{\mu} = \frac{(1.514x10^{-10})(999.4091)(9.8066)}{(1.2609x10^{-3})} \text{ x } 86400 = 106 \text{ m/d}.$$

The initial vertical velocity from Equation (3.32) was then:

$$v_0 = \frac{1}{2}\frac{K}{n}\frac{\Delta\rho}{\rho} = \frac{1}{2}\left[\frac{106}{0.39}\right]\left[\frac{1000.3701}{999.4091}\right] = 0.13 \text{ m/d}.$$

The horizontal ground-water velocity and, therefore, the horizontal velocity of the tracer body, was 0.42 m/d.

Table 3-8 shows the calculated vertical displacement for several combinations of dispersivity values and diameters of the source for the first 237 days of the tracer experiment. The values most closely based on the Cape Cod test are a radius of a = 1.7 m and a dispersivity of α = 0.13 m. The value of α is based on the values for α_L and α_T reported by Garabedian

and others (1991):

$$\alpha = \sqrt{\alpha_L \alpha_T} = \sqrt{(0.96)(0.018)} = 0.13 \text{ m.}$$

At 237 days, the vertical displacement for these values of a and α is 13.8 m. This is significantly greater than the observed displacement of 3.2 m.

Table 3-8. Calculated vertical displacement of a circular tracer body using the Gelhar model for various values of dispersivity and initial radius of the tracer cloud. Rate of vertical displacement without dispersion (v_0) is 0.13 m/day.

Time (days)	Vertical displacement (m)							
	a = 0.85 m	a = 1.7 m	a = 3.4 m	a = 10 m	a = 1.7 m			
	α= 0.13 m				α= 0.13 m	α= 0.30 m	α= 0.42 m	α= 0.95 m
10	1.0	1.2	1.3	1.3	1.2	1.1	1.0	0.8
20	1.6	2.2	2.5	2.6	2.2	1.9	1.7	1.4
40	2.7	3.9	4.7	5.1	3.9	3.1	2.8	2.2
60	3.5	5.3	6.8	7.6	5.3	4.2	3.7	2.8
90	4.5	7.1	9.6	11.4	7.1	5.5	4.9	3.5
120	5.3	8.7	12.2	15.0	8.7	6.6	5.8	4.2
160	6.3	10.6	15.4	19.8	10.6	7.9	6.9	4.9
200	7.2	12.3	18.4	24.4	12.3	9.0	7.9	5.6
237	8.0	13.8	20.0	28.7	13.8	10.0	8.7	6.1

The effect of dispersion can be seen in Figure 3-9. Without dispersion, the trajectory is a straight line with a slope of v_o = 0.13 m/d. Dispersion reduces the rate of sinking nonlinearly with time, and the trajectories are curved and concave upward. The smaller the initial radius of

the tracer body, the larger the reduction in the displacement rate. The nonlinear effects of dispersion and initial radius on the rate of downward movement are also shown in Figures 3-10 and 3-11 by using the calculated displacements at the end of 40 days. The displacement at 40 days when there is no dispersion, which can be accomplished by using an initial radius of zero or a dispersivity of zero, is simply $v_0 t$, or 5.2 m. The amount of downward movement is particularly sensitive to these parameters at low values of dispersivity and small values of the initial radius.

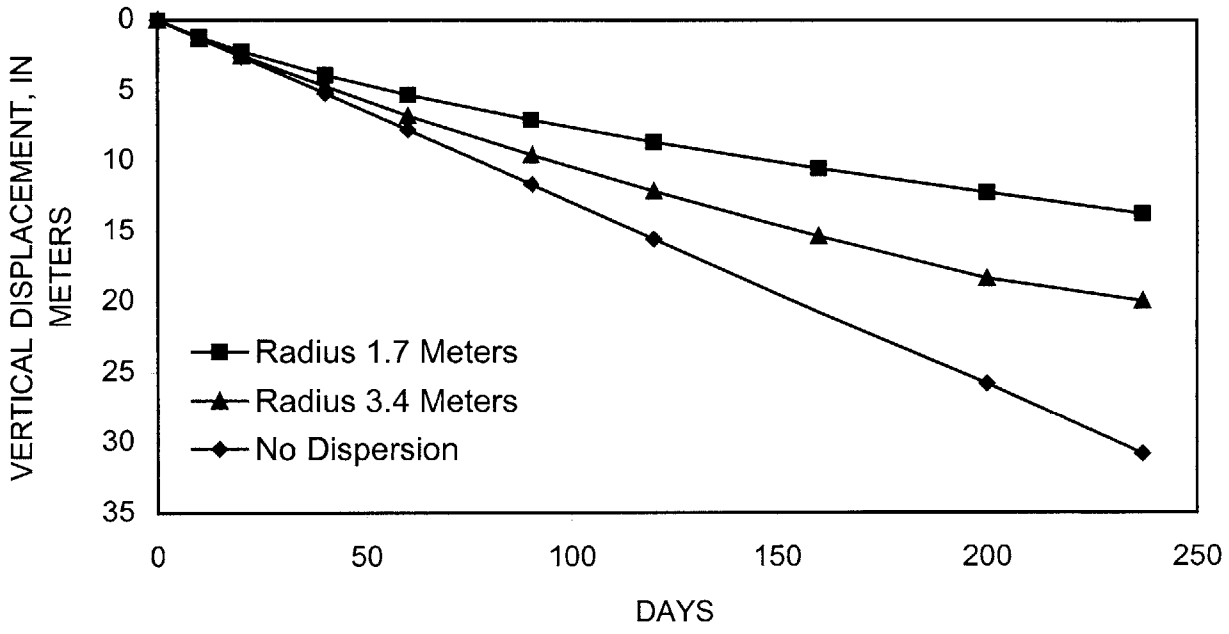

Figure 3-9. Predicted vertical displacement for two sizes of the initial tracer cloud using the Gelhar model. Dispersivity value $\alpha = 0.13$ m. Curve labeled v_0 shows downward movement without dispersion.

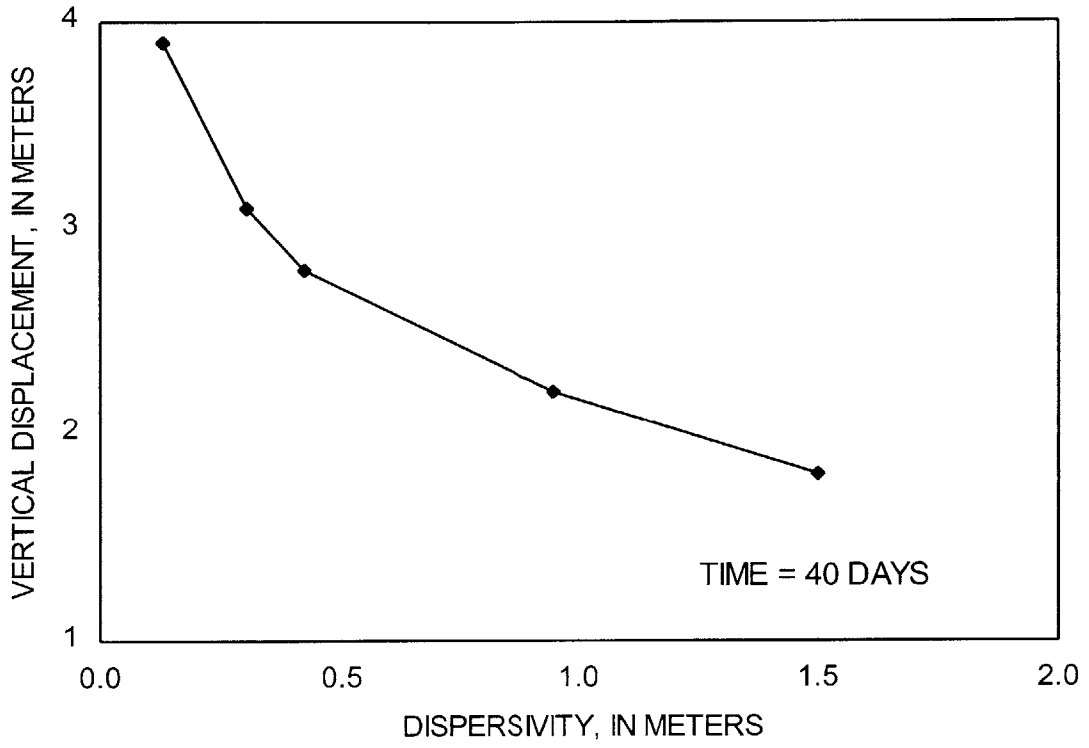

Figure 3-10. Predicted vertical displacement at 40 days as a function of dispersivity using the Gelhar model for an initial tracer cloud of radius a = 1.7 m. Maximum value of displacement with dispersivity equal to zero is 5.2 m.

Discussion

The analytical models of Hubbert (1953), Yih (1963), and Gelhar provide considerable insight into the factors that affect the rate of density-induced sinking of a tracer cloud. Although the models are based on many simplifying assumptions, essential characteristics of the sinking process can be deduced from the analytical expressions. One of the advantages of closed-form

analytical expressions is that one can deduce probable behaviors for a general set of problems without having to embark upon a detailed, site-specific analysis.

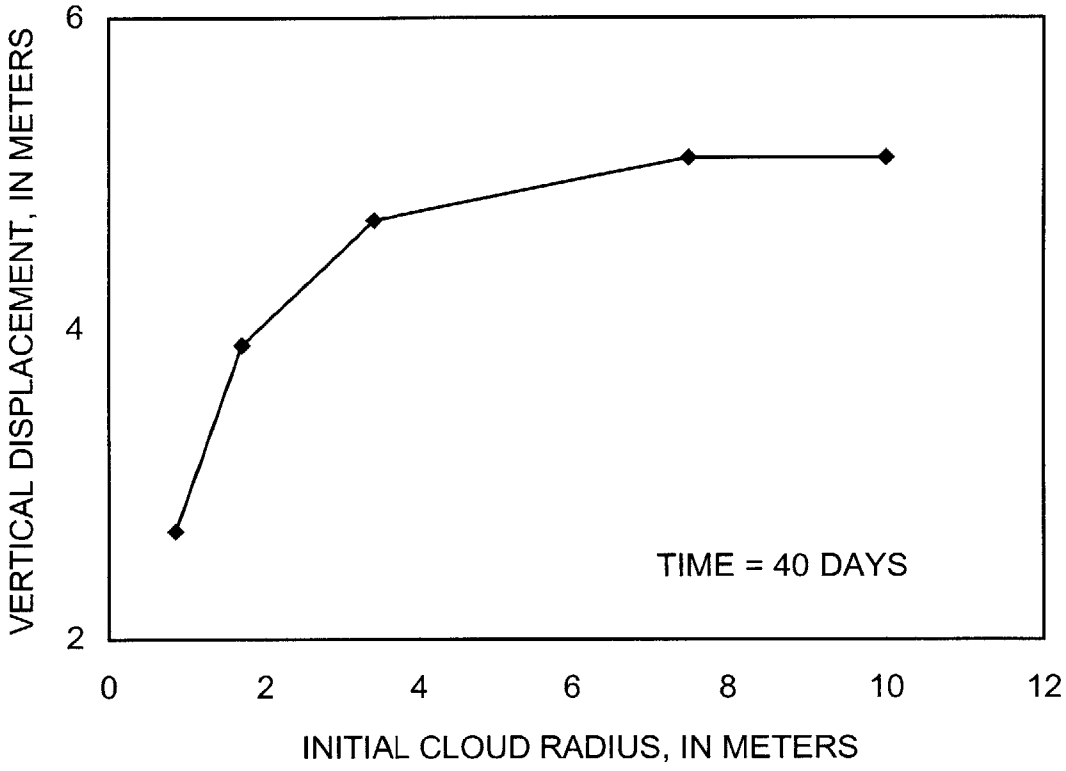

Figure 3-11. Predicted vertical displacement at 40 days as a function of initial cloud radius using the Gelhar model with a dispersivity $\alpha = 0.13$ m. Maximum value of displacement with an infinitely large radius is 5.2 m.

All of the models demonstrate that the rate of downward movement is dependent on the density difference between the ambient ground water and the tracer solution. The driving forces on the tracer fluid are dependent on the density contrast. The models of Hubbert and Yih do not

directly account for dilution of the tracer cloud, so they predict constant rates of downward movement for a given density contrast.

The Hubbert model relates the potential fields of the ambient ground water and tracer fluid in a simple expression involving only the density contrast. The tracer fluid is assumed to be dispersed within the ambient fluid. A straightforward analysis of the difference between direction of flow and the hydraulic gradient demonstrated that the anisotropy of permeability also affects the rate of downward movement. In most aquifers, the permeability is greatest in the horizontal direction, and the effect of anisotropy is to reduce the amount of downward movement for a given density contrast.

The Yih models assume that the tracer body has a particular shape and orientation. Although the tracer body moves without changing shape or becoming diluted by dispersion, the hydrodynamic effects of the sinking body on the ambient fluid are considered in the models. The ambient fluid is displaced by the sinking tracer cloud, and the resulting energy losses associated with this flow pattern reduce the rate of downward movement of the cloud. For a given density contrast, the Yih models predict considerably less downward movement than the Hubbert model.

The importance of the shape and orientation of the tracer body are highlighted by the Yih models. This effect is independent of the size of the tracer body, because the Yih models simulate an infinite porous medium, and the solutions apply to bodies of any size; only the geometry of the body is a factor. Because the ambient fluid that is displaced by the sinking cloud must move up and around the body to fill in the area left by the body, the rate of downward movement is particularly sensitive to the dimension of the body that is perpendicular to the gravitational force. A tracer cloud that presents a large cross-sectional area to the direction of

downward movement sinks more slowly than a narrow, "streamlined" body. Anyone who has tried to push a plate through water can understand this effect intuitively.

The Yih models also demonstrate the effect of dimensionality on the rate of downward movement. In many hydrologic studies involving the migration of contaminant plumes or clouds, the problem is represented as a two-dimensional, longitudinal, vertical section. The predicted rate of downward movement for a two-dimensional circular cloud was 25 percent less than the rate for a three-dimensional sphere. In the two-dimensional plane, the ambient ground water is forced to flow around the sinking cloud only in the plane, whereas the ground water can flow in all directions up and around a sinking three-dimensional body.

The Hubbert and Yih models assume that the density of the tracer fluid is constant and that the tracer cloud is not diluted by dispersion. The effect of dispersion is to reduce concentrations in the tracer cloud, which reduces the density difference and decreases the rate of downward movement. Gelhar extended Yih's model of a two-dimensional circular body to include the effects of dispersion. The analytical expression indicates that the rate of downward movement of a body that is subjected to dispersion is affected by the dispersivity and, most importantly, by the initial diameter of the tracer body. Size is important because, for a given dispersivity, the high concentrations at the center of a tracer cloud are farther from the boundary of the cloud and persist longer as the tracer cloud moves through the aquifer.

The observed tracer cloud moved downward about 3.2 m during the first 237 days of the tracer test. Table 3-9 shows that the analytical models over-predict the amount of downward movement for conditions that most closely resemble those during the field experiment. The over-predictions are even more significant if one considers that the observed movement was due in part to areal recharge during the field test (LeBlanc and others, 1991). The models are

idealized representations of the real system, and probably fail to include all of the factors that affect density-induced sinking.

Table 3-9. Predicted total amount of downward movement after 237 days for conditions similar to those during the Cape Cod test using the Hubbert (1953), Yih (1963), and Gelhar models. Values for common hydrologic parameters are shown in Table 3-4. All length units are in meters [Lengths in meters. Br^{max}, density decrease estimated from observed maximum bromide concentrations].

Model	**Source**	**Aniso-tropy** k_x/k_z	**Axes of ellipse** (a,b)	**Initial radius** (a)	**Dispersivity** (α)	**Predicted vertical movement**
Hubbert	From Table 3-1	1.2	--	--	--	53.1
Yih 3-D round	From Table 3-5	1.0	--	--	--	41.4
2-D round	"	1.0	--	--	--	31.0
2-D ellipse	"	1.0	(1.7,0.9)	--	--	21.5
Yih 3-D round	Table 3-7	1.2	--	--	From Br^{max}	10.8
2-D round	"	1.2	--	--	"	8.1
2-D ellipse	"	1.2	(1.7,0.9)	--	"	5.6
Gelhar	Table 3-8	1.0	--	1.7	0.13	13.8
Observed	LeBlanc and others (1991)	--	--	--	--	3.2

All of the models, for example, assume that the porous medium is infinite in extent. The tracer cloud in the field experiment, however, was introduced less than 1 m below the water table. Boundary effects could reduce the actual amount of downward movement by influencing the disturbance of the ambient flow field by the sinking tracer cloud.

The Yih models, including Gelhar's modification for the influence of dispersion, assume an idealized body with a regular geometry and uniform internal solute concentration. Although Gelhar's model dilutes the internal concentrations, thus decreasing the density difference with travel time, the model still assumes a circular shape for the tracer cloud, and the ambient ground water and tracer fluid are separated by a sharp boundary. In reality, the boundary between the tracer cloud and the ambient fluid would become indistinct with time. Internal flow within the cloud as gradations in solute concentration arise would distort the geometry of the tracer cloud. These processes could lead to less downward movement because of the energy losses associated with the more complex flow patterns.

CHAPTER 4

NUMERICAL SIMULATION TO DETERMINE FACTORS AFFECTING DOWNWARD MOVEMENT OF TRACER CLOUD

The hydrologic conditions that affect the movement of water and solutes in the aquifer are varied and may be difficult to incorporate in an analytical analysis. A numerical model can incorporate complex boundaries and spatially variable aquifer properties. In this chapter, a numerical model, SUTRA (Voss, 1984), is used to examine the factors that affect the rate of downward movement of a tracer cloud under conditions similar to those of the Cape Cod tracer experiment. The factors include hydrologic parameters, such as dispersivity and density, and characteristics of the model's design, such as boundary specifications and grid design. This analysis of sensitivity of downward movement to various factors was used to design the field-scale simulation of the Cape Cod experiment, which tests the hypothesis of density-induced downward movement.

Description of the Numerical Model

The numerical model that was chosen for this study is SUTRA (Voss, 1984). SUTRA is a computer program that simulates fluid movement and transport of energy or dissolved substances in the subsurface environment. The model solves the differential equations of flow and transport in a two-dimensional aquifer by using the finite-element method. SUTRA was selected for this study because it is a well-documented program that can simulate ground-water

flow and solute transport under conditions where solute concentration affects fluid density and, thus, fluid flow.

SUTRA can simulate a wide range of hydrologic and geochemical conditions, including saturated and unsaturated, steady and transient, density-dependent ground-water flow; and steady and transient transport of solutes subject to sorption and zero- or first-order reactions. The numerical algorithm allows for an irregularly spaced grid composed of quadrilateral elements, pinch nodes to change the mesh size rapidly, upstream weighting of advective transport terms, and directionally dependent longitudinal dispersivity in anisotropic porous media. The detailed development of these features is described in Voss (1984; updated in June 1990). This report summarizes only the features of SUTRA that are relevant to this analysis.

The form of the fluid mass balance as implemented in SUTRA is:

$$\rho S_{op} \frac{\partial p}{\partial t} + \left(\varepsilon \frac{\partial \rho}{\partial c} \right) \frac{\partial c}{\partial t} - \underline{\nabla} \cdot \left[\left(\frac{\underline{\underline{k}} \rho}{\mu} \right) \cdot \left(\underline{\nabla} p - \rho \underline{g} \right) \right] = Q_p , \qquad (4.1)$$

where

ρ = fluid density (Kg/m^3),

S_{op} = specific pressure storativity (Kg/(m·s^2),

p = fluid pressure (Kg/(m·s^2)),

t = time (s),

ε = porosity (dimensionless),

c = solute mass fraction (dimensionless),

$\underline{\underline{k}}$ = permeability of the solid matrix (m^2),

μ = fluid viscosity (Kg/(m·s)),

$\underline{g}$ = gravitational acceleration (m/s^2), and

Q_p = fluid mass source ($Kg/(m^3 \cdot s)$).

The first two terms on the left side of Equation (4.1) represent the change with time of fluid mass stored in the aquifer. The third term represents the balance of inflow and outflow (net flux) of fluid mass as the ground water flows in response to pressure gradients. The term on the right side of Equation (4.1) represents external sources or sinks of fluid mass, such as wells. Equation (4.1) is written in terms of pressure and permeability, rather than hydraulic head and hydraulic conductivity, because the fluid flow is dependent on density, which varies in space and time. A unique fluid potential cannot be defined for this case (Hubbert, 1940).

SUTRA uses a form of the specific pressure storativity that is based on the compressibilities of the fluid and bulk aquifer matrix:

$$S_{op} = (1-\varepsilon)\alpha + \varepsilon\beta, \tag{4.2}$$

where

α = porous-matrix compressibility $(Kg/(m \cdot s^2))^{-1}$, and

β = fluid compressibility $(Kg/(m \cdot s^2))^{-1}$.

Fluid viscosity is assumed to be independent of solute mass fraction and is set at a constant value. Density is assumed to be linearly related to solute mass fraction by the equation:

$$\rho = \rho_o + \frac{\partial \rho}{\partial c}(c - c_o), \tag{4.3}$$

where

ρ_o = base density of the fluid at the base solute mass fraction, c_o (Kg/m^3), and

c_o = base solute mass fraction (dimensionless).

The slope of the linear relation between density and solute mass fraction has the variable name DRWDU in the SUTRA code. The values used for viscosity and the coefficient relating density to solute mass fraction are described in a later section of this report.

The form of the solute mass balance as implemented in SUTRA is:

$$\varepsilon\rho\frac{\partial c}{\partial t}+\varepsilon\rho\underline{v}\cdot\underline{\nabla}c-\underline{\nabla}\cdot\left[\rho\varepsilon\left(D_m\underline{\underline{I}}+\underline{\underline{D}}\right)\cdot\underline{\nabla}c\right]=Q_p\left(c^*-c\right), \tag{4.4}$$

where

$\underline{v}$ = average linear ground-water velocity (m/s),

D_m = apparent molecular diffusivity (m^2/s),

$\underline{\underline{I}}$ = identity matrix,

$\underline{\underline{D}}$ = dispersion tensor (m^2/s), and

c^* = solute mass fraction of fluid source (Kg/m^3).

The first term on the left side of Equation (4.4) represents the change with time in solute mass in storage in the aquifer. The second term represents the net flux of solute mass because of advection by the flowing ground water. The third term represents the additional net diffusive flux of solute mass by molecular diffusion and hydrodynamic dispersion. In the sand and gravel at the Cape Cod site, ground-water velocities are high, and hydrodynamic dispersion is the dominant diffusive process. The term on the right side of Equation (4.4) represents the addition of solute mass from external fluid sources such as wells. The equation is in nonconservative form, having been derived by combination of the original conservative form of the equation with the phase-balance equation (Equation 5.1).

The average linear ground-water velocity in the terms representing advective and dispersive transport is obtained from the pressure solution by application of Darcy's Law:

$$\underline{v} = -\left(\frac{\underline{\underline{k}}}{\varepsilon\mu}\right)\cdot\left(\underline{\nabla}p - \rho\underline{g}\right). \tag{4.5}$$

The velocity values are used in Equation (4.4) during calculation of the advective and dispersive fluxes of solute mass.

The isotropic-media dispersion model described by Voss (1984) was used in this study to represent the dispersive flux of solute mass. This model accounts for dispersive flux forward and backward along the local direction of fluid flow, referred to as longitudinal dispersion, and perpendicular to the direction of fluid flow, referred to as transverse dispersion. The dispersion coefficients that govern the dispersion process are dependent on the absolute local magnitude of the average fluid velocity and the longitudinal and transverse dispersivities, α_L and α_T, which have units of length (m). In the isotropic-media dispersion model, longitudinal dispersivity acts along the direction of ground-water flow and not along the direction of maximum permeability or the direction parallel to the grid mesh of the model.

First-type (specified value) and second-type (specified flux) boundary conditions are applied to the fluid-flow and solute-transport equations (Equations 4.1 and 4.4). Assignment of these conditions, which will be described in a later section of this chapter, is a critical step in the modeling procedure and can greatly influence the simulated movement of the tracer cloud. A description of boundary conditions as implemented in SUTRA is given in Voss (1984).

The numerical model, composed of the differential equations and associated boundary conditions that describe fluid and solute mass balances, is solved in SUTRA by the finite-element method. The modeled area is divided into a finite-element mesh, and the continuous

differential equations are approximated by discretized numerical equations. Finite-element approximations developed with linear basis functions are used for the spatial derivatives, while implicit finite-difference approximations are used for the temporal derivatives. Although SUTRA provides the option to use upstream weighting of the advective transport term, this option increases the apparent dispersion process and was not used during this study. The set of discretized equations is solved for pressures and solute mass fractions using a band solver.

A solution is obtained at each time using a sequential iteration process. The equations for fluid mass balance are solved first. The velocity field is calculated, then the equations for the solute mass balance are solved. Because of the feedback between solute mass fraction and density, the new solute mass fractions are used in a second solution of the fluid balance equations. This iterative process continues until changes in pressure and solute mass fraction between subsequent iterations are below convergence criteria specified by the user. This solution sequence is repeated for subsequent time steps.

Because the model simulates transient fluid flow and solute transport, initial pressures and concentrations must be specified that are solutions to the modeled system or a deliberate perturbation of the system. Otherwise, the system's response for the first few time steps might include adjustments to an internally inconsistent set of initial conditions. For all simulations in this study, the initial pressure distribution was obtained by running a steady-state, density-independent flow simulation that represented conditions prior to emplacement of the solute cloud.

Spatial Moments of Solute Mass Fraction

The simulated distributions of pressure and solute mass fraction are outputted by SUTRA at time steps specified by the user. Graphical displays, such as contoured values of solute mass fraction, can be used to examine the results.

Integrated measures of the tracer cloud's spatial characteristics provide another way to examine the movement and spreading of solutes during transport. The spatial moments of solute mass fraction give insight into the average movement and rate of dispersion of the simulated tracer cloud. Garabedian and others (1991) used an analysis of the spatial moments of the bromide tracer cloud to describe its total mass (zeroeth moment), center of mass (first moment), and variance (second moment). The center of mass indicates the position of the cloud and can be used to track its path. The variance indicates the amount of spreading, or dispersion, of the cloud as it moves through the aquifer.

The same three spatial moments were considered in this study. These moments are obtained by spatial integration of the solute-mass-fraction distribution using the equation:

$$M_{ij} = \iint_{\Omega} \varepsilon c(x, y, t) x^i y^j dx dy , \tag{4.6}$$

where

M_{ij} = ij^{th} moment in space (i, j = 0, 1, 2),

Ω = domain of the problem, and

x, y = coordinates in space.

The proper indices are inserted into Equation (4.6) to obtain the various moments. The total mass is given by:

$$M_{00} = \iint_{\Omega} \varepsilon c dx dy \,. \tag{4.7}$$

The position of the center of mass, $(\bar{x}, \bar{y})$, relative to the origin is given by:

$$\bar{x} = \frac{M_{10}}{M_{00}} \tag{4.8a}$$

$$y = \frac{M_{01}}{M_{00}}, \tag{4.8b}$$

where

$$M_{10} = \iint_{\Omega} \varepsilon c x dx dy \tag{4.8c}$$

$$M_{01} = \iint_{\Omega} \varepsilon \; c y dx dy \,. \tag{4.8d}$$

The variances of solute-mass fraction relative to the center of mass, $\sigma_{xx}^2, \sigma_{xy}^2$, and σ_{yy}^2, are given by:

$$\sigma_{xx}^2 = \frac{M_{20}}{M_{00}} - (\bar{x})^2 \tag{4.9a}$$

$$\sigma_{xy}^2 = \sigma_{yx}^2 = \frac{M_{11}}{M_{00}} - \bar{x}\bar{y} \tag{4.9b}$$

$$\sigma_{yy}^2 = \frac{M_{02}}{M_{00}} - (\bar{y})^2 , \tag{4.9c}$$

where

$$M_{20} = \iint_{\Omega} \varepsilon c x^2 dx dy \tag{4.9d}$$

$$M_{11} = \iint_{\Omega} \varepsilon c x y dx dy \tag{4.9e}$$

$$M_{02} = \iint_{\Omega} \varepsilon c y^2 dx dy \,. \tag{4.9f}$$

These equations were integrated numerically over the modeled area by using linear basis functions identical to those used in the SUTRA computer program.

Design of Simulations

A series of SUTRA simulations was used to examine the hydrologic factors and characteristics of the model that influence the rate of downward movement of a tracer cloud. The series began with an initial simulation, which will be referred to as the "baseline run," that approximated conditions in the field during the Cape Cod tracer test. This section describes the design of the baseline run.

Grid Design

The modeled area is a vertical section of unit width that is 20 meters long and 12 meters high (Figure 4-1). The positions of the boundaries were chosen based on several preliminary

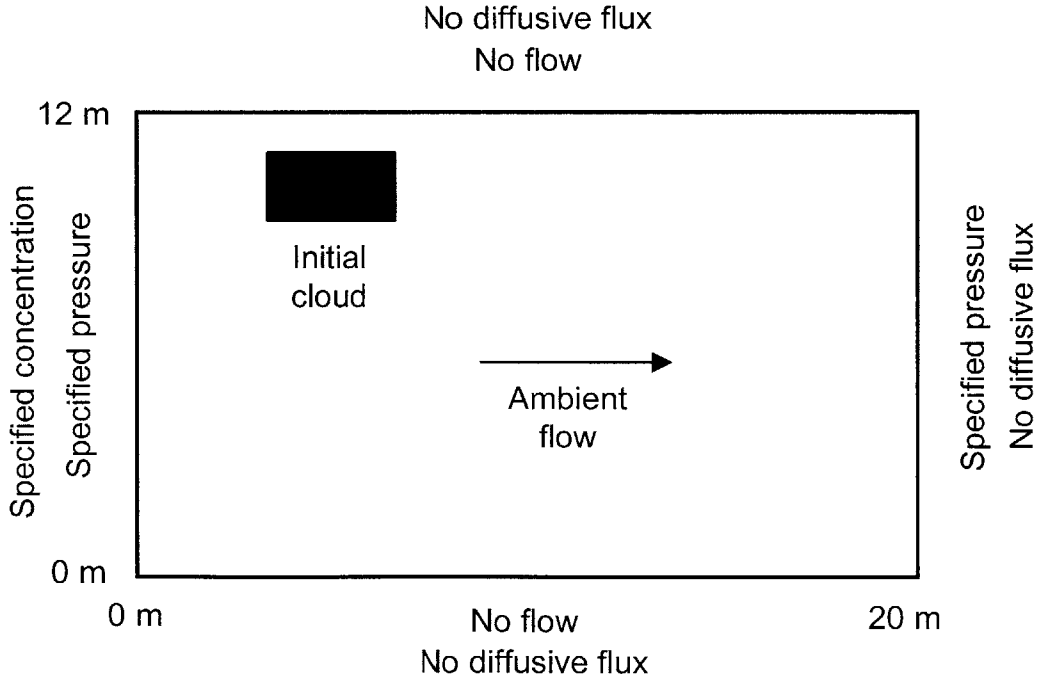

Figure 4-1. Modeled area, boundary conditions, and initial position of the tracer cloud for the baseline run, S3R19.

runs in which the influence of boundaries on transport of the cloud was examined. The horizontal dimension is sufficiently large that the left and right boundaries have little influence on downward movement of the cloud for the conditions of the Cape Cod test. Similarly, the vertical dimension is sufficiently large that downward movement of the cloud, which is placed initially near the upper boundary, is not affected by the distance to the lower boundary.

The modeled area is subdivided into a variably spaced rectangular finite-element mesh (Table 4-1). Nodes in the mesh are arranged in 45 rows and 89 columns; the mesh consists of 4,005 nodes and 3,872 rectangular elements. In the horizontal (x) direction, the spacing between columns in the grid (Δx) is 0.2 m in the central 15-m-long portion of the modeled area. The spacing increases to the left and right of the central area in order to move the boundaries away from the area of interest with a minimum number of additional columns. In the vertical (y) direction, the spacing between rows of the grid (Δy) is 0.1 m in the upper 3.2-m-high portion of the modeled area. The spacing increases below the central area to a maximum spacing of 2.6 m.

The grid spacing was chosen to allow use of the small dispersivities observed by Garabedian and others (1991) during the early part of the Cape Cod test. Voss (1984) recommended that the mesh Peclet number not exceed 4.0 in order to minimize oscillations in the numerical solution; a mesh Peclet number of 2.0 or less is needed to guarantee no oscillations of the solution. The mesh Peclet number along a flowline is given by:

$$P_e = \frac{v\Delta x}{D}. \qquad (4.10).$$

The dispersion coefficient can be represented by $D = \alpha_L v$. So the mesh Peclet number can be calculated by:

$$P_e = \frac{\Delta x}{\alpha_L}. \qquad (4.10).$$

Table 4-1. Spacing in the horizontal and vertical directions in the finite-element grid of the baseline run (S3R19).

Horizontal Direction (x)		
Grid spacing , Δ_x (m)	Number of Elements	Cumulative distance from left boundary (m)
0.4	1	0.4
0.3	2	1.0
0.2	75	16.0
0.3	4	17.2
0.4	4	18.8
0.6	2	20.0

Vertical Direction (y)		
Grid spacing, Δ_y (m)	Number of elements	Cumulative distance from bottom boundary (m)
2.60	1	2.60
1.90	1	4.50
1.30	1	5.80
0.90	1	6.70
0.60	1	7.30
0.40	1	7.70
0.30	1	8.00
0.20	1	8.20
0.15	4	8.80
0.10	32	12.00

Flow was predominantly horizontal during the test, so longitudinal dispersion was expected to act primarily in the horizontal direction. Simulations were planned with a longitudinal dispersivity as small as 0.05 m, which is slightly large than dispersivities reported in laboratory column experiments (Freeze and Cherry, 1979). The rule-of-thumb that the mesh

Peclet number be 4.0 or smaller was satisfied by using a horizontal grid spacing (Δx) of 0.2 m in the area through which the tracer cloud was expected to move.

Voss (1984) also recommended that the grid spacing perpendicular to the local flow direction be less than 10 times the transverse dispersivity. Simulations were planned with transverse dispersivities as small as 0.005 m, which is slightly larger than the transverse vertical dispersivity reported by Garabedian and others (1991). A vertical grid spacing (Δy) of 0.1 m was used in the area through which the cloud was expected to move, even though this spacing was larger than that recommended by Voss (1984). Preliminary runs with SUTRA indicated that the larger vertical spacing had little effect on transverse spreading of the simulated tracer cloud.

The effect of the increasing vertical spacing below the central part of the modeled area on vertical spreading of the tracer cloud was examined with a finite-difference model of one-dimensional diffusive transport. Only diffusive transport was simulated because ground-water flow is predominantly horizontal in the SUTRA simulations, and solute mass flux in the vertical direction will occur mostly by dispersion. The simulations were run with a finely discretized, evenly spaced grid and a variably spaced grid similar to that used in the vertical direction in the SUTRA simulations. The diffusion coefficient was the product of the ground-water velocity (0.42 m/d) and the transverse vertical dispersivity (0.005 m). A comparison of results using the two grids indicated that use of the mesh with increasing vertical spacing below the cloud caused no additional vertical dispersion beyond that specified by the diffusion coefficient.

Boundary Conditions

Boundary conditions were specified around the perimeter of the modeled area for the fluid flow and solute transport equations. These conditions are shown in Figure 4-1. For the

fluid-flow model, the top and bottom of the modeled area are second-type, zero-fluid-flow boundaries. The upper boundary is assumed to be at the location of the water table, which is a streamline across which no flow occurs unless there is recharge from precipitation. The position of the lower boundary was selected so it would not affect the simulations.

The left and right sides are specified-pressure, or first-type, boundaries. The pressure distributions were calculated from the hydraulic gradient at the tracer-test site and the density of the ambient ground water. The hydraulic gradient at the site was 0.0015 m/m during the tracer test; this is equivalent to a head difference of 0.03 m across the 20-m-long modeled area. To simplify calculation of appropriate pressure distributions, the hydraulic head (pressure head plus elevation head) along the right boundary was assumed to be zero, and the hydraulic head along the left boundary was assumed to be 0.03 m. Because ground-water flow is approximately horizontal at the site, the pressure distribution along each boundary was assumed to be hydrostatic. The pressure at each node was calculated using the relation:

$$p(x, y) = p_o + \rho_o g z, \tag{4.11}$$

where

p_o = reference pressure (assumed to be 0.0 Kg/(m^2·s^2)),

ρ_o = density of the ambient ground water (Kg/m^3),

z = height of the water column above the node (m).

A solute mass fraction is associated with each specified-pressure node in case the node becomes a source of fluid to the aquifer. For these simulations, the solute mass fraction for the specified-pressure nodes was set to 0.0.

For the solute-transport model, the top, bottom, and right sides of the modeled area are second-type boundaries at which the diffusive flux of solute mass across the boundaries is zero. Solute mass can cross these boundaries as advective flux, but only if fluid is flowing across the boundaries. The left side of the model, on the upstream side of the modeled area, is a specified solute-mass-fraction boundary; the mass fraction was set to 0.0 for these simulations.

Aquifer and Fluid Properties

Aquifer and fluid properties similar to those at the Cape Cod site were specified as input to the models. The properties that are needed are shown in the definitions of the two mass balance equations (Equations 4.1 and 4.4) and are listed in Table 4-2. The sources of the values are also shown in the table and, for several properties, are described in more detail below.

The permeability in the horizontal direction, k_{xx}, was calculated from fluid viscosity and hydraulic conductivity by using the relation:

$$k_{xx} = \frac{K_{xx}\mu}{\rho_o g}. \tag{4.12}$$

The values of μ, ρ_o, and g are given in Table 4-2. The ambient ground-water temperature was about 13°C (LeBlanc and others, 1991, p. 889). The average hydraulic conductivity, K_{xx}, is about 110 m/d (LeBlanc and others, 1991, p. 897).

For the baseline run, permeability was assumed to be isotropic. Anisotropy at the Cape Cod site is small; Hess and others (1992, p. 2022) used a stochastic analysis of hydraulic-conductivity measurements to estimate a ratio of 1.2 for horizontal to vertical conductivity. The effect of anisotropy on the movement of the tracer cloud is described in a later section of this report.

Table 4-2. Aquifer and fluid properties for the baseline run (S3R19)

Property	Variable	Value	Units	Source
Porosity	ε	0.39	none	Garabedian and others (1991, p. 916).
Permeability	k_{xx}	1.56×10^{-10}	m^2	LeBlanc and others (1991, p. 897); see text.
Anisotropy of permeability	k_{xx}/k_{yy}	1.0		See text.
Porous matrix compressibility	α	1.87×10^{-10}	$(m \cdot s^2)/Kg$	Aquifer test, Garabedian and others (1988); see text.
Longitudinal dispersivity	α_L	0.05	m	See text.
Transverse dispersivity	α_T	0.005	m	See text.
Fluid viscosity	μ	1.202×10^{-3}	$Kg/(m \cdot s)$	Weast (1989, p. F-37); fluid temperature 13°C
Fluid density at base solute concentration	ρ_o	999.4091	Kg/m^3	See text.
Coefficient of density/concentration relation	$\partial\rho/\partial c$	0.9610	Kg/m^3	See text.
Fluid compressibility	β	4.78×10^{-10}	$(m \cdot s^2)/Kg$	Weast (1989, p. F-15)
Molecular diffusivity	D_m	1.0×10^{-9}	m^2/s	Freeze and Cherry (1979, p. 103)
Gravitational acceleration	g	9.8066	m/s^2	

The compressibility of the porous matrix, α, was estimated from specific storage, S_s, by the relation:

$$\alpha = \frac{S_s}{\rho g} - n\beta . \tag{4.13}$$

A value for S_s of 3.66 x 10^{-6} m^{-1} was reported by Garabedian (1988, p. 59) for an aquifer test that was conducted in sand and gravel about 2 km from the tracer-test site. The values of ρ, g, n, and β are given in Table 4-2.

A longitudinal dispersivity of 0.05 m was used for the baseline simulation. This value is slightly larger than dispersivities reported for laboratory column experiments (Freeze and Cherry, 1979) and two orders of magnitude smaller than the asymptotic longitudinal dispersivity reported by Garabedian and others (1991, p. 918) for the Cape Cod tracer test. A small value of dispersivity is appropriate for the small scale of the simulations because the asymptotic value is reached only after tens of meters of transport (Garabedian and others, 1991). The small value also limited the effects of dispersion and facilitated examination of the influence of other factors on density-induced sinking.

The transverse dispersivity used in the baseline run was 0.005 m. This value is an order of magnitude larger than the transverse vertical dispersivity reported by Garabedian and others (1991, p. 920) for the Cape Cod test. Use of a value as small as the reported value, however, would have required a fine grid spacing; at the time that this work was done, computer simulation time would have been impractically large.

The fluid density, ρ_o, at the base solute concentration, and the coefficient, $\partial\rho/\partial c$, of the relation between density and concentration, were estimated from the measured concentrations of solutes in the ambient ground water and the injected tracer solution. The temperature of the

ambient ground water was about 13°C (LeBlanc and others, 1991, p. 899). At this temperature, the density of pure water is 999.3771 Kg/m^3 (Weast, 1989, p. F-4). The ambient ground water contained about 32 mg/L dissolved solids (LeBlanc and others, 1991, p. 900), or approximately 0.032 Kg/m^3. The density of the ambient ground water, ρ_o, was assumed to equal the density of pure water plus the additional mass of the dissolved constituents, or 999.4091 Kg/m^3.

The density of the tracer solution was estimated in a similar manner. The tracer solution was prepared by adding the tracers, as inorganic salts, to ground water pumped from the aquifer into a pair of tanks. The ambient ground water contained 32 mg/L, to which were added 640 mg/L bromide, 78 mg/L lithium, 133 mg/L molybdate (as MoO_4), and 50 mg/L fluoride (LeBlanc and others, 1991, Table 2). The total concentration of the dissolved constituents was 933 mg/L, or 0.933 Kg/m^3. The density of the tracer solution was assumed to equal the density of pure water plus the additional mass per liter of the dissolved constituents, or 1000.3701 Kg/m^3.

The coefficient of the linear relation between density and concentration was obtained by solving equation 4.3 for $\frac{\partial \rho}{\partial c}$:

$$\frac{\partial \rho}{\partial c} = \frac{\rho - \rho_o}{c - c_o} \quad . \tag{4.14}$$

For the sensitivity runs, the solute mass fractions were normalized to the mass fraction of the injected tracer solution. Therefore, the solute mass fractions were assumed to be 0.0 in the ambient ground water and 1.0 in the tracer solution. Using these mass fractions and the densities given above, a value of 0.9610 was obtained from Equation (4.14) for $\partial \rho / \partial c$. This coefficient has the variable name DRWDU in the SUTRA code.

The densities of the tracer solution and the ambient ground water differ by 0.961 Kg/m^3, or about 0.1 percent of the density of the ambient ground water. This small density contrast is difficult to measure directly. Estimation of the densities by addition of the ambient density and the additional mass of solutes is only an approximation because the two quantities are not strictly additive. Zhang and Schwartz (1995) used reported densities of solutions of sodium chloride at various concentrations (Weist, 1989) to develop a relationship between sodium chloride concentration and density. Their analysis suggested that the strictly additive approach may overestimate the densities by as much as 25 percent at concentrations of 1000 to 2,000 mg/L. However, the additive estimates were assumed to be adequate for this analysis.

Source Configuration

During the field tracer test, the tracer solution was injected into three wells over 16 hours. Because of local aquifer heterogeneity at the injection site, the initial tracer cloud probably had a complex three-dimensional shape. LeBlanc and others (1991) estimated that the initial volume of aquifer occupied by the tracer solution was about 19.5 m^3.

The solute source for the baseline run was represented as a two-dimensional area that is similar in cross-sectional area to the estimated initial volume of the tracer cloud. The thickness was assumed to be 1.8 m, or 50 percent greater than the screened interval of the injection wells to account for vertical spreading during injection. The length parallel to the ambient flow was assumed to be 3.2 m. The width, which was transverse to flow and not represented in the model, was assumed to be 3.4 m, or about twice the distance between the leftmost and rightmost injection wells to account for lateral spreading during injection.

The configuration of the solute source in the baseline run is shown in Figure 4-2. The

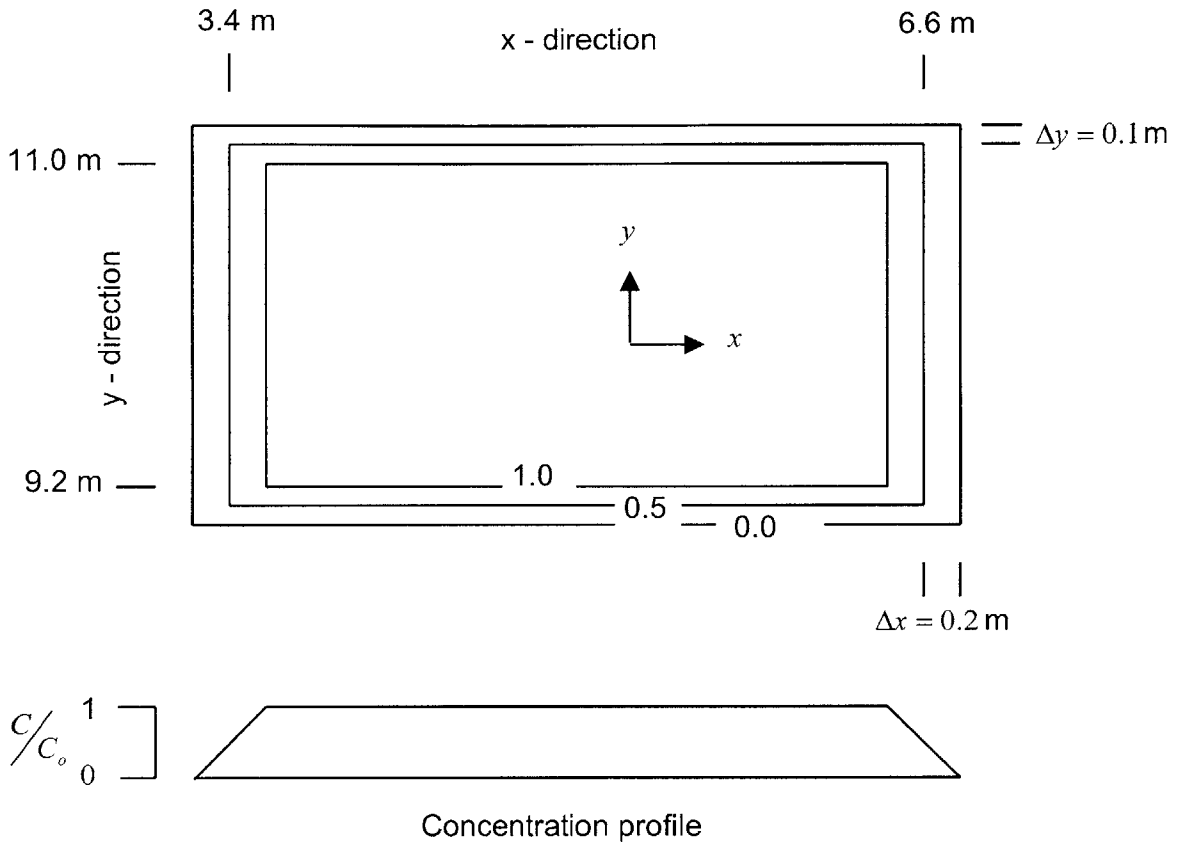

Figure 4-2. Source configuration for the baseline run, S3R19.

boundaries of the solute source were represented by a linear decrease in mass fraction over two nodes rather than by an abrupt transition. The mass-fraction profile across the solute source had a trapezoidal shape (Figure 4-2). This configuration helped to minimize numerical oscillations associated with the initially sharp front. The source dimensions given in this report include the area where the mass fraction is greater than 0.5. The zeroeth moment (total mass) calculated for the initial simulated tracer cloud for the baseline simulation is 2.2542 solute mass fraction units.

The source in the baseline run was centered at grid coordinates (5.00, 10.10)(Figure 4-1). Its upper boundary was 1.0 m below the top boundary of the modeled area. This distance was based on the screen positions below the water table and the 50-percent vertical spreading assumed above. The source's left, or upstream, boundary, was 3.4 m from the left boundary of the modeled area. Sensitivity simulations described later in this chapter indicate that this distance to the left boundary was sufficient to eliminate boundary effects.

Simulation Approach

The series of simulations to determine the effects on the downward trajectory of the tracer cloud was derived from the baseline run by changing the parameters of interest and comparing the results to the baseline run. A common procedure was used to run the simulations, including a common discretization in time for the transport simulations.

Simulation Procedure

The simulations were run in two steps. The first step was the steady-state simulation of fluid flow without solute transport. The purpose of this step was to create the ambient horizontal flow from the specified-pressure boundary conditions. The pressures for each node from this simulation were written to a file and used as the initial condition for the transient transport simulation. If transport was simulated without this step, pressures at early times in the transient simulation would change in response both to the original boundary specifications and the introduction of the dense tracer solution. The changes at early times would be mostly a numerical response to an unrealistic initial condition.

The second step was the transient simulation of transport of the solute cloud. The tracer cloud was assumed to appear instantaneously at the start of the simulation within the ambient pressure field associated with the steady-state, horizontal-flow condition. Although the tracer solution was injected into the aquifer during a 16-hour-period (0.7 days), the assumption of an instantaneous source simplified the simulations by ignoring the transient hydraulic response to the fluid injection.

During the transient simulations, SUTRA iterates between the flow and transport solutions until the changes in solute mass fraction and pressure between subsequent iterations are below convergence criteria set by the user. For these simulations, the pressure convergence criterion, RPMAX, was set to 10.0 Kg/($m^2 \cdot s^2$), or about 0.05 percent of typical pressure values in the model domain. The solute mass fraction criterion, RUMAX, was set to 0.01 (Table 4-3). The maximum number of iterations, ITRMAX, was set to 10, but only a few simulations that had significant downward movement of the solute cloud at early time required more than one iteration. The use of smaller convergence criteria did not significantly change the simulated results.

Temporal Discretization

Voss (1984, p. 234) provides the general guideline that sharp solute fronts require time discretization that allows them to move only a fraction of an element per time step. The Courant number provides a quantitative measure of this criterion:

$$C_r = \frac{v\Delta t}{\Delta x}. \qquad (4.15)$$

Even considering density effects, the flow is predominantly in the horizontal direction. The

horizontal ground-water velocity, v, is 0.42 m/d. The horizontal grid spacing varies from 0.2 to 0.6 m (Table 4-1), but is 0.2 m in the central portion of the modeled area through which the cloud is expected to pass. A time step of $\Delta t = 0.25$ days gives a Courant number of 0.525. Thus, a sharp front will move only about one half of a model cell in a time step.

Table 4-3. Model parameters for the baseline run, S3R19.

Property	**Variable**	**Value**	**Units**
Pressure convergence criterion	RPMAX	10.0	$Kg/(m^2 \cdot s^2)$
Concentration convergence criterion	RUMAX	0.01	none
Maximum number of iterations per time step	ITRMAX	10	
Time step	Δt	21,600	Seconds
Number of time steps	ITMAX	20	

The purpose of these simulations was to examine the factors that affect density-induced downward movement, not the maximum extent of movement. The effects of various factors was evident in a short time, so there was no need to simulate a long period of transport. Therefore, a simulation period of 5 days (20 time steps) was used for these model runs.

Numerical Oscillations

For these simulations, flow was predominantly in the horizontal direction. To minimize numerical oscillations, the horizontal grid spacing was selected so that the mesh Peclet number in the horizontal direction was less than 4.0.

The mesh Peclet number for these simulations is given by:

$$P_e = \frac{v\Delta x}{D} = \frac{\Delta x}{\alpha_L} = \frac{0.2m}{\alpha_L}. \tag{4.16}$$

For the baseline run, the longitudinal dispersivity, α_L, was 0.05, yielding a Peclet number of 4.0. To examine the effect of dispersivity on density-induced downward movement, several simulations were run with smaller dispersivities and, consequently, larger Peclet numbers. The results of these simulations are discussed in a later section of this report.

The simulated concentrations exhibited some numerical oscillation. Figure 4-3 shows longitudinal profiles of concentration through the center of the tracer cloud at 1.25 days for three simulations with input values of longitudinal dispersivity of 0.0 m (Run S3R23B), 0.10 m (Run S3R42B), and 1.0 m (Run S3R24B). Numerical oscillations were greatest for the smallest dispersivity, as was expected. The oscillations are not evident for the simulation with α_L = 1.0 m, which corresponds to a mesh Peclet number of 0.2.

The oscillations are greatest at the leading and trailing edges of the tracer cloud (Figure 4-3), where the concentration fronts are steepest. The location of the oscillation can also be seen in Figure 4-4, in which concentrations for Run S3R23B at 1.25 days have been contoured. Concentration overshoot, where simulated concentrations exceed the input solute mass fraction of 1.0, is evident just behind the leading edge of the solute cloud. Many small oscillations are also evident as "ripples" in the areas behind and below the simulated tracer cloud. The ripples, which are formed by zero contours, represent undershoot and overshoot at mass fractions of less than 0.01 percent of the input solute mass fraction, except in areas that are close to the tracer cloud.

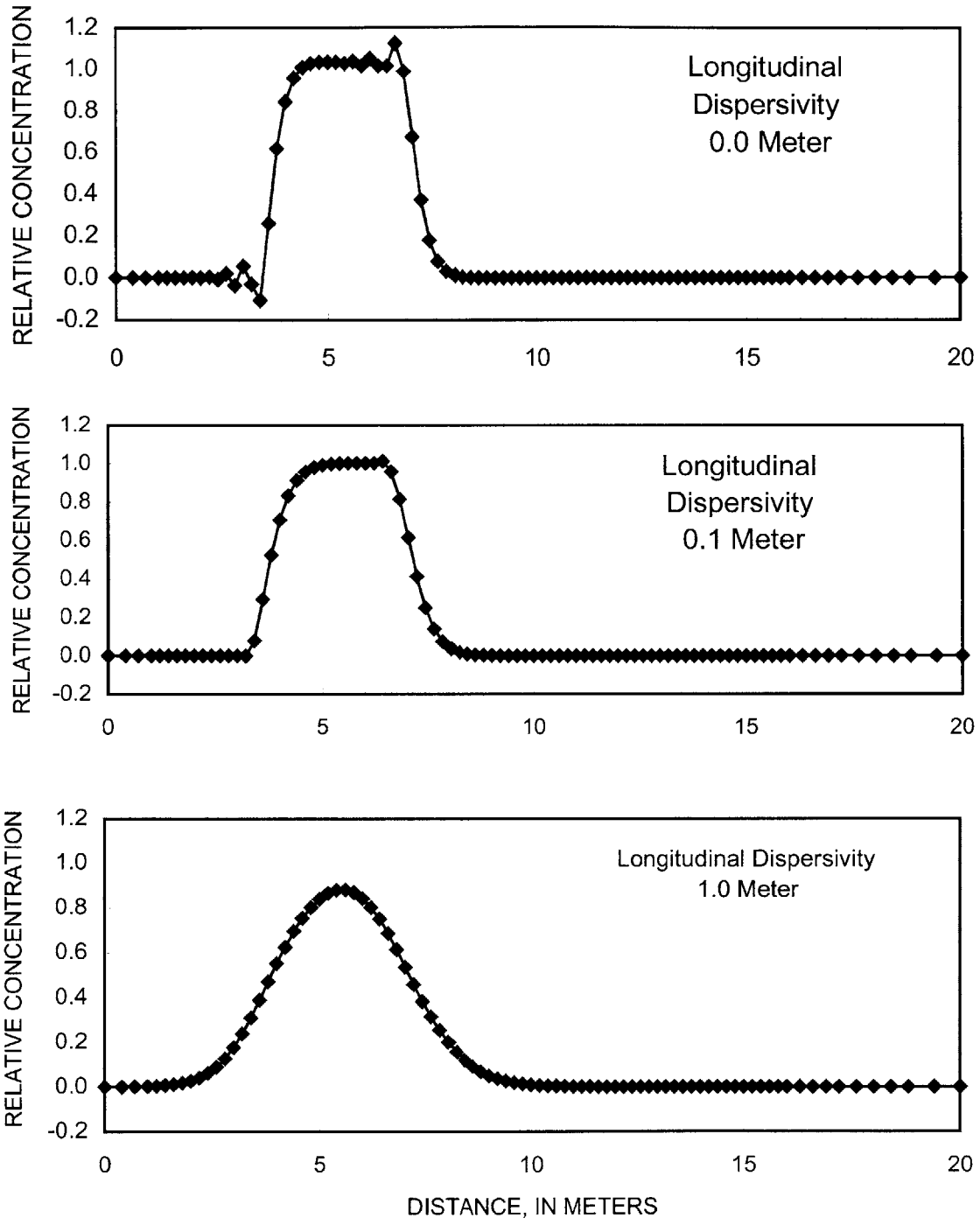

Figure 4-3. Longitudinal profiles of solute mass fraction through the center of the tracer cloud at 1.25 days for runs S3R23B (α_L = 0.0m), S3R42B (α_L = 0.10 m), and S3R24B (α_L = 1.0 m).

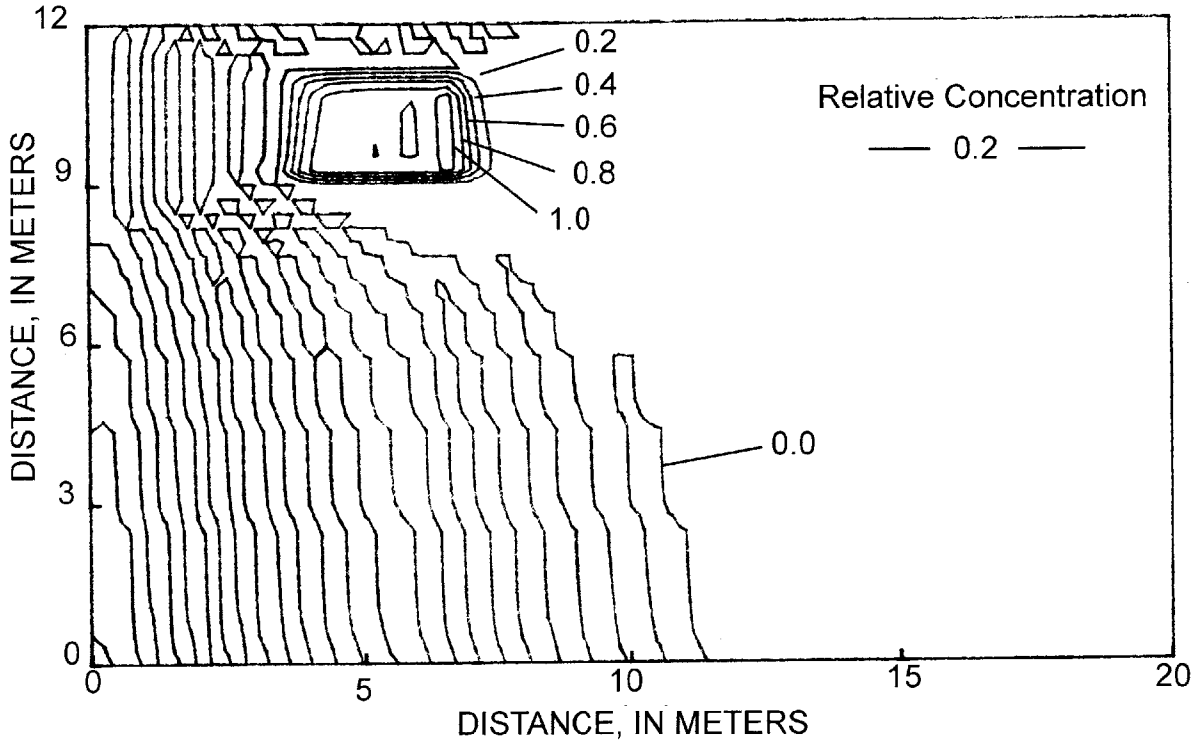

Figure 4-4. Simulated tracer cloud at 1.25 days for run S3R23B. Input value of longitudinal dispersivity is 0.0 m.

A reduction in the mesh Peclet number by increasing the longitudinal dispersivity or decreasing the grid spacing will reduce the oscillations. The effect of the oscillations also diminishes with time as the cloud disperses during transport and the concentration fronts become less steep.

In these simulations, the effective value for longitudinal dispersivity, α_L*, is larger than the SUTRA input value, ALMAXF, because there is additional numerical dispersion related to

the time discretization. For unidirectional flow, it can be shown (Michael Celia, written commun., 1992) that the effective longitudinal dispersivity is given by:

$$\alpha_L^* = \alpha_L^{true} + \frac{(2\Theta - 1)}{2} v\Delta t, \tag{4.17}$$

where α_L* = effective longitudinal dispersivity (m), α_L^{true} = input value of longitudinal dispersivity, and Θ = weighting of the time derivative. Equation (4.17) shows that decreasing the ground-water velocity, the time step, or the weighting factor can reduce numerical dispersion.

Flow is approximately unidirectional (horizontal) for these simulations, so Equation (4.17) can be used to approximate the effective dispersivity from the model parameters. SUTRA uses a fully implicit finite-difference approximation to the time derivative, so Θ = 1.0, v = 0.42 m/d, and Δt = 0.25 d. Therefore, Equation (4.17) becomes:

$$\alpha_L^* = \alpha_L^{true} + 0.0525, \tag{4.18}$$

in which the last term, 0.0525 m, is an estimate of the numerical dispersion. The model-input and estimated effective longitudinal dispersivity values for runs S3R23B, S3R42B, and S3R24B are shown in Table 4-4.

The effective dispersivity can also be calculated from the second moment, or the variance, of the tracer-cloud concentrations in the longitudinal direction. The variance of the cloud in the x-direction, σ_{xx}^2, was calculated from the simulated concentrations by using Equation (4.9a). The change in longitudinal variance with travel time for the three simulations is shown in Figure 4-5. If the ground-water velocity is unidirectional and constant, the dispersivity can be calculated from the change in variance with travel distance:

$$\alpha_L = \frac{1}{2} \frac{\Delta \sigma_{xx}^2}{\Delta \bar{x}}, \tag{4.19}$$

where $\Delta\bar{x}$ = change in the first moment, or the position of the center of mass. The calculated effective longitudinal dispersivities for the three runs are shown in Table 4-4.

Table 4-4. Comparison of longitudinal dispersivity from the model input value, the estimated effective value with numerical dispersion, and the moments of the simulated tracer cloud for runs S3R23B, S3R42B, and S3R24B.

Run	Longitudinal dispersivity, meters		
	Model input value	**Estimated with numerical dispersion (Equation 4.17)**	**Calculated from second moment of simulated tracer cloud**
S3R23B	0.0	0.0525	0.0536
S3R42B	0.10	0.1525	0.1417
S3R24B	1.00	1.0525	1.0006

The results presented in Table 4-4 show that Equation (4-17) is a good predictor of the effective longitudinal dispersion. The difference between the predicted and simulated dispersivities may be the result of terms and factors that are not accounted for in the derivation of Equation (4.17). For runs S3R19B and S3R24B, boundary effects may also contribute to the difference. For large dispersivity values (for example, α_L = 1.0 m in run S3R24B), the cloud spreads rapidly in the both longitudinal directions, and mass is lost from the model domain across the boundaries, particularly the upgradient specified zero-concentration boundary. Because the mass at the tails of the distribution is heavily weighted in the moments calculations, there is less apparent spreading as measured by the second moment, and the apparent effective longitudinal dispersivity is less than the predicted value.

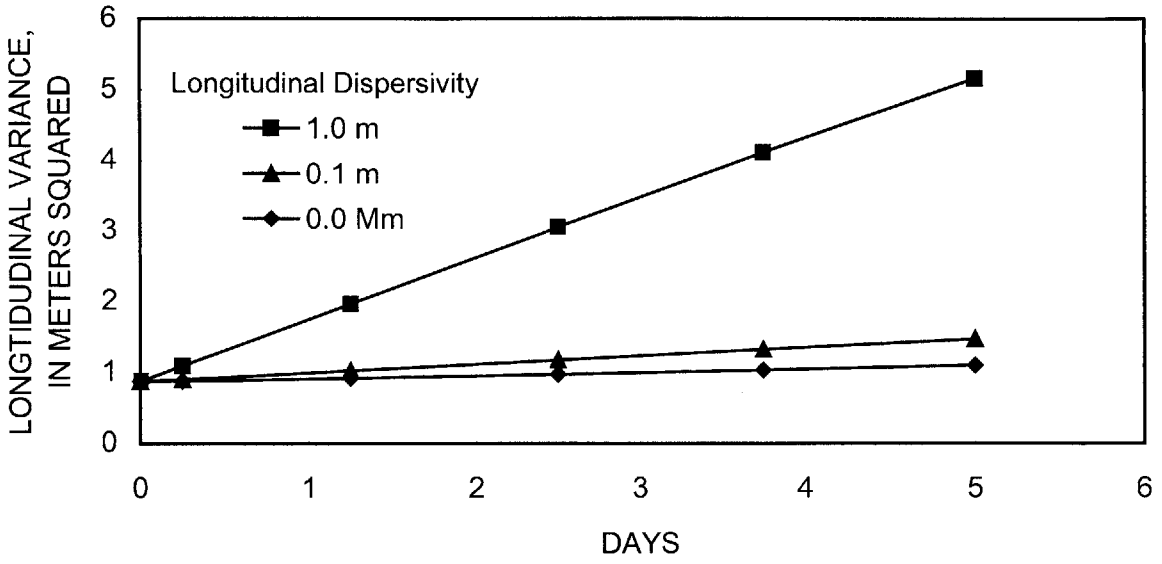

Figure 4-5. Second moment, or longitudinal variance, of simulated tracer cloud with travel time for runs S3R23B, S3R42B, and S3R24B.

The oscillations in run S3R23B, for which the input α_L was 0.0 m, were not as great as might have been expected given that the equivalent mesh Peclet number is infinity. The effective longitudinal dispersivity results in an effective Peclet number of about 3.8 and, therefore, decrease the magnitude of the oscillations.

The numerical oscillations can pose a particular problem in simulations of density-induced downward movement. The density of the fluid is linearly related to the calculated solute mass fraction by Equation (4.3). Therefore, significant overshoot and undershoot of concentrations result in a proportional overshoot and undershoot of fluid density. Because

density affects the simulated pressure gradients that drive the flow, erroneous flow directions and magnitudes can develop in areas with significant numerical oscillation. For these simulations, the oscillations were assumed to be sufficiently small and localized that their influence on the overall downward movement of the tracer clouds was small.

Pattern of Flow around Sinking Tracer Cloud

The next section of this report describes the effect of various factors on the vertical trajectory of the first moment, or center-of-mass, of the simulated tracer cloud. These effects can be explained best if the flow patterns that form around a sinking tracer cloud are understood. The changes in flow are subtle for the small density contrasts considered in most of the simulations. Therefore, a separate simulation with a large density contrast was run to illustrate this flow pattern more clearly.

The model design was similar to the baseline run, but the model domain and the source size were smaller. The model domain, which is shown in Figure 4-6, was 2.5 m high and 15.0 m long. The uniform grid spacing was $\Delta x = 0.2$ m and $\Delta y = 0.05$ m. The initial source area was centered at (x, y) = (4.0 m, 1.75 m) relative to the lower left corner of the grid. The density of the initial tracer cloud was four times the density of the ambient ground water to cause a significant perturbation of the ambient flow system. The simulation was run for 10 days with a time step of 0.25 days.

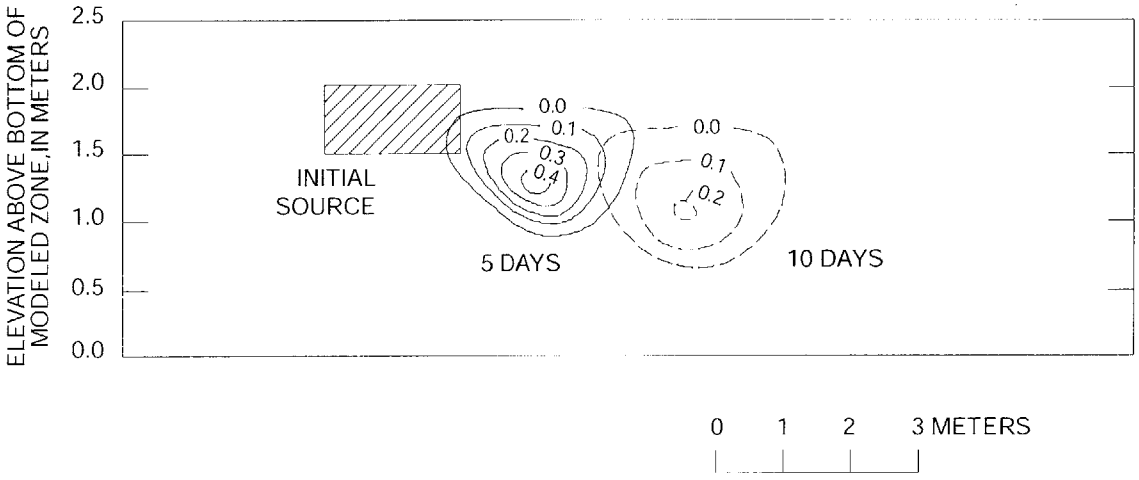

Figure 4-6. Simulated tracer cloud at 0, 5, and 10 days for run S2R4G. Density of the solute tracer cloud was four times the density of the ambient ground water.

The tracer cloud develops a saddle shape (Figure 4-6) as it is transported laterally with the ambient flow at about 0.42 m/d. The saddle shape develops because the center of the cloud, where concentrations are highest and downward forces caused by density are greatest, moves downward more rapidly than the edges of the cloud, where concentrations are diluted by dispersion and downward forces are weaker. The density contrast gradually diminishes as the maximum concentration decreases and the cloud becomes more dispersed. But the shape that is caused by the initial rapid sinking persists at later time (for example, compare the cloud shapes at 5 and 10 days), even though the downward movement also diminishes with time.

The downward movement also affects directions of flow in the ambient fluid as the sinking tracer cloud displaces the fluid. Figure 4-7 is a vector plot of calculated ground-water velocities at 5 days. The greatest downward flow is in the area of the tracer cloud. A less pronounced area of upward flow is immediately behind and above the cloud, where ambient water moves to fill the area left by the sinking cloud. Another area of subtle upward flow is ahead of the cloud where it is pushing water aside as it sinks.

A circulation develops within the ambient flow field as the sinking cloud displaces ambient water. Unless the density contrast is so great that the cloud "sinks like a stone," the ambient flow field continues to dominate and flow remains largely in the horizontal direction. However, a circulation up and around the cloud as it sinks is superimposed on the ambient flow. The magnitude of the circulation diminishes as the cloud is diluted and the rate of downward

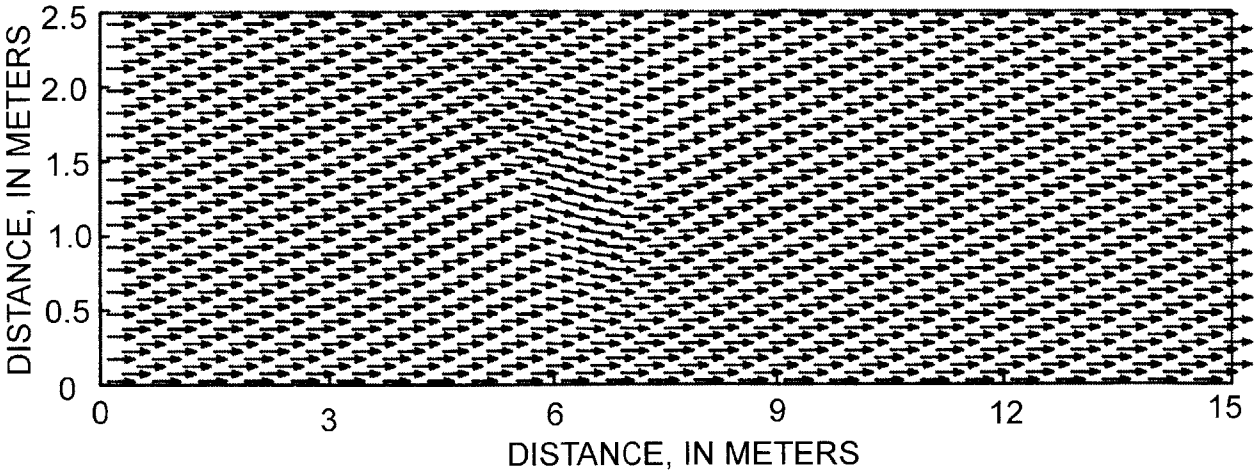

Figure 4-7. Vector plot of the ground-water velocity field at 5 days for run S2R4G. Only every fourth velocity vector is shown for clarity.

movement decreases. It should be noted that a component of the downward force would persist as long as any density difference remains between the dispersed tracer cloud and the ambient fluid.

Factors Affecting Density-Induced Downward Movement

The effects of various factors on density-induced downward movement of a solute cloud were examined in a set of 27 simulations. The baseline transport simulation, run S3R19B, served as the basis for evaluation of the influence of the various factors. The factors are divided into two groups: hydrologic factors and model-design considerations. The hydrologic factors include aquifer parameters, hydrologic stresses, and source configuration. The model-design considerations include the location of boundaries relative to the tracer cloud and the type of boundaries.

The set of simulations is summarized in Table 4-5. The table is organized so that the baseline run forms the second column. The runs on either side vary from the baseline run only in the characteristic shown in the table. All other parameters for runs in a given row are identical to those in the baseline run.

The sensitivity of downward movement to changes in a given factor is shown graphically by plotting the vertical position of the center of mass (the first moment in the y-direction) versus time. It should be noted that the horizontal distances traveled in a given time varied from simulation to simulation because of the different trajectories followed by the tracer clouds. However, horizontal flow dominated in most simulations, so the differences in horizontal displacement between runs generally were small.

Table 4-5. Model runs and factors examined for effect on density-induced downward movement.

FACTOR	**RUN NUMBER**				
Density DRWDU	**S3R20B** 0.4805	**S3R19B** 0.9610	**S3R18B** 1.9220		
Longitudinal Dispersivity α_L; α_T = 0.005 m	**S3R23B** 0.0 m	**S3R19B** 0.05 m	**S3R42B** 0.10 m	**S3R24B** 1.0 m	
Anisotropic Permeability K_V:K_h (K_V/K_h)		**S3R19B** 1:1 (1.0)	**S3R22B** 1:1.2 (0.83)	**S3R21B** 1:5 (0.20)	
Recharge to Top Boundary cm/day		**S3R38B** 0.0 cm/d	**S3R39B** 0.14 cm/d	**S3R40B** 3.545 cm/d	**S3R41B** 14.18 cm/d
Source Size X_L x Y_L (m) AR = Aspect ratio (total mass)	**S3R27B** 2.2 x 1.3 AR 1.69 (1.09)	**S3R19B** 3.2 x 1.8 AR 1.78 (2.25)	**S3R26B** 4.4 x 2.5 AR 1.76 (4.39)		
Source Aspect Ratio X_L/Y_L (X_L x Y_L) (m)	**S3R28B** 1.02 (2.4 x 2.35)	**S3R19B** 1.78 (3.2 x 1.8)	**S3R29B** 4.0 (4.8 x 1.2)		
Source Length x-dimension (m) (y-dimension)	**S3R26B** 4.4 m (2.5 m)		**S3R30B** 3.4 m (2.5 m)	**S3R31B** 2.4 m (2.6 m)	
Top Boundary Position distance above top of cloud y-total = 12.0 m	**S3R33B** 1.4 m	**S3R19B** 1.0 m	**S3R32B** 0.6 m	**S3R36B** 0.3 m	
Type of Top Boundary boundary 1 m above top of cloud		**S3R19B** Zero flux	**S3R37B** Specified pressure		
Left Boundary Position distance to left side of cloud	**S3R34B** 1.4 m	**S3R19B** 3.4 m	**S3R35B** 5.4 m		

FACTOR	RUN NUMBER				
Type of Left Boundary boundary 3.4 m from left side of cloud		**S3R19B** Specified pressure	**S3R38B** Specified flux		
Bottom Boundary Position distance below bottom of cloud (total grid height) DRWDU = 1.9220	**S3R16B** 4.7 m (7.5 m)		**S3R15B** 6.2 m (9.0 m)	**S3R18B** 9.2 m (12.0 m)	

Hydrologic Factors

A series of simulations was done to examine various hydrologic factors that affect density-induced downward movement of a solute cloud. The factors include flow and transport parameters, such as density, dispersivity, and anisotropy of permeability; recharge; and source characteristics, such as source size, aspect ratio, and length of the initial cloud in the longitudinal direction.

Density

Two simulations were run, one in which the density of the initial tracer cloud was twice the density used in the baseline run, and one in which the density was half of that used in the baseline run. As was expected, the downward movement of the tracer cloud increases as the density of the tracer cloud increases (Figure 4-8). The density response was approximately linear, as can be seen in Table 4-6. Although the results are not shown, the cloud did not move downward when density was decoupled from the solute mass fraction and assumed to be uniform throughout the modeled domain.

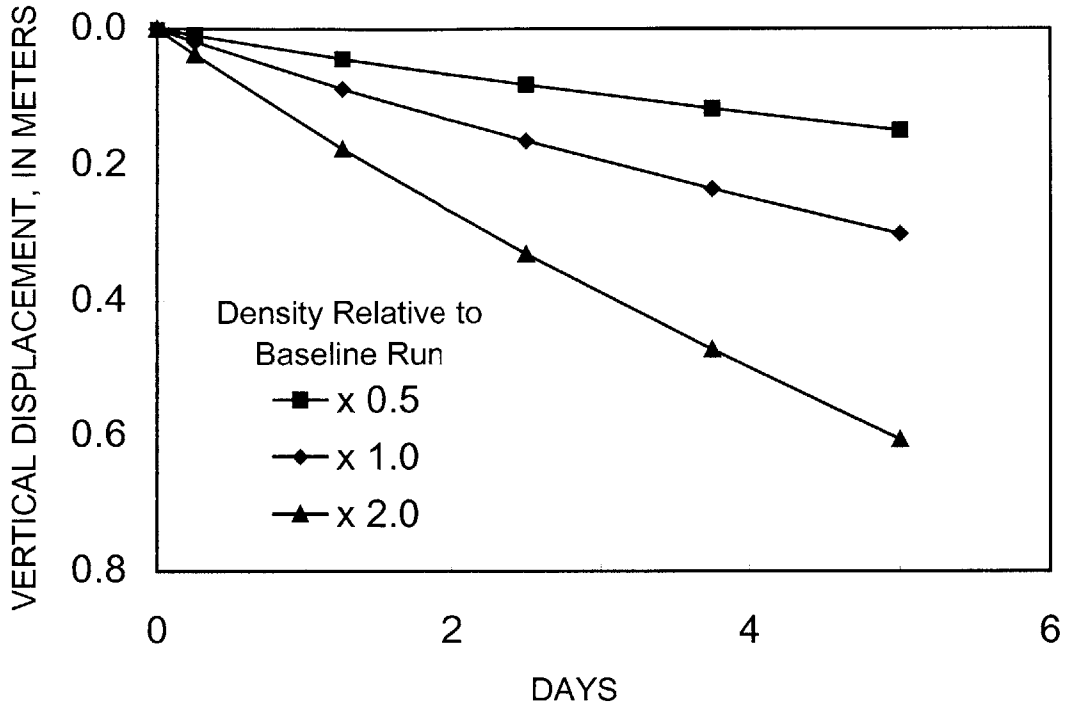

Figure 4-8. Vertical position of the center of mass of the simulated tracer cloud during a 5-day-long period for initial density differences of 0.5, 1.0, and 2.0 times the density difference of the baseline run.

Longitudinal Dispersivity

The downward movement was sensitive to the rate at which concentrations in the tracer cloud are diluted by dispersion. Figure 4-9 shows that downward movement of the center of mass decreased as the value of longitudinal dispersivity increased. As dispersion spreads the solute cloud and dilutes the concentrations, the density driving force decreases and the rate of sinking diminishes. This is most evident for run S3R24B, which has an input longitudinal dispersivity of 1.0 m, or about the asymptotic value report by Garabedian and others (1991) for

Table 4-6. Comparison of the relative downward movement of the center of mass of the simulated tracer cloud to the initial relative density contrast of the tracer solution after a 5-day-long period.

Run	Cloud density factor, DRWDU	Ratio of cloud density to baseline value	Downward movement after 5 days	Ratio of downward movement to baseline run
S3R20B	0.4805	0.5	0.149 m	0.50
S3R19B	0.9610	1.0	0.301 m	1.00
S3R18B	1.9220	2.0	0.606 m	2.01

the Cape Cod tracer test. The cloud sinks rapidly at first, but the vertical trajectory flattens out quickly as concentrations in the center of the cloud are decreased rapidly by dispersion.

As was discussed above, the effective longitudinal dispersivity is greater than the input value because of additional numerical dispersion. The trajectories shown in Figure 4-9 reflect the effective dispersion that was spreading the clouds. The additional numerical dispersion, which increases the effective dispersion (Equation 4.18), decreases the amount of downward movement that would otherwise be predicted for a given input value of longitudinal dispersivity.

Simulations were not run to examine the effect of transverse dispersivity on downward movement. For these simulations, the transverse dispersivity was 0.005 m. An increase in this value would increase the rate of dilution and decrease the rate of downward movement.

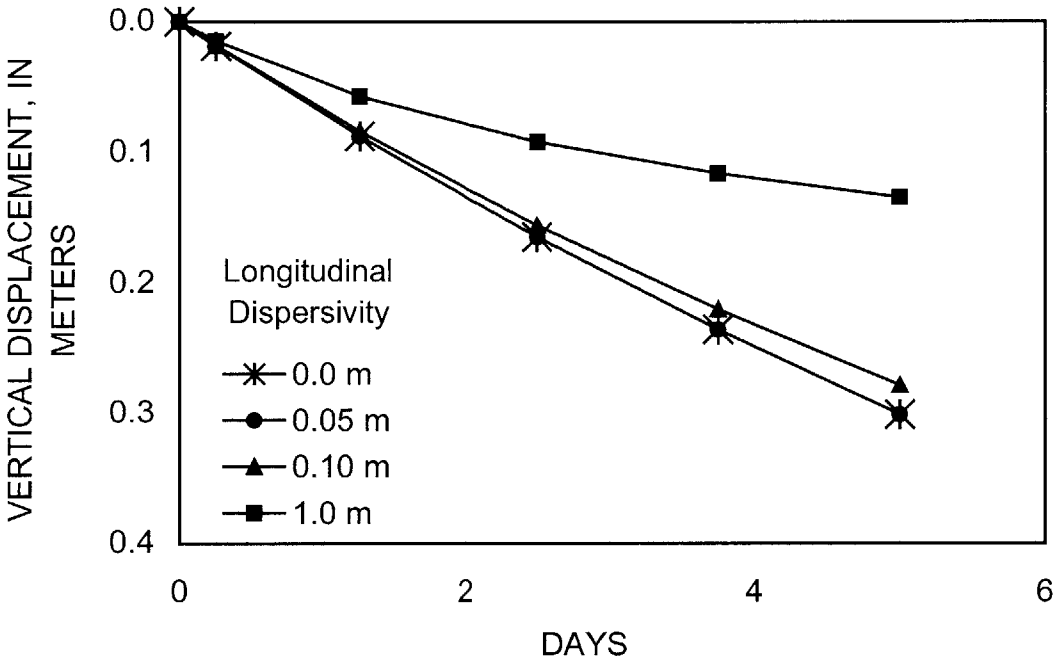

Figure 4-9. Vertical position of the center of mass of the simulated tracer cloud during a 5-day-long period for input longitudinal dispersivity values of 0.0, 0.05, 0.10, and 1.00 m.

Anisotropy of Permeability

The effect of anisotropy was examined in three simulations. An isotropic permeability (1:1) was used in the baseline run. However, Hess and others (1992) estimated an anisotropy of 1.2:1 (horizontal to vertical permeability) for the Cape Cod sand and gravel. This value is nearly isotropic compared to estimates reported for many other aquifers. A value of 5:1 is commonly used in numerical models of glacial sand and gravel aquifers.

For all three runs, the initial size and density of the clouds were the same. Prior to the introduction of the tracer cloud, the flow fields also were identical because the same value for horizontal permeability was used for all of the simulations, and the boundary conditions established strictly horizontal flow that was parallel to the maximum permeability direction. The simulations differed only in the input value for the vertical permeability.

An increase in anisotropy decreased the downward movement of the tracer cloud (Figure 4-10). The small value of anisotropy reported by Hess and others (1992) decreased the total downward movement over 5 days only slightly (about 10 percent). However, a greater value of

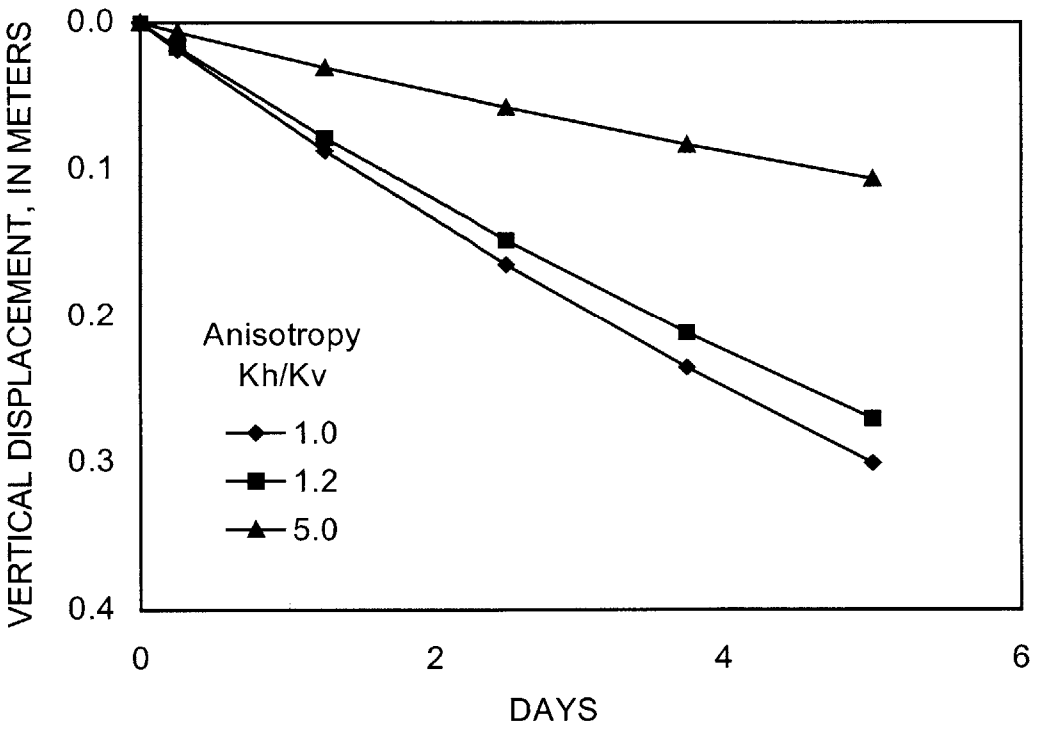

Figure 4-10. Vertical position of the center of mass of the simulated tracer cloud during a 5-day-long period for ratios of horizontal to vertical permeability of (1:1), (1.2:1), and (5:1).

anisotropy (5:1) flattened the trajectory of the tracer cloud and decreased the total downward movement over 5 days by about 65 percent.

The tracer cloud perturbs the ambient flow field by introducing pressure variations that result from the spatial variations in fluid density. The vertical components of the pressure gradient increase as the dense tracer cloud sinks and the ambient fluid moves up and around the cloud. However, the resulting flow directions are skewed in the direction of the maximum permeability direction by the anisotropic permeability. All else being equal, the amount of downward movement decreases as the preference for flow along the maximum permeability direction increases.

Areal Recharge

The water-table aquifer at the Cape Cod site is recharged by precipitation. The flux of water at the water table creates a downward component of flow that increases the downward movement of the tracer cloud. The amount of additional downward movement depends on the recharge amount and the proximity of the tracer cloud to the water table.

Four simulations were run to examine the downward movement of the tracer cloud when both density differences and recharge are factors. The recharge was applied uniformly along the top boundary of the model grid at a constant rate over time.

Four recharge rates were simulated. No recharge was applied during the baseline run. Three hydrologically reasonable recharge rates were estimated from LeBlanc and others (1991), including an average annual daily rate and two rates estimated from an intense storm on August 26-27, 1985. A summary of the estimated rates is shown in Table 4-7.

Table 4-7. Recharge rates applied uniformly in time and space along the top row of model cells in runs S3R39B, S3R40B, and S3R41B.

Run	Nominal recharge rate	Notes
S3R38B	0.0	From baseline run with specified-flux upstream (left) boundary
S3R39B	50 cm/yr 1.58×10^{-8} m/s	Estimated average annual recharge rate (LeBlanc and others, 1991, p. 897)
S3R40B	7.09 cm/48 hours 4.10×10^{-7} m/s	Estimated recharge for an August 1985 storm (7.09 cm) assumed to have occurred over a 48-hr period (LeBlanc and others, 1991, fig. 5)
S3R41B	7.09 cm/12 hours 1.64×10^{-6} m/s	Estimated recharge for an August 1985 storm (7.09 cm) assumed to have occurred over a 12-hr period

The recharge was input into the model as a specified fluid source with a solute mass fraction of 0.0 along the top row of nodes of the model grid. In SUTRA, sources of fluid are specified node-by-node as total mass per second. Therefore, even with a uniform recharge rate, the nodal inputs vary depending on the grid spacing (Voss, 1984, p. 268). The nodal values for the four simulations were calculated from the rates shown in Table 4-7, the horizontal grid spacing (Δx), and a unit thickness perpendicular to the modeled section, and a density of the recharged water of 1,000 Kg/m^3.

The ambient flow in the baseline run was established by lateral specified-pressure boundaries. The fluid flux across the boundaries would be changed by the additional inflow across the upper boundary. At sufficiently high recharge rates, a pressure divide could form and outflow could occur at both lateral boundaries. In the real system, inflow across the upstream

boundary also would increase because the increased recharge would not be restricted to the modeled area.

To approximate the real situation, the upstream boundary was converted from a specified-pressure boundary to a specified-flux boundary. The baseline flow model (S3R19) was run to obtain a steady-state solution, and the node-by-node inflows at the specified-pressure boundary were obtained as model output. The fluxes were used to specify an upstream flux boundary in a new simulation without recharge (S3R38B) to insure that the calculated steady-state pressure field was the same for both types of boundary conditions. The new upstream (left) specified-flux boundary was then used, along with recharge at the top of the model and the specified pressures at the downstream (right) boundary from the baseline run, to calculate a new steady-state pressure field for the transient transport simulations.

As expected, the addition of recharge along the upper boundary increased the downward movement of the tracer cloud (Figure 4-11). The additional downward movement was small for the simulation that used the average annual recharge rate (0.14 cm/d, S3R40B). In the 5-day-long simulation period, only about 0.68 cm of water was added above the tracer cloud, which would fill a 0.018-m interval when corrected for the porosity (Table 4-8). The vertical position of the cloud for this simulation was about 0.014 m lower than for the zero-recharge simulation, so the two values are comparable. The additional downward movement because of recharge was much larger for the higher recharge rates. At the highest rate, which occurred over a 12-hour period (Table 4-7), about 17.8 cm of water was added above the tracer cloud in 1.25 days, which would occupy a 0.45-m interval when corrected for the porosity. The vertical position of the cloud for this simulation (14.19 cm/d, S3R41B) was about 0.36 m lower than for the zero-recharge simulation.

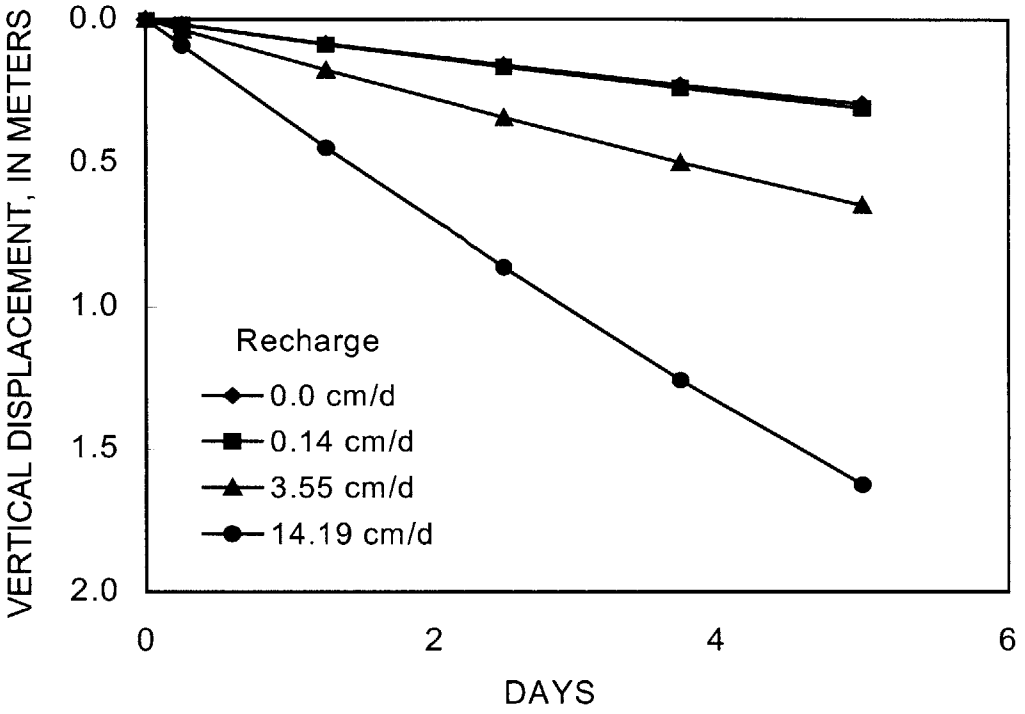

Figure 4-11. Vertical position of the center of mass of the simulated tracer cloud during a 5-day-long period with recharge to the top boundary of the model at rates of 0.0, 0.14, 3.55, and 14.19 cm/d.

The additional downward flow because of recharge is greatest at the water table and diminishes to zero at the no-flow boundary along the bottom of the modeled area. Therefore, the amount of downward movement of the tracer cloud because of recharge is dependent upon the thickness of the simulated section and the vertical position of the cloud relative to the upper and lower model boundaries. Recharge will affect the vertical movement of a tracer cloud most strongly when the cloud is near the recharge boundary. The amount of downward movement is less than the equivalent thickness of the recharge water in the porous medium because flow is not

Table 4-8. Comparison of estimated vertical thickness occupied by cumulative recharge in the aquifer to simulated additional downward movement of the tracer cloud for four recharge rates at 1.25 and 5 days [Interval equals cumulative recharge divided by porosity].

Run	Recharge rate (cm/d)	1.25 Days		5.00 Days	
		Estimated vertical thickness	Additional downward movement	Estimated vertical thickness	Additional downward movement
S3R38B	0.0	0.0 m	0.0 m	0.0 m	0.0 m
S3R39B	0.14	0.004 m	0.004 m	0.018 m	0.014 m
S3R40B	3.55	0.11 m	0.092 m	0.45 m	0.35 m
S3R41B	14.19	0.45 m	0.36 m	1.82 m	1.33 m

strictly in the vertical direction, and the recharge water is being carried laterally at an increasing rate to compensate for the additional flux being added to the system along the flow path.

Source Size

The effect of source size was tested in several simulations in which the relative shapes of the initial tracer clouds were approximately the same despite their different sizes. The aspect ratio of the clouds (x-length divided by y-height) was about 1.75, but the initial masses ranged from half (1.09) to twice (4.39) the initial mass (2.25 solute mass fraction units) of the baseline run (Table 4-5). The distance from the top of the source to the upper no-flow boundary of the model was 1.0 m for all of the simulations to eliminate possible boundary effects.

Figure 4-12 shows that downward movement increased with increasing size of the initial source. Elevated concentrations should persist longer in a large solute cloud than in a small solute cloud as the cloud disperses. Therefore, the downward movement of a large cloud should be greater than the movement of a small cloud that has the same initial density. The maximum simulated concentrations at 5 days ranged from 1.03 solute mass fraction units for the largest

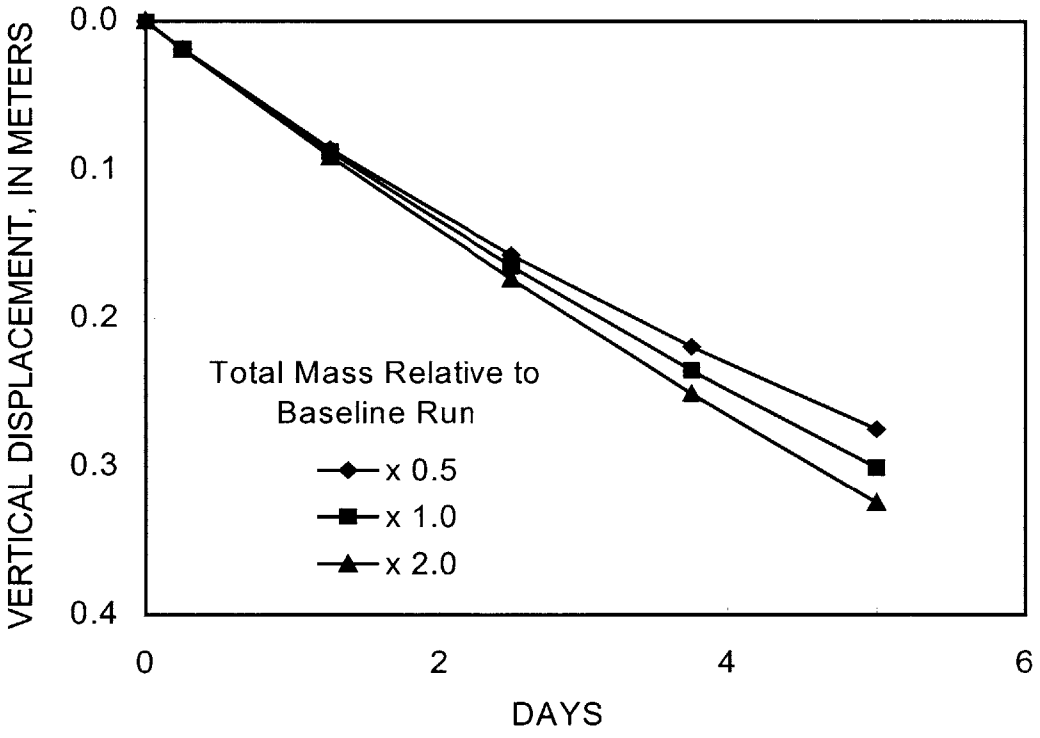

Figure 4-12. Vertical position of the center of mass of the simulated tracer cloud during a 5-day-long period for initial clouds with total masses of about half and twice the mass of the baseline run, but with similar relative shapes.

source (run S3R26B) to 0.93 for the smallest source (run S3R27B). The mass fraction exceeds 1.0 for S3R26B because of numerical oscillations.

Source Aspect Ratio

The analytical models of Yih (1963) indicate that the shape of the initial source affects the rate of density-induced sinking. The effect of source shape was examined for three rectangular tracer clouds that had the same initial mass (about 2.25 mass fraction units), but different ratios of length (x-dimension) to height (y-dimension). For all three simulations, the top of the tracer clouds was set at 1.0 m below the top boundary to eliminate possible boundary effects. The shape is characterized by the aspect ratio, which is the ratio of the length to the height of the initial tracer cloud. The aspect ratio for the baseline run was 1.78.

Figure 4-13 shows that the rate of downward movement is significantly affected by the shape of the initial cloud. The downward movement decreased with increasing elongation, or greater aspect ratio, of the initial tracer cloud. After 5 days, the cloud with an aspect ratio of about 1.0 (run S3R28) moved downward 2.4 times farther than the cloud with an aspect ratio of 4.0 (run S3R29). The maximum concentrations at 5 days were similar for the three simulations (Table 4-9), which indicates that the differences in downward movement are related to the shape and not to the rate of dilution of the concentrations.

A comparison of Figures 4-12 and 4-13 suggests that the shape of the initial cloud has a greater effect on downward movement than the size of the initial cloud. The circulation of the ambient fluid that occurs during sinking caused by density may develop more easily around the

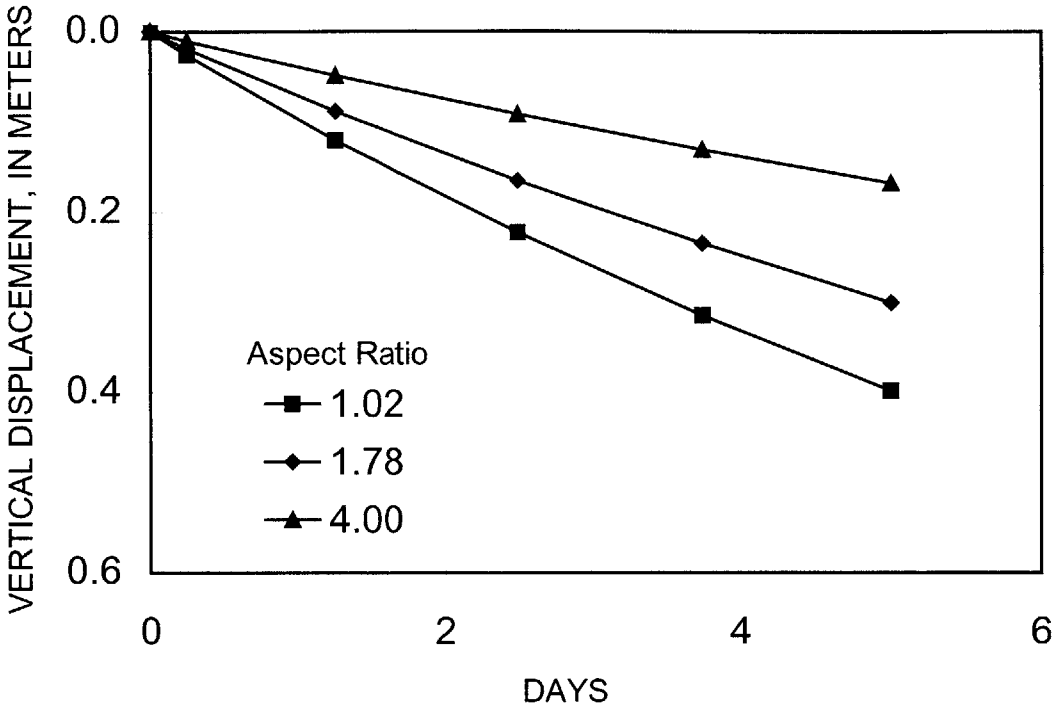

Figure 4-13. Vertical position of the center of mass of the simulated tracer cloud during a 5-day-long period for initial clouds with a total mass of about 2.25 solute mass fraction units and aspect ratios (x-dimension divided by y-dimension) of 1.02, 1.78, and 4.00.

square-shaped initial cloud (run S3R28B) than around the more elongated initial clouds (runs S3R19B and S3R29B).

Source Length

The downward movement increased as the cloud size increased for a given aspect ratio (Figure 4-12). The downward movement also increased as the aspect ratio decreased for a given

cloud size (Figure 4-13). However, these relationships are not independently applicable, as a comparison of runs S3R26B and S3R28B indicates (Table 4-10). The larger, but more elongated cloud (S3R26B), moved downward less than the smaller, but less elongated, cloud (S3R28B).

Table 4-9. Downward movement of the tracer cloud and maximum solute mass fraction after a 5-day-long period for initial tracer clouds with a total mass of 2.25 mass fraction units and aspect ratios (x-dimension divided by y-dimension) of 1.02, 1.78, and 4.00.

Run	**Total mass, in mass fraction units**	**Aspect ratio**	**Downward movement at 5 days**	**Maximum concentration at 5 days**
S3R28B	2.21	1.02	0.40 m	0.99
S3R19B	2.25	1.78	0.30 m	1.00
S3R29B	2.25	4.00	0.17 m	1.00

Table 4-10. Downward movement of the tracer cloud after a 5-day-long period for a larger, but more elongated, initial cloud (S3R16B) and a smaller, but less elongated, tracer cloud (S3R28B).

Run	**Total mass, in mass fraction units**	**Aspect ratio**	**Downward movement at 5 days**	**Maximum concentration at 5 days**
S3R26B	4.30	1.76	0.32 m	1.03
S3R28B	2.21	1.02	0.40 m	0.99

This trend suggests that the length of the tracer cloud perpendicular to the direction of the density driving force significantly affects the rate of downward movement. Three simulations were run in which the tracer clouds were 2.5 m thick (in the y-direction), but their lengths (in the x-direction) were different. Figure 4-14 shows that the amount of downward movement increased with decreasing length, even though cloud size also decreased with decreasing length.

This result makes intuitive sense when one considers the flow pattern around a tracer cloud that is sinking in an ambient flow field because of density differences. Water is displaced as the dense tracer cloud moves downward. The flowpaths of the displaced water are longer for a cloud that is long transverse to the direction of sinking than for a cloud that is thin transverse to

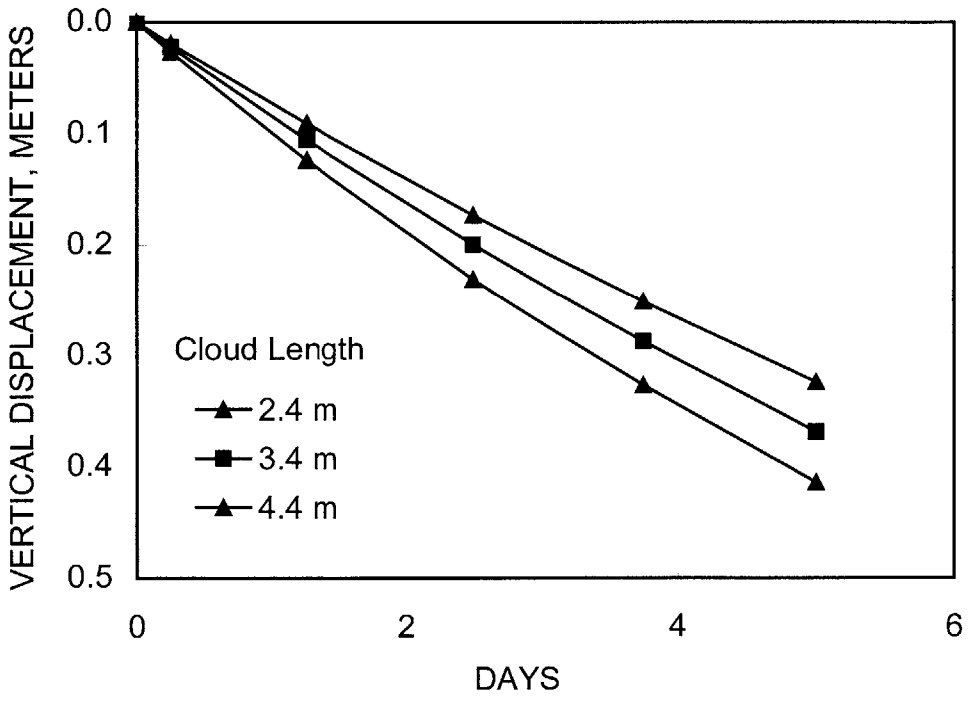

Figure 4-14. Vertical position of the center of mass of the simulated tracer cloud during a 5-day-long period for initial clouds with a thickness (y-dimension) of 2.5 m and lengths (x-dimension) of 2.4, 3.4, and 4.4 m.

the flow direction. The greater displacement that is needed produces a greater resistance to downward movement. In an analogous manner, a sleek naval destroyer moves more efficiently through the water than a blunt-nosed barge.

Model-Design Factors

The hydrologic factors considered thus far are based on the real-world physical system. Density, dispersivity, and cloud shape and size can vary from field site to field site. However, representation of the field situation with numerical models gives rise to model-design considerations that also may affect the predicted amount of downward movement of a dense tracer cloud. In an earlier section of this chapter, simulated concentrations and, therefore, densities, were shown to be affected by spatial and temporal discretization. A coarse spatial discretization can cause numerical oscillations, whereas a coarse temporal discretization can cause significant numerical dispersion for this time-stepping algorithm. This section examines the effects of boundary location and type on the simulated downward movement of the tracer cloud. All the simulations use the same density, shape, and size of the initial tracer cloud. The position of the cloud relative to the boundaries and the types of boundaries were changed for the various simulations.

Distance to Top Boundary

Four simulations were run to examine the effect of the distance from the top boundary of the model domain to the top of the initial tracer cloud. The distance was varied by repositioning the initial cloud vertically without changing the y-dimension of the model domain (12.0 m).

Figure 4-15 shows that the rate of downward movement decreased as the cloud was located closer to the top, no-flow boundary. The cloud whose top edge was located 0.3 m from the top boundary (S3R36B) moved downward about 21 percent less than the cloud whose top edge was located 1.4 m from the top boundary (S3R33B). The boundary affects the amount of downward movement by affecting the ease with which water can move into the area above the sinking tracer cloud. When the cloud is located close to the top boundary, this circulation must occur through a narrow zone, and pressures drop accordingly above the cloud to induce the inflow. The pressure drop decreases the effective downward forces on the solute cloud and reduces the rate of downward movement.

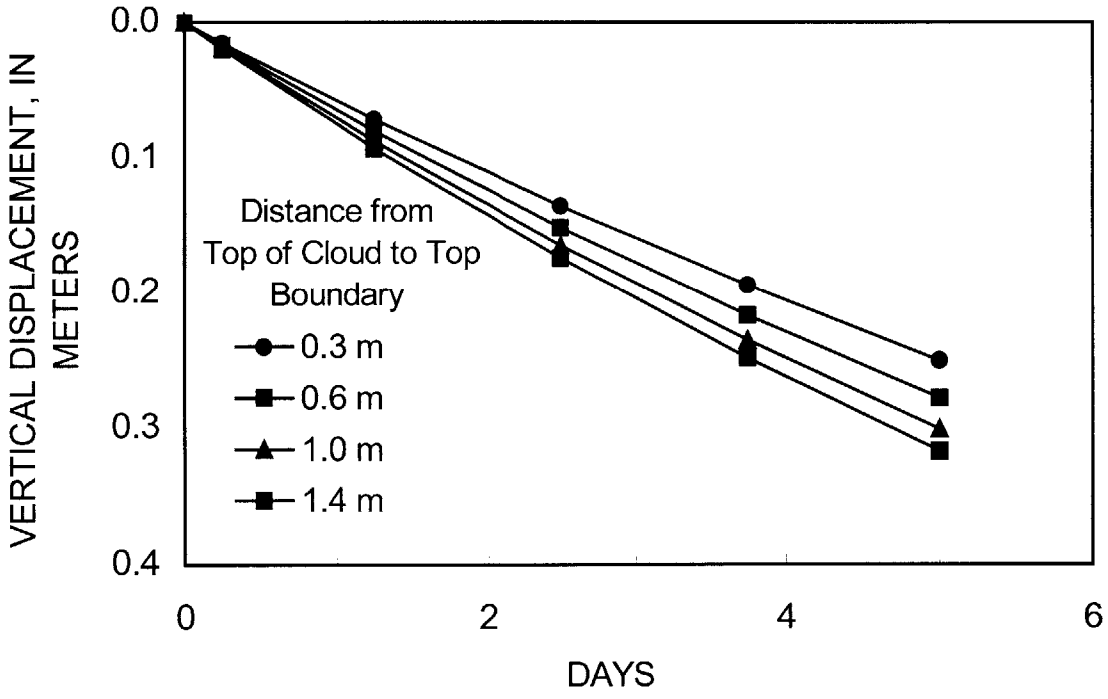

Figure 4-15. Vertical position of the center of mass of the simulated tracer cloud during a 5-day-long period for distances of 0.3, 0.6, 1.0, and 1.4 m from the top edge of the initial tracer cloud to the upper no-flow boundary of the model.

Type of Top Boundary

The importance of the top boundary is even more evident when the type of boundary condition is considered. In the baseline run (S3R19B), the top boundary was specified as a no-flow boundary. In a second simulation (S3R37B), the top boundary was set as a specified-pressure boundary across which fluid flow can occur in response to changes in pressure in the modeled area.

The ambient flow field from the baseline run was duplicated by assigning pressures along the top boundary that preserved the horizontal flow field and total fluid flux across the model domain. The pressures were calculated for the nodes along the top row of the model grid by assuming a linear decrease in the horizontal hydraulic gradient across the model domain. The ambient pressure field was obtained from a steady-state flow simulation with the specified-pressures boundaries on the left and right sides from the baseline run and the newly specified-pressure boundary at the top of the model. A comparison of the baseline run to the newly simulated flow field indicated that the pressure fields were identical and fluid flux across the top specified-pressure boundary was zero prior to introduction of the solute tracer cloud. The fluid flux was obtained from the SUTRA output, which reports the flux rate at each specified-pressure node in Kg/s (assuming a unit width transverse to the model section)

Figure 4-16 shows that the downward movement of the tracer cloud was significantly greater with a specified-pressure boundary than with a no-flow boundary. After 5 days, the vertical displacement of the tracer cloud with the no-flow boundary was about 73 percent of the vertical displacement with the specified-pressure boundary. The cause for the increased downward movement with a specified-pressure top boundary is evident in a graph of fluid flux across the top boundary (Figure 4-17). As the tracer cloud begins to move downward because of

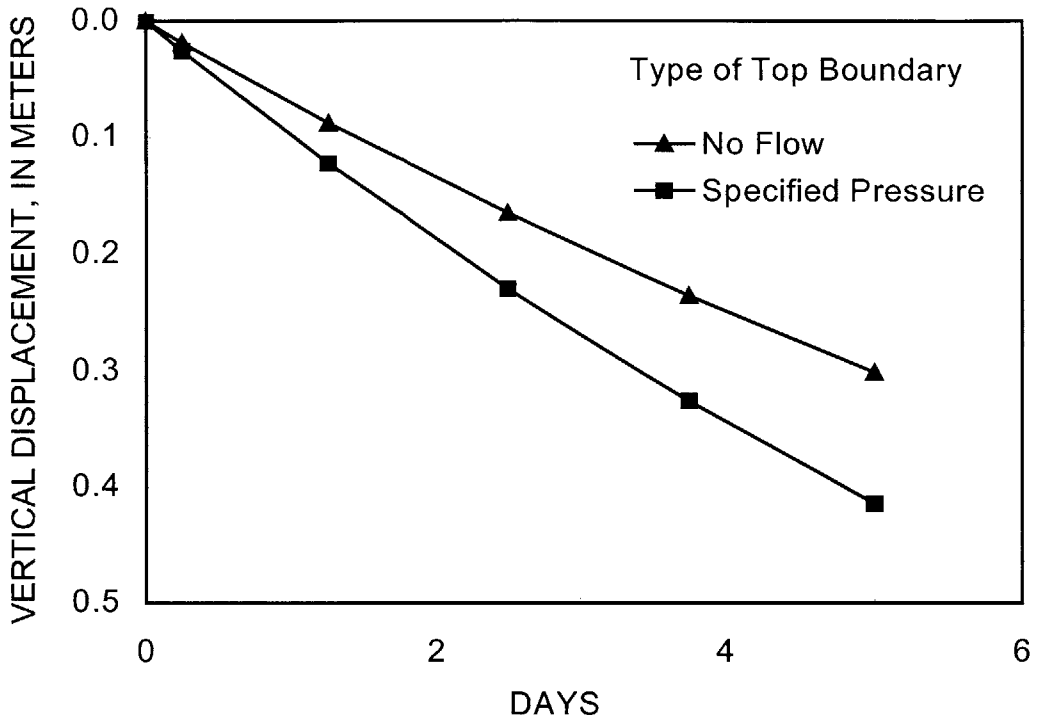

Figure 4-16. Vertical position of the center of mass of the simulated tracer cloud during a 5-day-long period for no-flow and specified-pressure boundaries at the upper boundary of the modeled area.

density differences, water moves into the model domain across the specified-pressure boundary to fill in the area being left by the sinking tracer cloud, rather than having to flow up and around the cloud. The amount of inflow decreases as the tracer cloud sinks farther below the boundary.

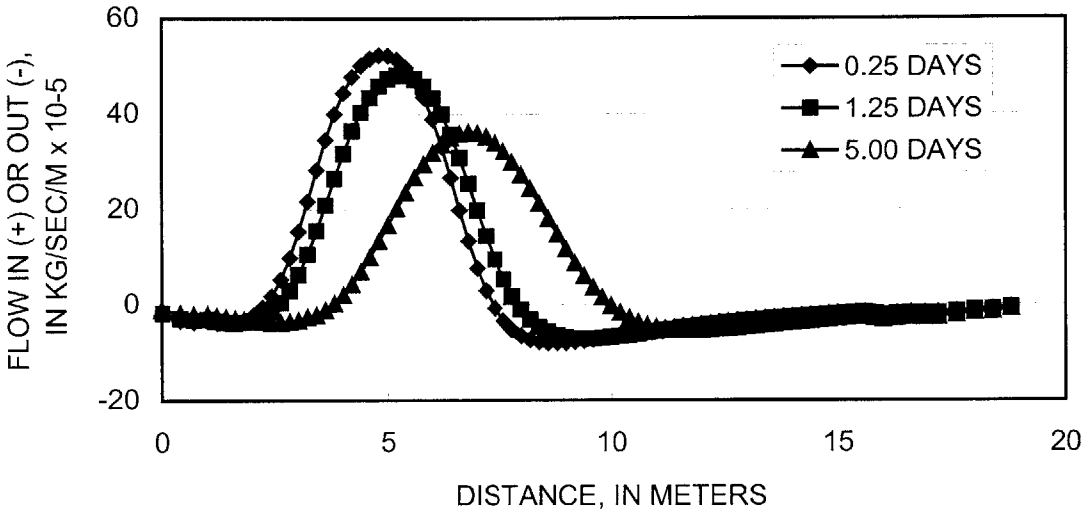

Figure 4-17. Calculated fluid flux across the specified-pressure boundary along the upper boundary of the modeled area at 0.25, 1.25, and 5 days after introduction of the tracer cloud.

The inflow across the specified-pressure boundary directly above the sinking cloud is partly offset by smaller flows out of the model domain upstream and downstream of the tracer cloud. These inflows occur because of subtle pressure gradients that develop in the areas of upward flow adjacent to the cloud as water is displaced laterally by the sinking cloud. The flows across the top specified-pressure boundary are small compared to the total flow across the model domain. At 1.25 days, the simulated inflow above the tracer cloud was only about 5 percent of the simulated flow into the model domain across the upstream (left) specified-pressure boundary. The relatively small inflow, however, locally affected the circulation around the cloud and increased the rate of downward movement.

Distance to Left Boundary

The initial position of the tracer cloud in the baseline run was near the upstream specified-pressure boundary on the left side of the model domain. Three simulations were run to examine the effect of the distance from the left edge of the tracer cloud to the boundary. The distance was varied without changing the vertical position of the initial cloud.

The distance to the left boundary had only a small effect on the amount of downward movement for the three cases that were simulated (Figure 4-18). For the cases in which the left

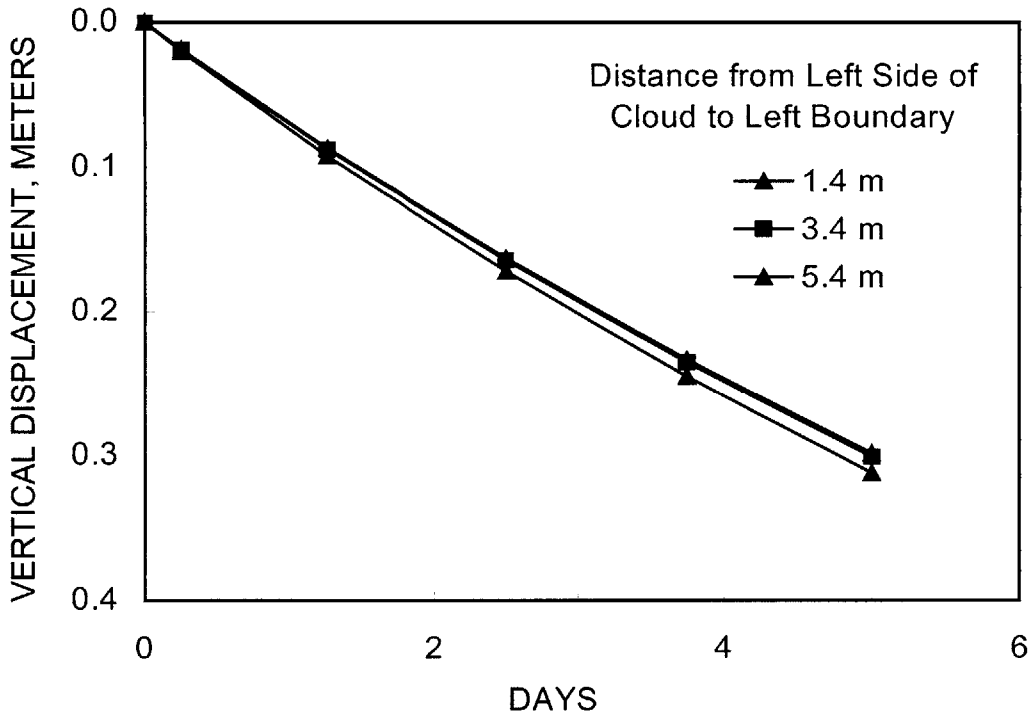

Figure 4-18. Vertical position of the center of mass of the simulated tracer cloud during a 5-day-long period for distances of 1.4, 3.4, and 5.4 m from the left edge of the initial tracer cloud to the upstream (left) specified-pressure boundary.

edge of the cloud was 3.4 m and 5.4 m from the boundary, the simulated amount of downward movement after 5 days was almost the same. The downward movement after 5 days was only slightly greater (0.014 m, or 4 percent) when the left edge of the cloud was 1.4 m from the boundary instead of 5.4 m from the boundary.

The small increase in downward movement when the cloud was nearest the upstream specified-pressure boundary probably was the result of changes in fluid flux along the boundary. As the cloud moved downward because of the density differences, pressure changes transmitted to the boundary caused local increases and decreases in inflow along the boundary. The changes in flow short-circuited the circulation that developed around the sinking cloud and enabled water to be replaced above the cloud more easily. The very small additional downward movement (about 0.002 m in 5 days) as the cloud was shifted from 3.4 to 5.4 m from the boundary indicates that the influence of the upstream boundary on the rate of downward movement is minimal in the baseline run.

Type of Left Boundary

The minimal influence of the upstream, specified-pressure boundary when the left edge of the tracer cloud is at least 3.4 m from the boundary was confirmed by changing the boundary to a specified-flow boundary. The method used to obtain the flow rates for each node along the boundary is described in an earlier section of this report. With the specified-flux boundary, flows cannot change in response to the sinking tracer cloud. Figure 4-19 shows that the downward movement was slightly greater after 5 days (0.006 m greater) for the specified-pressure boundary than for the specified-flux boundary. The cause for slight difference is the short-circuiting of the circulation around the sinking cloud at the specified-pressure boundary.

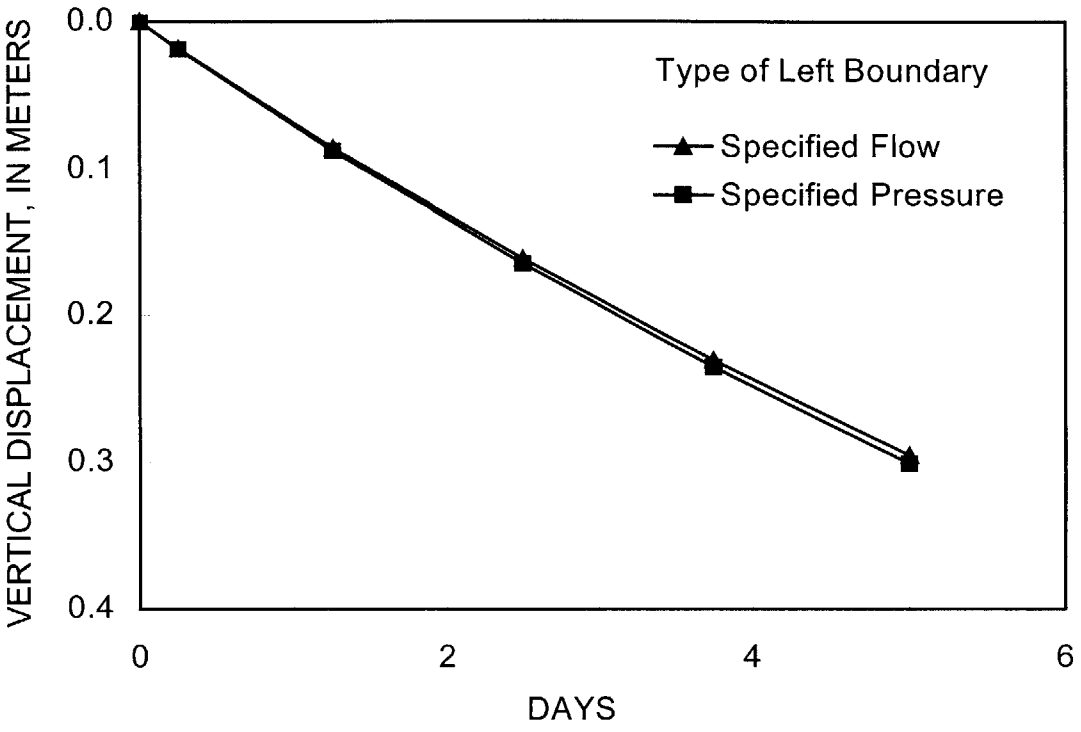

Figure 4-19. Vertical position of the center of mass of the simulated tracer cloud during a 5-day-long period for specified-flux and specified-pressure boundaries at the upstream (left) boundary of the modeled area.

Distance to Bottom Boundary

All of the simulations described in this chapter thus far were based on the baseline model grid, which is a vertical section that is 12 m high and 20 m long (Table 4-1). The effect of the distance from the initial tracer cloud to the bottom boundary of the modeled area was tested in three simulations with different total grid sizes in the vertical direction (Table 4-11) and different

distances from the bottom edge of the cloud to the bottom of the modeled area. The initial clouds were the same size and were at the same distance from the top and left boundaries as the baseline run. The density difference, however, was twice the value used in the baseline run to cause a more rapid downward movement of the tracer cloud.

Table 4-11. Grid spacing in the vertical direction for three simulations used to examine the effect of the bottom boundary on downward movement.

S3R16B (Bottom edge of cloud 4.7 m above bottom boundary)		**S3R15B** (Bottom edge of cloud 6.2 m above bottom boundary)		**S3R18B** (Bottom edge of cloud 9.2 m above bottom boundary)	
Grid spacing (m) times number of cells	**Cumulative distance from bottom boundary (m)**	**Grid spacing (m) times number of cells**	**Cumulative distance from bottom boundary (m)**	**Grid spacing (m) times number of cells**	**Cumulative distance from bottom boundary (m)**
--	--	--	--	2.60 x 1	2.6
--	--	1.50 x 1	1.5	1.90 x 1	4.5
1.30 x 1	1.3	1.30 x 1	2.8	1.30 x 1	5.8
0.90 x 1	2.2	0.90 x 1	3.7	0.90 x 1	6.7
0.60 x 1	2.8	0.60 x 1	4.3	0.60 x 1	7.3
0.40 x 1	3.2	0.40 x 1	4.7	0.40 x 1	7.7
0.30 x 1	3.5	0.30 x 1	5.0	0.30 x 1	8.0
0.20 x 1	3.7	0.20 x 1	5.2	0.20 x 1	8.2
0.15 x 4	4.3	0.15 x 4	5.8	0.15 x 4	8.8
0.10 x 32	7.5	0.10 x 32	9.0	0.10 x 32	12.0

Figure 4-20 shows that there was little difference (less than 0.009 m) in downward movement among the three simulations. As expected, downward movement increased, although slightly, as the distance to the bottom no-flow boundary increased. The results indicate that boundary effects related to the bottom boundary were very small for the simulations in this analysis.

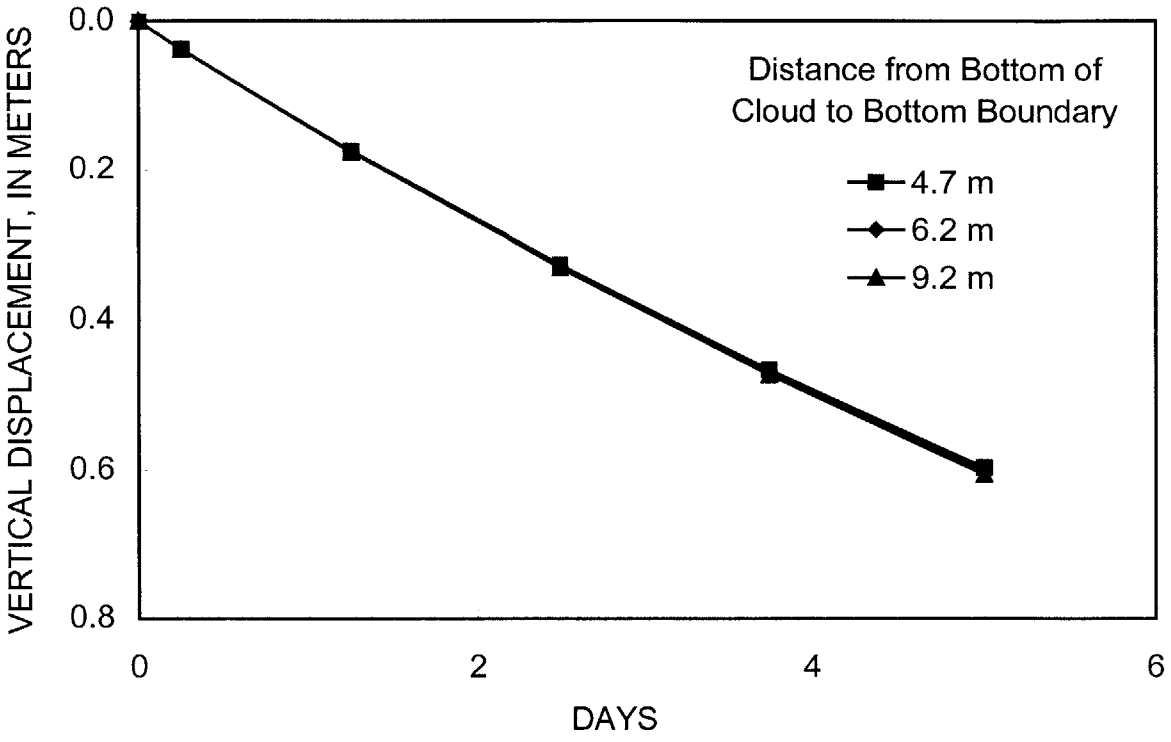

Figure 4-20. Vertical position of the center of mass of the simulated tracer cloud during a 5-day-long period for distances of 4.7, 6.2, and 9.2 m from the bottom edge of the initial tracer cloud to the bottom, no-flow boundary of

Discussion

This analysis demonstrated that the density-induced downward movement of a tracer cloud is affected by many hydrologic factors, such as density, dispersivity, anisotropic permeability, and the shape of the tracer cloud. The analysis also demonstrated that the simulated rate of downward movement is greatly affected by modeling considerations, especially

boundary specifications and discretization in time and space. Hydrologic factors and modeling issues both must be considered in the field-scale simulation of density-induced sinking during a tracer test.

As was expected, the density difference between the tracer solution and the ambient fluid is an important factor in determining the rate of downward movement. Dispersion is an important parameter because it affects the rate at which the tracer cloud is diluted and the density-difference is diminished. The dispersion process must be represented at the appropriate scale for the problem being considered. Garabedian and others (1991) used a spatial-moments analysis to show that dispersivity increased with travel distance during the Cape Cod tracer test until it reached an asymptotic value. The scale dependence of dispersivity has been described theoretically by Gelhar and Axness (1983) and Dagan (1982). The amount of density-induced downward movement could be significantly under-predicted if an inappropriately large dispersivity is used during the early part of a tracer test.

The preceding analysis examined only the effect of changes in the value of longitudinal dispersivity. Although transverse dispersivity is an order of magnitude or more smaller than the longitudinal value, transverse dispersion could still be a significant factor in some situations. For example, concentrations in a very long, thin tracer cloud that is moving parallel to its long dimension could be diluted rapidly by transverse dispersion.

The permeability also affects the downward movement. The forces caused by density operate in the vertical direction. In most field situations, however, these forces are added to the ambient, predominantly horizontal potential gradients. Although the downward component of the driving force may be substantial, the resulting flow direction will be affected by the anisotropy of the permeability field. Because most aquifers are more permeable in the horizontal

than in the vertical direction, flow will be biased toward the horizontal direction. The simulations suggest that, even in an aquifer than would be considered only weakly anisotropic (for example, k_H/k_V = 5:1), the amount of downward movement can be substantially less than in an equivalent isotropic medium.

The initial shape of the tracer cloud also greatly affects the rate of downward movement. Because the ambient fluid must move up and out of the way of the sinking tracer cloud, the horizontal dimensions of the cloud are the most important consideration in determining the downward movement. A sinking cloud with a small horizontal cross-sectional area will encounter the least resistance from the ambient fluid. Even a cloud with a large total mass may sink less than a cloud that has a smaller mass, but also a smaller cross-sectional area. The importance of the cloud shape poses a particular problem in the simulation of field tracer tests, in which the shape of the actual cloud is usually unknown and is represented as an idealized regularly shaped volume in the subsurface. A locally present high-permeability layer could cause the injected cloud to be a thin, areally extensive body rather than a circular blob; this would reduce the amount of downward movement relative to the predicted amount.

The representation of areal recharge in a two-dimensional cross-sectional model is problematic because of the difficulty of representing fluxes at the upstream and downstream boundaries accurately. Despite these difficulties, the simulations showed that recharge can cause significant downward movement over several time scales. Recharge from individual storms, such as those that occurred in late August 1985 during the Cape Cod tracer test, can have a rapid and substantial effect on the observed downward movement and mask the additional, slow but steady, downward movement caused by density differences.

Modeling considerations can have a significant effect on the predicted amount of density-induced sinking. Boundary effects can be particularly important, depending on the geometry of the problem and the size of the modeled domain. In these analyses, the bottom boundary had little effect on the downward movement because the boundary was set sufficiently far below the path and hydraulic influence of the tracer cloud. However, the no-flow boundary could limit downward movement if the density contrast was larger or the recharge rate was greater than in these simulations. The upstream boundary at the left side of the model also had little effect on the downward movement, although its influence would increase significantly if the initial tracer cloud were too close to the boundary.

The most critical boundary in these simulations was the top boundary because the initial tracer cloud was only 1 m from the boundary and the density forces act in the vertical direction. As the tracer cloud moves downward, the ambient fluid is displaced and moves up and around the cloud to fill the area left by the sinking cloud. Pressures drop above the sinking cloud to induce inflow of the ambient water. The type and position of the top boundary affect this circulation, which must occur in order for the cloud to sink. With a no-flow upper boundary, all of this inflow must come from the modeled area. If the tracer cloud is too close to the boundary, the smaller area for inflow reduces the ability of the cloud to move downward through the ambient fluid. With a specified-pressure upper boundary, water can move easily across the boundary into the model to fill in the area left by the sinking cloud. In essence, the flow is short-circuited and the resistance to downward movement is decreased.

The no-flow and specified-pressure boundaries are only approximations to the water table, which is the upper boundary at the Cape Cod field site. The water table is a free surface whose position changes in response to stresses in the flow system. When the tracer cloud begins

to move downward, the pressure drop above the cloud probably causes a dimple to form in the water table above the cloud. This dimple, which is like a cone of depression, allows water to move into the area left by the sinking cloud by both dropping the free surface and inducing lateral flow. As the cloud sinks farther below the water table, the effectiveness of lateral flow increases and the dimple diminishes with time.

The specified-pressure boundary also provides a source of water as the cloud begins to move downward. Because this is limitless source of water, it causes an over-prediction of the downward movement. On the other hand, the no-flow boundary forces all the water to come from lateral inflow and probably causes an under-prediction of the downward movement. A saturated-unsaturated flow and transport model that explicitly simulates the free surface would be a better representation of the physical system, but this more sophisticated approach introduces additional parameters with significant uncertainties that can influence the predicted downward movement.

These simulations represented flow and transport in a two-dimensional vertical plane. In the previous chapter, it was demonstrated using the models of Yih (1963) that downward movement would be greater in a three-dimensional system. However, the relative importance of the hydrologic and modeling factors that were examined in this chapter would be the same in the two- and three-dimensional systems.

The simulations also assumed a homogeneous aquifer, but a heterogeneous permeability is characteristic of most aquifers, including the Cape Cod aquifer (Hess and others, 1992). A low-permeability layer beneath the tracer cloud could impede downward movement and decrease the apparent influence of the density differences. Heterogeneity also could affect the shape of the initial tracer cloud, which has been shown to significantly affect downward movement. If the

tracer solution was injected into the aquifer during a finite period, rather than being emplaced instantaneously in the ambient fluid, the cloud is likely to have an irregular shape that reflects the presence of higher permeability zones. This irregular shape would be imprinted upon the cloud as it moves with the ambient fluid and moves downward because of density and recharge.

CHAPTER 5

NUMERICAL SIMULATION OF THE CAPE COD TRACER TEST

LeBlanc and others (1991) reported that the tracer cloud moved downward about 3.2 m during the first 237 days of the 1985-88 Cape Cod tracer test. This amount is about 70 percent of the total downward movement observed during the entire 511-day experiment. LeBlanc and others (1991) noted that vertical flow caused by accretion of recharge could account for only part of the downward movement. They hypothesized that the additional downward movement was caused by the density difference between the ambient ground water and the tracer solution.

In this chapter, the numerical model SUTRA is used to test the density hypothesis. The simulation focused on the first 237 days of the experiment, when the density effects would have been greatest. The information developed in the previous chapter was used to design the simulation so it represented as closely as practical the conditions during the field experiment.

Design of the Simulations

The numerical code SUTRA, which was described in the previous chapter, was used for the field-scale simulation of the Cape Cod tracer test. Application of the model to the Cape Cod test was similar, in most regards, to the use of the model to examine the sensitivity of density-induced sinking to various hydrologic and model-design factors. Many of the parameters used in the baseline run (S3R19B) and shown in Table 4-2 were also used for the field-scale simulation. This section will discuss the significant changes that were made to simulate the field test,

particularly the changes related to boundary conditions, grid size and discretization, and recharge.

Several conclusions from the sensitivity analysis described in the previous chapter were used to guide the design of the field-scale simulation. It is obvious that accurate specification of the ambient flow rate, density of the tracer cloud, and anisotropy is important to the success of the simulations. The source shape was shown to be particularly important, but an initial shape that was more complex than a rectangular source could not be justified from the field data. Dispersivity also is an important parameter because it controls the dilution of the tracer cloud. The previous analysis showed that grid design and temporal discretization must be selected carefully to control undesirable numerical oscillations and numerical dispersion. Finally, the location and type of the boundaries, particularly the top boundary that represents the water table, can greatly affect the predicted downward movement caused by density differences.

Modeled Area

The first step in the design of the simulations was the identification of the model domain, or the overall extent of the modeled area. The observed path and size of the tracer cloud were the primary considerations in setting the extent of the domain. The modeled area was selected so that the upper boundary coincided with the water-table position, and the cloud remained in the modeled area for the entire 237-day-long simulation. The thickness of the aquifer was also considered in setting the height of the modeled area.

Height of the Modeled Area

The estimated location of the water table and the trajectory and shape of the cloud during the first 237 days of the experiment were the main factors in determining the height (y-direction) of the modeled area. The tracer cloud was injected near the water table, so the top boundary was set to coincide with the water-table position. At the start of the field test, the water-table altitude was about 13.8 m above sea level.

The spatial moments of the concentration data in Garabedian and others (1991, Table 1) describe the observed path and size of the tracer cloud relative to sea level as it moved and dispersed over the 237 days (Table 5-1). The vertical location and thickness of the observed cloud at 237 days can be estimated from the first and second moments in the vertical direction:

$$\bar{y} \pm 2s_{y'}, \tag{5.1}$$

where $\bar{y}$ = first moment (center of mass) in the vertical direction and $s_{y'}$ is the square root of the principal component of the second moment (the variance) in the vertical direction. Using the values from Table 5-1, 95 percent of the mass (two standard deviations) at 237 days was located between 11.4 and 7.2 m above sea level, or from 2.4 to 6.6 m below the water table.

The thickness of the aquifer also was considered in the height of the modeled area. LeBlanc and others (1991) stated that the permeable, stratified sand and gravel was 30 m thick at the tracer-test site. Sediment cores collected at a site adjacent to the path of the tracer cloud showed coarse sand and gravel to a depth of 29 m underlain by silty sediments. The water table at this site was 4 m below land surface, so the thickness of the saturated sand and gravel was about 25 m.

Table 5-1 Observed spatial moments and estimated size of the tracer cloud for first 237 days of the Cape Cod tracer test (adapted from Garabedian and others, 1991, Table 1)[Only moments along vertical section aligned with path of cloud are shown. The y and z directions in Garabedian and others (1991) are shown as x and y directions for consistency. $\bar{x}'$, total travel distance relative to injection point; $\bar{y}$, altitude above sea level; $s^2_{x'}$, principal component of variance in longitudinal direction; $s^2_{y'}$, principal component of variance in transverse direction].

Days after injection	**Center of mass (first moment, m)**		**Principal components of variance (second moment, m²)**		**Estimated size of tracer cloud (95 percent of mass, m)**	
	$\bar{x}'$	$\bar{y}$	$s^2_{x'}$	$s^2_{y'}$	$\bar{x}' \pm 2s_{x'}$	$\bar{y} \pm 2s_{y'}$
0	0	12.5	--	--	--	--
13	7.4	12.3	6.5	0.37	2.3-12.5	11.1-13.5
33	17.1	11.7	20.2	0.46	8.1-26.1	10.3-13.1
55	26.1	11.1	34.8	0.50	14.3-37.9	9.7-12.5
83	39.4	10.6	52.4	0.72	24.9-53.9	8.9-12.3
111	51.7	10.3	85.6	0.73	33.2-70.2	8.6-12.0
139	65.6	10.4	118	0.74	43.9-87.3	8.7-12.1
174	78.7	9.6	134	1.03	55.5-101.9	7.6-11.6
203	90.0	9.4	162	1.02	64.5-115.5	7.4-11.4
237	101.3	9.3	189	1.06	73.8-128.8	7.2-11.4

Based on the vertical trajectory and size of the observed cloud and the thickness of the permeable sediments, the height of the modeled area was set at 25 m (Figure 5-1). At 237 days, the bottom of the observed cloud was more than 18 m above the bottom of the modeled zone.

The influence of the bottom boundary on the simulated rate of downward movement of the cloud should be negligible at this distance.

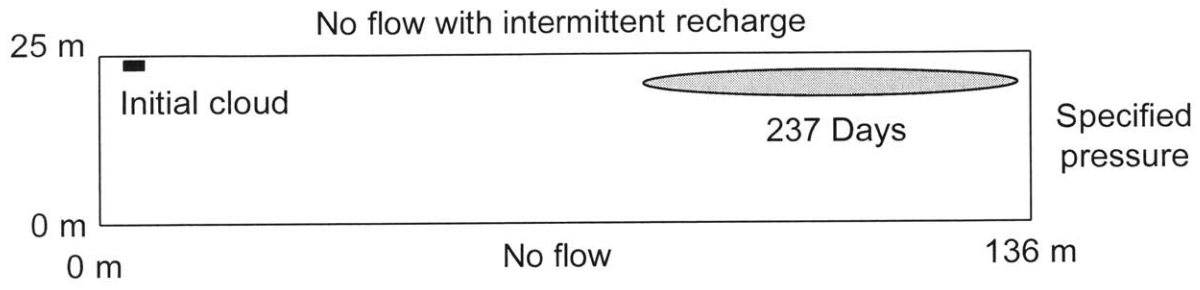

Figure 5-1. Modeled area for the field-scale simulation of the Cape Cod tracer test, including boundary conditions and expected position of the tracer cloud at 0 and 237 days.

Length of Modeled Area

The length of the modeled area was selected so that the entire tracer cloud remained in the area for the first 237 days of the tracer test. As was described in the previous chapter, the influence of the upstream boundary was small when the left edge of the 3.2-m-long cloud was at least 3.4 m from the boundary. With this configuration, the center of the cloud was 5 m from the boundary. A similar cloud size was used in the field-scale simulation (see below).

The horizontal position of the tracer cloud at 237 days was estimated from the first and second moments of the observed concentrations in the horizontal direction:

$$\bar{x}' \pm 2s_{x'}, \tag{5.2}$$

where $\bar{x}'$ = total travel distance along the path of the tracer cloud and $s_{x'}$ is the square root of the principal component of the second moment (the variance) in the horizontal direction. Using the

values from Table 5-1, 95 percent of the mass (two standard deviations) was located between 74 and 129 m from the injection point at 237 days.

Based on the horizontal positions of the tracer cloud relative to the injection wells at the start of the simulation and at 237 days, the length of the modeled area would be 134 m (5 m upgradient plus 129 m downgradient of the initial cloud). The length was increased slightly to 136 m (5.6 m upgradient and 130.4 m downgradient of the center of the initial cloud) during the grid design (Figure 5-1) to accommodate a regular spatial discretization scheme. Therefore, the final model domain was 25 m high (y-direction) and 136 m long (x-direction).

Boundary Conditions

Boundary conditions were specified around the perimeter of the modeled area for fluid flow and solute transport. The specified conditions for the fluid-flow model are shown in Figure 5-1.

For the fluid-flow model, the bottom boundary is a no-flow boundary that coincides with the bottom of the permeable sand and gravel. The top boundary coincides with the water table. In the previous chapter, it was shown that the downward movement of the tracer cloud is sensitive to the type of boundary above the cloud, particularly because the initial cloud is located within about 1 m of the water table. The simulation of the field test was designed to examine the combined effects of the density differences and recharge. Therefore, the top boundary was specified as a no-flow boundary along which there was an intermittent fluid source from the areal recharge. Although the downward movement would have been greater during periods of no recharge if a specified-pressure boundary were used, the specification of pressures and fluid

sources at the same nodes during periods of recharge would not have made hydrologic or numerical sense.

The left (upgradient) boundary was set as a specified-flow boundary, while the right (downstream) boundary was a specified-pressure boundary. The flows and pressures were specified so that the ambient steady-state flow prior to introduction of the tracer cloud was uniformly horizontal at a ground-water velocity of 0.42 m/d. The specification of flows, rather than pressures, along the upstream boundary insured that the effective direction of flow would remain from left to right, even during periods of significant areal recharge.

The inflow rates assigned along the left boundary were determined from a preliminary simulation in which the left and right boundaries were specified-pressure boundaries. The hydraulic gradient at the site was about 0.0015 m/m during the tracer test. This is equivalent to a hydraulic-head difference of about 0.2 m across the 136-m-long model domain. As in the previous chapter, the pressure distributions along each boundary were calculated using Equation (4.11) by assuming hydrostatic conditions in the vertical direction and a zero hydraulic head along the right boundary. The flow model was run to obtain a steady-state solution, and the node-by-node boundary inflows from the preliminary simulation were then used as specified fluid sources along the upstream (left) boundary in the simulation of the tracer test.

For the solute-transport simulations, the solute mass fraction of specified inflow along the left boundary was zero, the same as the solute mass fraction of the ambient ground water. Areal recharge also was assigned a zero solute mass fraction. The top, bottom, and right sides of the modeled area were specified as zero-diffusive-flux boundaries. Solute mass can cross the right boundary as advective flux.

Source Configuration

The rationale for the dimensions of the initial tracer cloud is described in the previous chapter. For the baseline run (S3R19B), the initial cloud was 3.2 m long, 1.8 m high, and 3.4 m wide (transverse to flow and not represented in the model). The initial tracer cloud was increased slightly in length to 3.4 m in the field-scale simulation to accommodate a regular grid spacing. As in the baseline run, the boundaries of the tracer cloud were represented by a linear decrease in mass fraction over two nodes rather than an abrupt transition to minimize numerical oscillations associated with sharp fronts (see Figure 4-2). For a unit width normal to the plane of the simulations, a porosity of 0.39, and an initial solute mass fraction of 1.0, the zeroeth moment (total mass) calculation for the initial simulated tracer cloud was 2.3946 mass fraction units.

The location of the initial tracer cloud relative to the top and left boundaries in the field-scale simulation was slightly different than the location in the baseline sensitivity simulation (S3R19B). The altitude of the water table at the start of the tracer test was about 13.8 m above sea level, or about 0.7 m above the top of the 1.2-m-long screened interval of the injection wells. Assuming that the initial cloud was about 50 percent thicker (see previous chapter) than the screened interval, or 1.8 m thick in the y-direction, the top and center of the initial cloud were 0.4 and 1.3 m below the top boundary, respectively. As was described above, the center of the initial tracer cloud in the field-scale simulation was located 5.6 m from the left boundary of the model. Therefore, the upstream (left) edge of the initial 3.4-m-long cloud was 3.9 m from the boundary, which is sufficiently far to insure a minimal influence of the boundary on the simulated downward movement. The final location of the initial tracer cloud with respect to the modeled area is shown in Figure 5-1.

Aquifer Properties

The aquifer properties that were used in the field-scale simulation are generally the same as those used in the baseline sensitivity run (Table 4-2). For example, the porosity and permeability of the aquifer matrix were not changed. The densities of the ambient fluid and tracer solution also remained unchanged. However, the values for longitudinal dispersivity and anisotropy of permeability were changed to reflect the characteristics of the field site. Table 5-2 lists some of the properties of particular relevance to the field-scale simulation.

Anisotropy of Permeability

The baseline simulation (S3R19B) assumed an isotropic permeability. Hess and others (1992) estimated an anisotropy of 1.2:1 (horizontal to vertical permeability) for the Cape Cod sand and gravel. They obtained this estimate from a stochastic analysis of nearly 1,500 measurements of hydraulic conductivity obtained by borehole flowmeter tests and permeameter analysis of cores Although this nearly isotropic value for anisotropy was shown in the previous chapter to have a small effect on the rate of downward movement, the field-based value was used for the field-scale simulations.

Longitudinal Dispersivity

The dispersion process affects the rate of downward movement by controlling the rate at which the solute cloud is diluted and density differences are diminished. The sensitivity analysis in the previous chapter showed that the dispersivity value could have a significant effect on the downward movement early in a tracer test by influencing how long the large initial density

Table 5-2. Selected aquifer and fluid properties for the field-scale simulation of the Cape Cod tracer test

Property	Variable	Value	Units
Porosity	ε	0.39	none
Permeability	k_{xx}	1.56×10^{-10}	m^2
Anisotropy	k_{xx}/k_{yy}	1.2	none
Viscosity	μ	1.202×10^{-3}	Kg/(m·s)
Longitudinal dispersivity	α_L	See Equation (5.3)	m
Transverse dispersivity	α_T	0.005	m
Fluid density of ambient ground water	ρ_o	999.4091	Kg/m^3
Fluid density of initial tracer solution	ρ_{max}	1000.3701	Kg/m^3
Coefficient of density/ concentration relation	$\partial\rho / \partial c$ DRWDU	0.9610	Kg/m^3

difference persists. In the simulation with α_L = 1 m (Figure 4-9), for example, the vertical trajectory of the tracer cloud had nearly flattened out after only a few days of transport.

The sensitivity simulations in the previous chapter used a constant value of longitudinal dispersivity. However, stochastic models of the dispersion process by Gelhar and others (1979), Gelhar and Axness (1983), and Dagan (1982, 1984) identify an early period when the dispersivity increases with time (or the travel distance of the center of mass). An asymptotic,

maximum value of longitudinal dispersivity is reached only after the tracer cloud has been transported a sufficient distance through the heterogeneous aquifer. The use of an inappropriately large asymptotic dispersivity value early in a tracer test, when the density difference is greatest, could result in a significant under-prediction of the amount of density-induced downward movement of the tracer cloud.

Garabedian and others (1991) calculated the field-scale longitudinal dispersivity by using Equation (4.19) and determined that there was an early period of about 60 days in which the longitudinal dispersivity increased as the cloud traveled through the aquifer; the dispersivity reached an asymptotic value of 0.96 m after about 26 m of transport. Garabedian and others (1988), in an earlier analysis of the Cape Cod test, estimated that the asymptotic dispersivity value was reached after 95 days, or about 40 m of travel distance. Hess and others (1992) applied the three-dimensional, time-dependent, stochastic transport theory of Dagan (1988) to predict the time rate of change of the longitudinal dispersivity from the hydraulic-conductivity measurements at the site. They determined that a constant value for α_L should be reached in about 80 days, after the cloud had traveled about 35 m through the aquifer sediments.

The difference among these estimates is reasonable given the uncertainties associated with the field measurements and the assumptions made in the estimation methods. For the simulation of the field-scale tracer test, the asymptotic value of longitudinal dispersivity was assumed to be reached after 30 m, or 71 days, of transport. A linear rate of increase to the asymptotic value was assumed, as is shown in Figure 5-2. At any time, t, in days, the value of longitudinal dispersivity, α_L, in meters, can be obtained from the following equation:

$$\alpha_L(t) = \frac{0.96}{70} t, \quad t \leq 70 \text{ days} \tag{5.3}$$

$$\alpha_L = 0.96, \quad t > 70 \text{ days.}$$

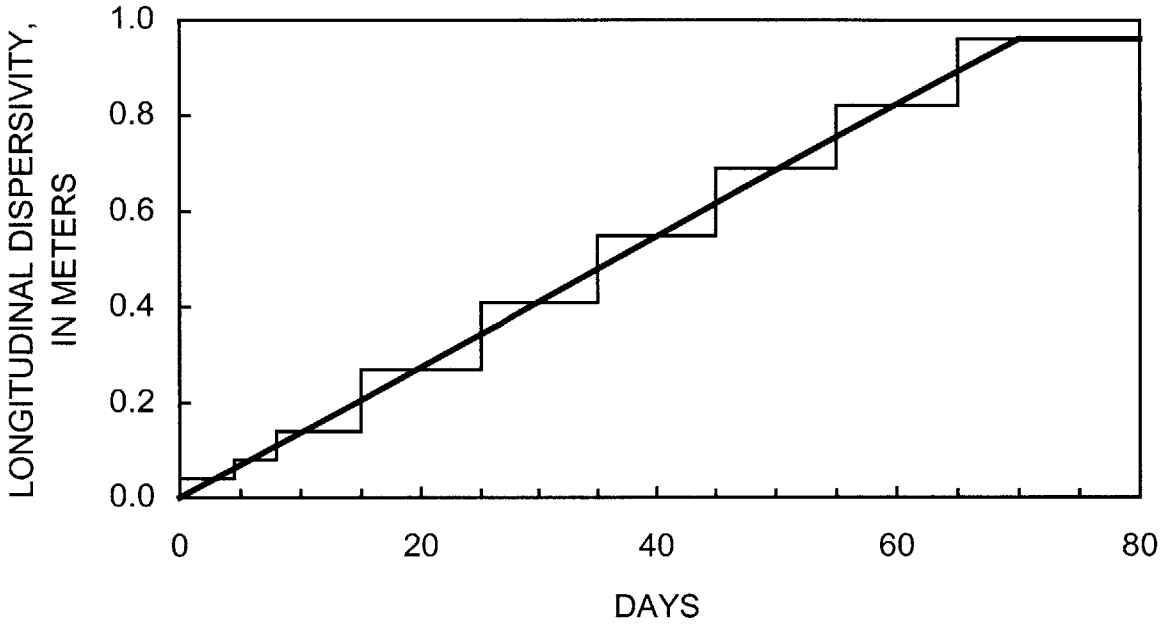

Figure 5-2. Linear increase in longitudinal dispersivity with travel time and stepwise approximation for the first 80 days of the Cape Cod tracer test. Linear increase estimated from the second spatial moment of the observed concentrations (Garabedian and others, 1988, 1991).

Spatial and Temporal Discretization

The model domain for the field-scale simulation was 25 m high and 136 m long. The length of the simulation period was 237 days. The expected trajectory and shape of the cloud, the time-varying dispersivity, numerical oscillations, and numerical dispersion were all considered in selecting the discretization in time and space.

Vertical Discretization

The objective of the grid design in the vertical direction was to use a fine mesh in the zone through which the cloud was expected to pass and to use a coarse mesh below that zone to the bottom of the modeled area. The moments data in Table 5-1 were used to estimate the cloud's trajectory. The center of mass moved downward about 3.2 m during the first 237 days of the experiment. The downward movement carried the center of mass from a starting depth of about 1.3 m below the water table to an ending depth of about 4.5 m below the water table. Therefore, the finest grid spacing, $\Delta y = 0.1$ m, was used in the upper 4.5 m of the model domain (Table 5-3).

At 237 days, the tracer cloud was estimated to extend about 2.1 m below its center of mass ($+2s_y$ in Equation 5.1), or about 6.6 m below the water table. A grid spacing of $\Delta y = 0.15$ m was used from 4.5 to 6.6 m. Below 6.6 m, where the cloud was not expected to pass, the spacing was increased by a factor of about 1.5 for each successively lower element until the mesh extended vertically to 25 m.

Horizontal and Temporal Discretization

The objective of the grid design in the horizontal direction was to select the cell sizes (Δx) and time steps (Δt) along the path of the tracer cloud so that, at any given time, the criteria for limiting numerical oscillations and preserving sharp fronts were met in the area encompassing most of the solute mass of the cloud, and so that the cloud experienced the appropriate level of time-varying longitudinal dispersivity. At the same time, Δx and Δt were increased as quickly as possible to reduce the computational times needed to solve the model.

Table 5-3. Spacing in the horizontal and vertical directions for the finite-element grid of the field-scale simulation of the Cape Cod tracer test.

Horizontal Direction			**Vertical Direction**		
Grid spacing (Δ_x) (meters)	Number of elements	Cumulative distance from left boundary (meters)	Grid spacing (Δ_y) (meters)	Number of elements	Cumulative distance from top boundary (meters)
0.3	7	2.1	0.1	45	4.5
0.2	47	11.5	0.15	14	6.6
0.3	7	13.6	0.2	1	6.8
0.4	1	14.0	0.3	1	7.1
0.5	11	19.5	0.4	1	7.5
0.75	2	21.0	0.6	1	8.1
1.0	5	26.0	0.9	1	9.0
1.5	5	33.5	1.3	1	10.3
2.0	2	37.5	1.95	1	12.25
2.5	2	42.5	2.7	1	14.95
3.0	2	48.5	4.05	1	19.0
3.5	25	136.0	6.0	1	25.0

The concepts that were used to meet these design considerations are illustrated in Figure 5-3 for transport of the tracer cloud during the period from 25 to 35 days. Two clouds are shown schematically at 25 days and 35 days. The size and location of the cloud at a given time were determined by linear interpolation of the moments data in Table 5-1, as shown in Figure 5-4. During the time period from 25 to 35 days, the center of mass of the cloud moved from 10.5 m to 14.7 m horizontally along the flow path. The horizontal extent of the cloud is represented by the area encompassing about 95 percent of the mass, or $\bar{x}' \pm 2s_{x'}$ (Equation 5.2). At 25 days, the cloud was positioned from about 1 to 20 m along the flow path, while at 35 days, the cloud was positioned from 2 to 27 m along the flow path.

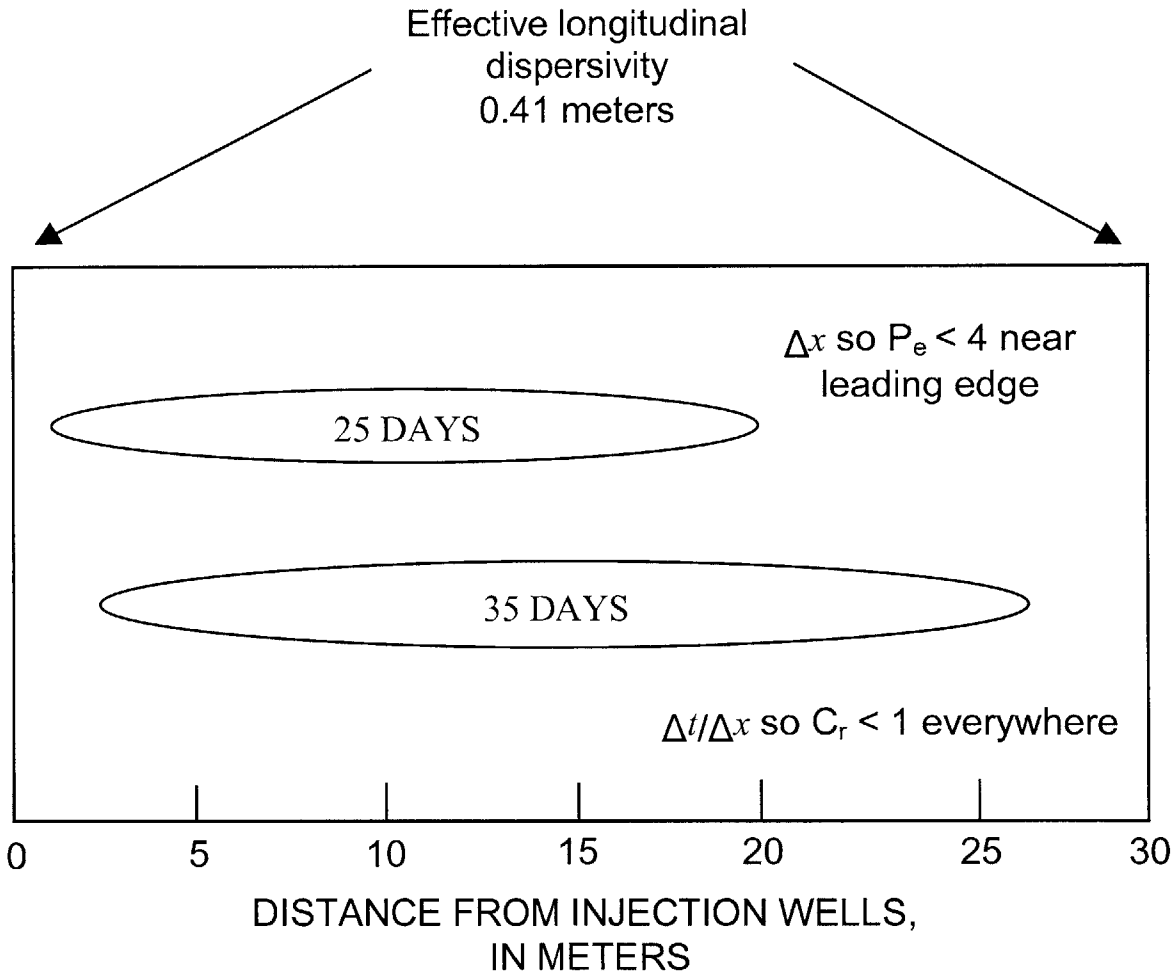

Figure 5-3. Schematic diagram of the tracer cloud at 25 and 35 days, and the factors that were used in design of the horizontal and temporal discretization.

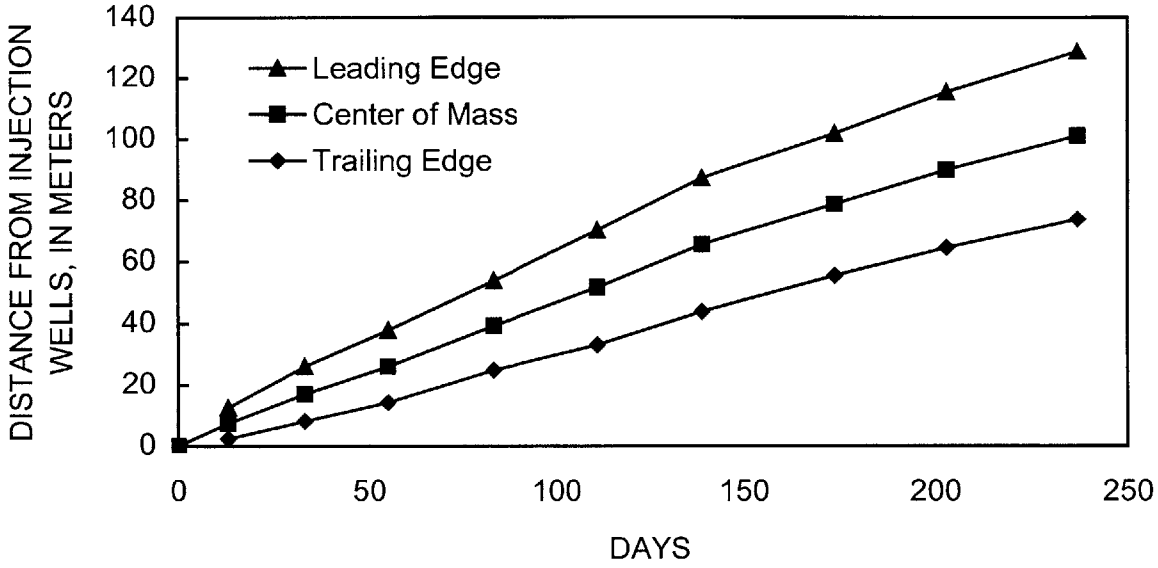

Figure 5-4. Location of the observed trailing and leading edges and center of mass of the tracer cloud during the first 237 days of the Cape Cod tracer test [based on spatial moments of observed concentrations, Garabedian and others, 1991, Table 1].

The first consideration was the effective longitudinal dispersivity experienced by the tracer cloud, which was determined from a stepwise approximation of the observed linear increase in dispersivity. Equation (5.3) was used to generate values of dispersivity at specific times up to 70 days, when the asymptotic dispersivity value was reached. These values are shown in Table 5-4. The values were assumed to apply over a discrete time interval to approximate the smooth linear function by the stepwise approximation that is shown in Figure 5-2.

Table 5-4. Longitudinal dispersivity values at selected travel times during the first 237 days of the Cape Cod tracer test [based on Garabedian and others, 19881991; Hess and others, 1992).

Time from start of tracer test (days)	**Longitudinal dispersivity (m)**	**Time interval over which α_L is effective in stepwise approximation**	
		Start of time interval (days)	**End of time interval (days)**
3	0.04	0	4.5
6	0.08	4.5	8.0
10	0.14	8.0	15.0
20	0.27	15.0	25.0
30	0.41	25.0	35.0
40	0.55	35.0	45.0
50	0.69	45.0	55.0
60	0.82	55.0	65.0
70	0.96	65.0	75.0
80	0.96	75.0	237.1

During the period from 25 to 35 days, the effective longitudinal dispersion is estimated to be 0.41 m (Figure 5-2 and Table 5-4). Therefore, the objective was to select a Δt for the 10-day time period such that as much of the cloud as possible experienced the appropriate effective dispersivity. The effective dispersivity is the sum of the input value of dispersivity and the numerical dispersion associated with the time step according to Equation (4.17) (reproduced from Chapter 4):

$$\alpha_L^* = \alpha_L^{true} + \frac{(2\Theta - 1)}{2} v\Delta t . \qquad (4.17)$$

For a given Δt, Equation (4-17) was used to calculate the input value that, with the numerically generated value, would result in the appropriate effective longitudinal dispersivity for that transport interval.

The second consideration was the criteria for numerical oscillations and preservation of sharp fronts. As the tracer cloud moved forward in the 10-day period, the trailing and leading edges of the cloud passed through the zone from 1 to 27 m along the flow path. The horizontal cell size, Δx, was selected so that the mesh Peclet number,

$$P_e = \frac{v\Delta x}{D} = \frac{\Delta x}{\alpha_L}, \qquad (5.4)$$

remained less than 4.0. Because Δx increased with distance along the travel path, the Peclet number criterion was most applicable at the leading edge of the tracer cloud.

The horizontal cell size, Δx, and the time step, Δt, that were effective in a given zone also were selected so that the Courant number,

$$C_r = \frac{v\Delta t}{\Delta x}, \qquad (5.5)$$

remained less 1.0 to insure preservation of sharp concentration fronts. Because the ground water velocity, v, was constant at 0.42 m/day during the simulation, the ratio $\Delta t / \Delta x$ had to remain less than about 2.4 days/m throughout the modeled area.

This complex mix of considerations was accounted for in the design of the final mesh and time-stepping schemes for the field-scale simulation. Table 5-6 is a detailed tabulation of the various criteria and factors that were evaluated to select the horizontal grid spacing and time-stepping scheme. It is organized in blocks according to the stepwise increase in effective

longitudinal dispersivity. The design proceeded by sequential consideration of the various stepwise targeted values for effective dispersivity. For each step, the positions of the cloud at the start and end of the time interval were determined. Based largely on the farthest extent of the cloud at the end of the time interval, the appropriate Δx and Δt were selected to meet the criteria described above. The same approach was used at later times, when the asymptotic value of dispersivity had been reached, even though the targeted value for effective dispersivity no longer changed along the flow path. The final horizontal and temporal discretization used in the field-scale simulation is shown in Table 5-3 and Table 5-5, respectively.

Table 5-5. Temporal discretization for the 237-day-long field-scale simulation of the Cape Cod tracer test.

Time step interval (Δt) (days)	**Number of time steps**	**Cumulative time from start of simulation (days)**
0.2	23	4.6
0.4	9	8.2
0.45	82	45.1
0.7	14	54.9
0.95	10	64.4
1.2	15	82.4
3.0	9	109.4
4.1	7	138.1
4.5	22	237.1

Table 5-6. Cloud size and grid-design criteria and final horizontal grid spacing and time steps used to simulate the field-scale Cape Cod tracer test.

α_L^*	t_i	t_{i+1}	Δt	α_L^{num}	α_L^{input}	# of steps	Σ # steps	$\bar{x}$ at t_{i+1}	$\bar{x}-2s_x$ at t_i	$\bar{x}-2s_x$ at t_{i+1}	Δx	x_j	x_{j+1}	# of elem	Σ # elem	P_e	C_r^{max}	C_r^{min}
--	--	--	--	--	--	--	--	--	--	--	0.3	-5.5	-3.4	7	7	--	--	--
--	--	--	--	--	--	--	--	--	--	--	0.2	-3.4	0.0	17	24	--	--	--
0.050	0.0	4.6	0.2	0.042	0.008	23	23	1.89	-5.5	6.0	0.2	0.0	6.0	30	54	4.0	0.42	0.42
0.084	4.6	8.2	0.4	0.084	0.0	9	32	3.40	-2.2	8.0	0.3	6.0	8.1	7	61	2.5	0.84	0.84
0.14	8.2	15.4	0.45	0.0945	0.0455	16	48	6.43	-1.2	14.0	0.4	8.1	8.5	1	62	2.85	0.94	0.38
											0.5	8.5	14.0	11	73	3.57		
0.27	15.4	25.3	0.45	0.0945	0.1755	22	70	10.58	-1.4	20.0	0.75	14.0	15.5	2	75	2.78	0.94	0.19
											1.0	15.5	20.5	5	80	3.70		
0.41	25.3	35.2	0.45	0.0945	0.3155	22	92	14.74	1.0	27.0	1.5	20.5	28.0	5	85	3.65	0.94	0.13
0.55	35.2	45.1	0.45	0.0945	0.4555	22	114	18.9	2.4	32.0	2.0	28.0	32.0	2	87	3.64	0.94	0.094
0.69	45.1	54.9	0.70	0.147	0.543	14	128	23.0	5.3	38.0	2.5	32.0	37.0	2	89	3.62	0.98	0.12
0.82	54.9	64.4	0.95	0.200	0.620	10	138	27.0	8.2	43.0	3.0	37.0	43.0	2	91	3.66	0.998	0.13
0.96	64.4	82.4	1.2	0.252	0.708	15	153	34.6	11.6	54.0	3.5	43.0	57.0	4	95	3.64	1.008	0.14
0.96	82.4	109.4	3.0	0.630	0.330	9	162	45.9	27.0	70.0	3.5	57.0	71.0	4	99	3.64	0.84	0.36
0.96	109.4	138.1	4.1	0.861	0.099	7	169	58.0	37.0	87.0	3.5	71.0	88.5	5	104	3.64	0.57	0.49
0.96	138.1	174.1	4.5	0.945	0.015	8	177	73.1	44.0	102.0	3.5	88.5	106.0	5	109	3.64	0.54	0.54
0.96	174.1	201.1	4.5	0.945	0.015	6	183	84.5	55.0	116.0	3.5	106.0	116.5	3	112	3.64	0.54	0.54
0.96	201.1	237.1	4.5	0.945	0.015	8	191	99.6	64.0	129.0	3.5	116.5	130.5	4	116	3.64	0.54	0.54

Notes: Time in days from the start of the tracer test. Distances in meters from center of tracer cloud at time t = 0 days.

α_L^*	=	effective longitudinal dispersivity from field observations (Table 5-4 and Figure 5-3), m
t_i	=	time at start of interval over which effective longitudinal dispersivity applies, days
t_{i+1}	=	time at end of interval over which effective longitudinal dispersivity applies, days
Δt	=	time step, days
α_L^{num}	=	numerical longitudinal dispersivity from Equation (4-17) with v = 0.42 m/day and Θ = 1
α_L^{input}	=	model input value of longitudinal dispersivity, m
# of steps	=	number of time steps in interval over which effective longitudinal dispersivity applies
Σ # steps	=	cumulative number of time steps from start of simulation
$\bar{x}$ at t_{i+1}	=	center of mass location at end of time interval, m
$\bar{x}' - 2s_{x'}$ at t_i	=	trailing edge of tracer cloud at beginning of time interval, m
$\bar{x}' + 2s_{x'}$ at t_{i+1}	=	leading edge of tracer cloud at end of time interval, m
Δx	=	horizontal grid spacing, m
x_j	=	start of grid interval over which Δx applies, m
x_{j+1}	=	end of grid interval over which Δx applies, m
# of elem	=	number of grid cells in grid interval
Σ # elem	=	cumulative number of grid cells from left boundary of model
P_e	=	grid Peclet number for grid interval, $P_e = \Delta x / \alpha_L^*$
$C_r^{\min}$	=	Courant number, $C_r = v\Delta t / \Delta x$, for leading edge of cloud at t_{i+1}
$C_r^{\max}$	=	Courant number, $C_r = v\Delta t / \Delta x$, for trailing edge of cloud at t_i

This page is blank.

Areal Recharge

The center of mass of the tracer cloud moved downward about 3.2 m in the first 237 days of the Cape Cod tracer test (Table 5-1). LeBlanc and others (1991, Figure 5) reported that 87 cm of precipitation were recorded from July 1985 through March 1986 at a weather station located about 1.8 km from the site. They estimated that this precipitation resulted in about 45 cm of recharge in the same period (LeBlanc and others, 1991, Figure 5). Given a porosity of 0.39, this is equivalent to about 1.2 m of water in the aquifer, which is less than half of the vertical movement observed during the 237 days.

The sensitivity analysis in the previous chapter examined the effect of continuous recharge at several hydrologically reasonable rates that were based on the data from LeBlanc and others (1991). The analysis indicated that recharge can cause significant downward movement of the tracer cloud over several time scales. The representation of recharge as an average rate will likely result in a smoother downward trajectory than a representation of recharge as shorter, but higher intensity, pulses during the same time period.

Therefore, for the simulation of the first 237 days of the field-scale tracer test, recharge was applied to the upper boundary of the model as a time-varying stress. The average monthly values presented in Figure 5 of LeBlanc and others (1991) were replaced with daily values taken from climatological records. The same water-balance approach was used to estimate recharge, but it was applied on a daily basis instead of a monthly basis to capture the short-term influence of individual storms. This consideration was particularly important because there were several major precipitation events in late August 1985, only about 35 days after the tracer injections, when density-induced downward movement was still significant.

Daily Potential Evapotranspiration

The first step in determining the daily recharge rate was estimation of daily values for potential evapotranspiration (PET). LeBlanc and others (1991) used the methods of Thornthwaite (1944) and Thornthwaite and Mather (1957) to estimate monthly values for potential evapotranspiration for the years 1985-1987. The Thornthwaite and Mather methods are based on empirical studies of evaporation rates, and estimate potential evapotranspiration from measurements of mean monthly temperature and daylight length, which is a function of the latitude of the site in question. The measurements of mean monthly temperatures were obtained from a weather station in Hyannis, Massachusetts, about 25 km east of the tracer-test site. The potential evapotranspiration values were calculated using a computer program that was prepared for another study (LeBlanc and others, 1986) and implements the Thornthwaite and Mather method.

The monthly estimated potential evapotranspiration values for the period from June 1985 to March 1986, which includes the first 237 days of the tracer experiment, are shown in Figure 5-5. The Thornthwaite and Mather method provides only monthly estimates. For the field-scale simulation, daily values for recharge were desired. Therefore, a linear approximation to the monthly values was obtained that is represented by the following equations:

$$
\begin{aligned}
PET &= (12 + 0.125t)/31 && 0 \le t \le 20 \\
PET &= (16.48 - 0.099t)/30.55 && 21 \le t \le 153 \\
PET &= 0 && 154 \le t \le 243 \\
PET &= (-23.52 + 0.977t)/31 && 244 \le t \le 274
\end{aligned}
\qquad (5.6)
$$

where PET = potential evapotranspiration, in cm, and t = time, in days, from July 1, 1985. The divisors in the equations convert the monthly rates to daily rates. These equations were used to

generate daily estimates of potential evapotranspiration for the period of July 1, 1985, to March 31, 1986.

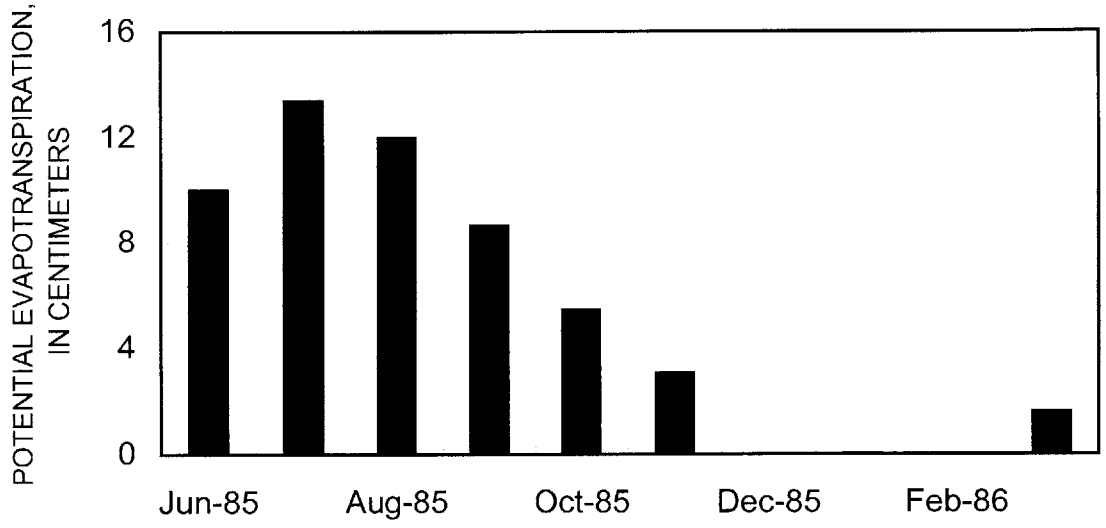

Figure 5-5. Estimated monthly potential evapotranspiration (PET) for June 1985 through March 1986. Values estimated using the Thornthwaite and Mather (1957) method and temperature data from Hyannis, Mass.

Daily Precipitation and Recharge

Daily measurements of precipitation were obtained from a weather station in Hatchville, Massachusetts, about 1.8 km from the tracer-test site. The Thornthwaite and Mather (1957) water-balance method was used to estimate daily recharge from the estimated daily potential evapotranspiration and the measured daily precipitation data. In any given accounting period, the potential evapotranspiration is satisfied first by the precipitation, and then by the available

soil moisture. Recharge is the excess precipitation that remains after the potential evapotranspiration and the soil-moisture deficit are satisfied.

The soil-moisture capacity, or maximum amount of water stored in the soil that is available for evapotranspiration, is specified for the water-balance calculations. The tracer-test site, which is located in an abandoned gravel borrow pit, has bare, sandy soils and little vegetation. Therefore, the soil-moisture capacity for the tracer-test site was estimated to be 5.08 cm (2 inches), which is less than the 4 inches assumed by LeBlanc and others (1986) for the typical vegetated sandy soils of Cape Cod.

The estimated daily recharge that was obtained from the Thornthwaite and Mather analysis, and the corresponding record of daily measured precipitation, for July 1985 through March 1986, are shown in Figure 5-6. The total precipitation was about 87 cm, as mentioned earlier. The total recharge from the daily calculations was about 50 cm, which is about 11 percent greater than the total recharge from the monthly calculations reported in LeBlanc and others (1991, Figure 5). The difference between the estimates based on daily and monthly rates reflects the nonlinear effects of the fixed maximum soil-moisture storage on the balance calculations. With month-long averaging, any precipitation that falls in the month is mathematically available to meet the potential evapotranspiration for the month. This results in the physically impossible evaporative consumption of some precipitation before it falls, and tends to underestimate the amount of excess precipitation in a given month.

The daily recharge rates shown in Figure 5-6 were further manipulated for use in the field-scale simulation. Only recharge for the first 237 days of the tracer test was simulated in the model run. This period extended from July 18, 1985, to March 12, 1986. The estimated total recharge during this period is about 5 cm less than the amount for the full months from July 1985

through March 1986 because there was a large storm on March 15, three days after the simulation period. Thus, the total recharge for the simulation period was 45 cm.

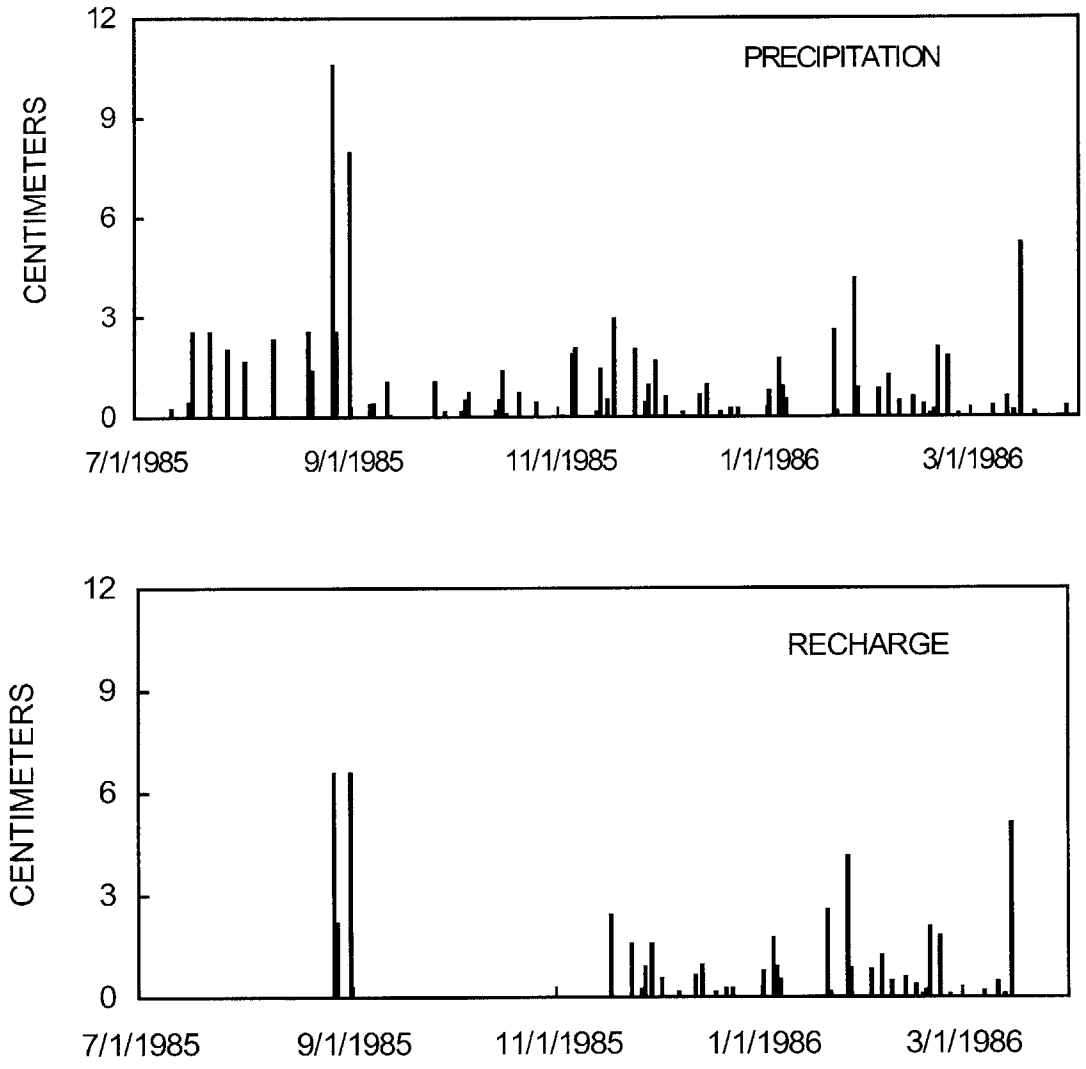

Figure 5-6. Estimated daily recharge and measured daily precipitation for the period from July 1985 to March 1986.

The recharge occurred in two major periods during the field experiment (Figure 5-6). About 15 cm of recharge, 33 percent of the total, occurred in late August 1985, 38 to 44 days after the start of the tracer test. On two separate days (August 26 and 31), the estimated recharge rate was more than 6.5 cm/day. The remaining 30 cm occurred between mid-November and mid-March, when evapotranspiration rates are low and most precipitation results in recharge (LeBlanc and others, 1986).

Simulated Recharge

The recharge was included in the field-scale simulation as a time-dependent fluid flux into the model along the top row of nodes. The daily spatially uniform recharge values in cm (implicitly per cm^2) were converted to total recharge rates for each node for each time step in units of Kg/sec. The conversion was accomplished through pre-processing of the recharge estimates and manipulation by a computer code that was inserted into the SUTRA subroutine BCTIME.

The procedure included the conversion of the daily recharge values to recharge rates for each of the 191 time steps shown in Table 5-6. The daily values were apportioned among the time steps according to the proportion of the day represented by each Δt value. The result was a set of 191 recharge values, in units of cm (implicitly per cm^2), one for each time step. The values were then divided by the lengths of the time steps (Δt) to obtain a recharge rate in cm/sec.

The next step was to convert the recharge rates for each time step into recharge rates for each node along the top boundary of the model. This was accomplished by determining the length of the boundary represented by each node. These lengths were then multiplied by the

recharge rates and the assumed unit width of the model domain to obtain volumetric flux rates for each node for each time step in cm^3/sec.

The final step was to convert the volumetric flux rates into fluid mass flux rates. The fluid mass flux rates were obtained by converting cm^3/sec to m^3/sec and multiplying by the fluid density, which was assumed to equal the density of the ambient ground water. The final result was a recharge rate in Kg/sec for each node along the top boundary for each time step.

Simulation Approach

Simulation of the Cape Cod tracer test was divided into 15 sequential simulations covering the 237 days of the test. This section describes the simulation procedure, including the changes that were made at each pause in the simulation. A principal components approach to calculate the spatial moments of the simulated concentrations, and the use of iterative solutions to insure fluid and solute mass balance are also described.

Simulation Procedure

The first step was the simulation of steady-state fluid flow without solute transport. The simulated flow between the upstream specified-flux boundary and the downstream specified-pressure boundary was horizontal because there was no areal recharge. The simulated ambient flow rate was about 0.42 m/day. The pressure field from this simulation was used as the initial condition for the transient solute-transport simulation.

The second step was transient solute-transport simulation of the tracer cloud. The cloud was assumed to appear instantaneously at the start of the simulation. The progress of the cloud

through the modeled area was then simulated in a sequence of 15 model runs having transport periods ranging from 0.6 to 99 days and numbers of time steps ranging from 2 to 22 steps. The various runs are summarized in Table 5-7. The periods represented by the runs were based mostly on the time-step and input-dispersivity scheme outlined in Table 5-6. However, as discussed in the next section, one period (37.9 to 38.8 days, Run S4R16B) was chosen specifically to include the large recharge events in late August 1985.

Each simulation was run for a specified number of time steps. For each time step, the numerical accuracy of the simulations was checked by examining the fluid and solute mass balances, and the number of iterations needed to convergence to a solution. At the end of selected time steps, the pressure, concentration, and velocity fields were output for analysis. In particular, the spatial moments of the concentration field were calculated to track the simulated movement and spreading of the solute cloud.

At the end of the simulation period, the final pressures and concentrations for each node at the end of a simulation period were output to use as starting values for the next simulation period. Before the next period was simulated, the input dispersivity value, the new time-step size (Δt), and the number of time steps were changed manually in the input data sets according to the schemes shown in Tables 5-6 and 5-7. A pointer in the data set of recharge values was reset to indicate where to start reading the next set of values. Then, the next simulation in the sequence was run. The procedure was repeated until the full 237-day period had been simulated.

Table 5-7. Characteristics of the 15 sequential model runs used to simulate the 237-day-long Cape Cod tracer test [α_L, longitudinal dispersivity].

Run number	Starting day	Ending day	Time step (days)	Number of time steps	Input α_L (m)	Iterative solution
S4R08B	0.0	0.6	0.2	3	0.008	Yes
S4R09B	0.6	4.6	0.2	20	0.008	No
S4R10B	4.6	8.2	0.4	9	0.0	No
S4R11B	8.2	15.4	0.45	16	0.0455	No
S4R12B	15.4	25.3	0.45	22	0.1755	No
S4R13B	25.3	35.2	0.45	22	0.3155	No
S4R14B	35.2	37.9	0.45	6	0.4555	No
S4R16B	37.9	38.8	0.45	2	0.4555	Yes
S4R17B	38.8	45.1	0.45	14	0.4555	Yes
S4R18B	45.1	54.9	0.70	14	0.543	No
S4R19B	54.9	64.4	0.95	10	0.620	No
S4R20B	64.4	82.4	1.2	15	0.708	No
S4R21B	82.4	109.4	3.0	9	0.330	No
S4R22B	109.4	138.1	4.1	7	0.099	Yes
S4R23B	138.1	237.1	4.5	22	0.015	Yes

Iterative Solution

Because there is a feedback between the solute mass fraction and the density, an iterative procedure is used to solve the fluid flow and solute transport equations for each time step. The iterative process continues until the changes in pressure and solute mass fraction are below convergence criteria specified by the user. For the runs in the field-scale simulation, the pressure convergence criterion was set to 10.0 $Kg/(m \cdot s^2)$, and the solute mass fraction criterion was set to 0.01, the same values that were used for the simulations in the previous chapter (Table 4-3).

The iteration procedure adds considerable computation time to each computer run. Most of the sensitivity simulations in the previous chapter required only two iterations to converge to a solution. This is the minimum number needed to identify convergence and, in essence, indicated that an iterative approach was not needed. Several preliminary runs of the field-scale simulation confirmed that an iterative approach was unnecessary except when there were large changes in density or fluid flow during the time step.

Two situations were identified when an iterative approach was needed. The first situation is at the start of the overall simulation, when the tracer cloud instantaneously appears in the flow field. At that instant, the pressure field is not consistent with the concentration field, and there are significant changes in the flow field that cause corresponding changes in the solute concentrations over a short time interval. Accurate simulation of these changes required three iterations for each of the first two time steps to reach convergence.

The second situation is during time steps with significant recharge along the top boundary of the model. In this situation, the sudden influx of water caused large changes in pressures and flow velocities and corresponding movement of the solute cloud that required several iterations

to be resolved. A poor mass balance for the non-iterative solution demonstrated the need for an iterative solution in these cases. For example, the first major recharge event in late August 1985 was simulated in run S3R16B (Table 5-7). Three iterations were needed in the first time step to converge to a solution, and the mass balance was excellent (Table 5-8). The run was repeated with a non-iterative solution (run S3R15B), which yielded a poor mass balance. The zeroeth moment (total mass) of the solute cloud also showed a spurious decrease as compared to the iterative solution.

Table 5-8. Total mass of the solute cloud from the zeroeth moment for the non-iterative (run S3R15B) and iterative (run S3R16B) solutions of the time period from 37.9 to 38.8 days
[smfu, solute mass fraction units; mass balance error, percent difference between rate of change of stored fluid mass (water and solute) because of pressure and concentration changes, and net mass flux rate (water and solutes) from fluid sources and sinks (Voss, 1984, p. 145-146)].

End of time step (days)	**Run S3R16B (iterative)**			**Run S3R15B (non-iterative)**		
	Number of iterations	Total solute mass (smfu)	Fluid and solute mass balance error	Number of iterations	Total solute mass (smfu)	Fluid and solute mass balance error
37.90	--	2.3939	--	--	2.3939	--
38.35	3	2.3939	0.0 %	--	2.3923	15 %
38.80	2	2.3939	--	--	2.3919	--

Therefore, non-iterative solutions were used for most of the runs shown in Table 5-7. The indicated exceptions were the first several time steps after the cloud was initially introduced, and the three simulation periods that included time steps with significant pulses of recharge.

Principal Components of the Variance Tensor

The second moment, or the variance, of the concentration distribution is a measure of the spreading of the solute cloud relative to the center of mass. The second moment was calculated along the major coordinate axes of the model. The product of the second-moments calculation was a 2 x 2 symmetric matrix of the form:

$$\begin{bmatrix} \sigma_{xx}^2 & \sigma_{xy}^2 \\ \sigma_{yx}^2 & \sigma_{yy}^2 \end{bmatrix},$$

in which the subscripts indicate the variance components relative to the x (horizontal) and y (vertical) model coordinates, and $\sigma_{xy}^2 = \sigma_{yx}^2$.

For the initial tracer cloud, the rectangular cloud was aligned with the major coordinate axes of the model, and the off-diagonal components of the variance tensor were zero. As the cloud was transported by the ambient flow and moved downward because of density differences, however, the off-diagonal terms became non-zero, indicating a slight rotation of the tracer cloud's main axis from its initially horizontal orientation.

Garabedian and others (1991) reported the principal components of the variance tensor and the angle of rotation of the cloud's principal axis relative to the major grid coordinates of the model. For direct comparison to their results, the principal components of the variance tensor of the simulated concentrations were calculated. The procedure was to find the eigenvalues and associated eigenvectors of the matrix, and to rotate the matrix into the coordinate system defined by the eigenvector directions. The result was a diagonal matrix in which the off-diagonal terms were zero.

Calculation of the principal components of the variance matrix was done for each time step in the field-scale simulation. The maximum angle of rotation of the tracer cloud was about 1.6 degrees and was less than 1 degree for most time steps. The effect on the magnitude of the major components, σ_{xx}^2 and σ_{yy}^2, of the variance was less than 0.5 percent. Although the difference between the two sets of variances was insignificant for this analysis, the principal components are reported later in this report for consistency with the results of Garabedian and others (1991).

Density Calculation

The model grid was designed to minimize numerical oscillations. However, as was described in the previous chapter, small oscillations occurred at the leading and trailing edges of the tracer cloud, which resulted in simulated concentrations that were outside the range of concentrations,

$$0 \le C \le C_{\max}, \tag{5.7}$$

where $C_{\max} = 1.0$, the solute mass fraction of the initial tracer cloud. Because fluid density was assumed to be linearly related to solute mass fraction (Equation 4.14), the oscillations could result in densities that were negative or greater than the initial density of the tracer cloud. In order to limit the influence of these spurious density calculations on the simulated downward movement of the tracer cloud, the linear relationship as implemented by SUTRA was modified to limit the density values to the range shown in Equation (5.7). For solute mass fractions less than zero, the fluid density was set to the density of the ambient ground water; for solute mass fractions greater than one, the fluid density was set to the density of the initial tracer solution. In

preliminary simulations, this change did not measurably affect the transport and downward movement of the simulated tracer cloud.

Simulated Downward Movement of the Cape Cod Tracer Cloud

The first 237 days of the Cape Cod tracer test, when the downward movement was greatest, were simulated using the procedures described above. The simulated movement and characteristics of the tracer cloud were tracked by calculation of the spatial moments of the concentration distribution at the end of each of the 191 time steps. The vertical trajectory of the tracer cloud was compared to the observed trajectory to determine if density-induced sinking contributed significantly to the downward movement observed during the field experiment.

Shape and Path of the Simulated Tracer Cloud

The simulated tracer cloud moved predominantly in the horizontal direction across the modeled area. The path and size of the cloud, as defined by the 0.01 solute-mass fraction level, is shown in Figure 5-7. The significant spreading in the longitudinal direction and the lack of spreading in the vertical direction are evident in the series of vertical sections. This behavior was expected given that the targeted asymptotic longitudinal dispersivity value (0.96 m) was more than 190 times larger than the input value of transverse dispersivity. By 237 days, the length of the zone in which concentrations exceeded 0.01 mass fraction units was about 50 m long.

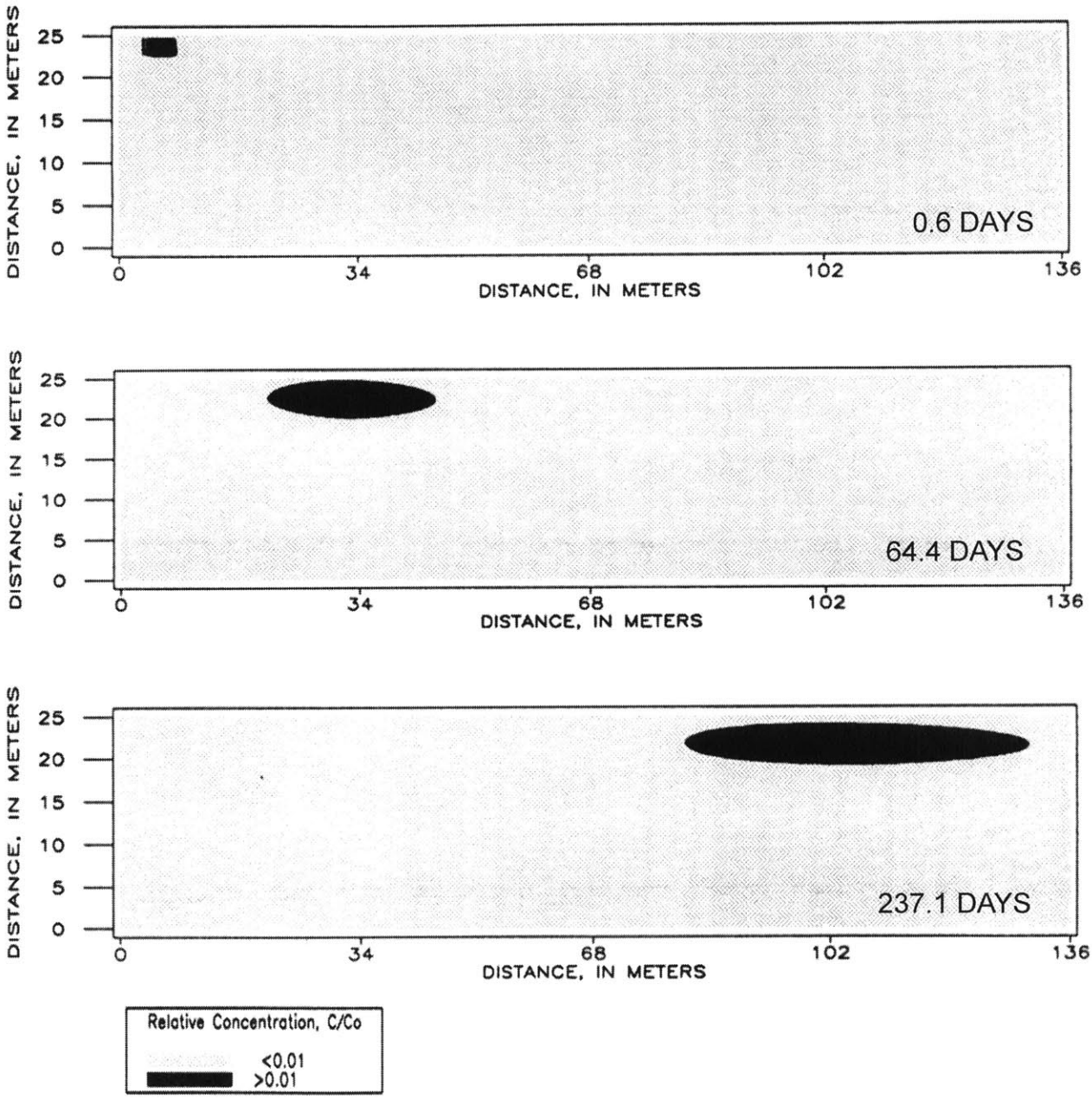

Figure 5-7. Location of the simulated tracer cloud at 0.6, 64.4, and 237.1 days since the start of the simulation period. Cloud locations are defined by the zones in which the solute mass fraction exceeded 0.01.

Contoured plots of concentrations show the same features that were described for run S2R4G in the previous chapter (Figure 4-6). At 0.6 days (Figure 5-8), the rectangular shape of the initial cloud was still evident, and numerical oscillations were present near the leading and

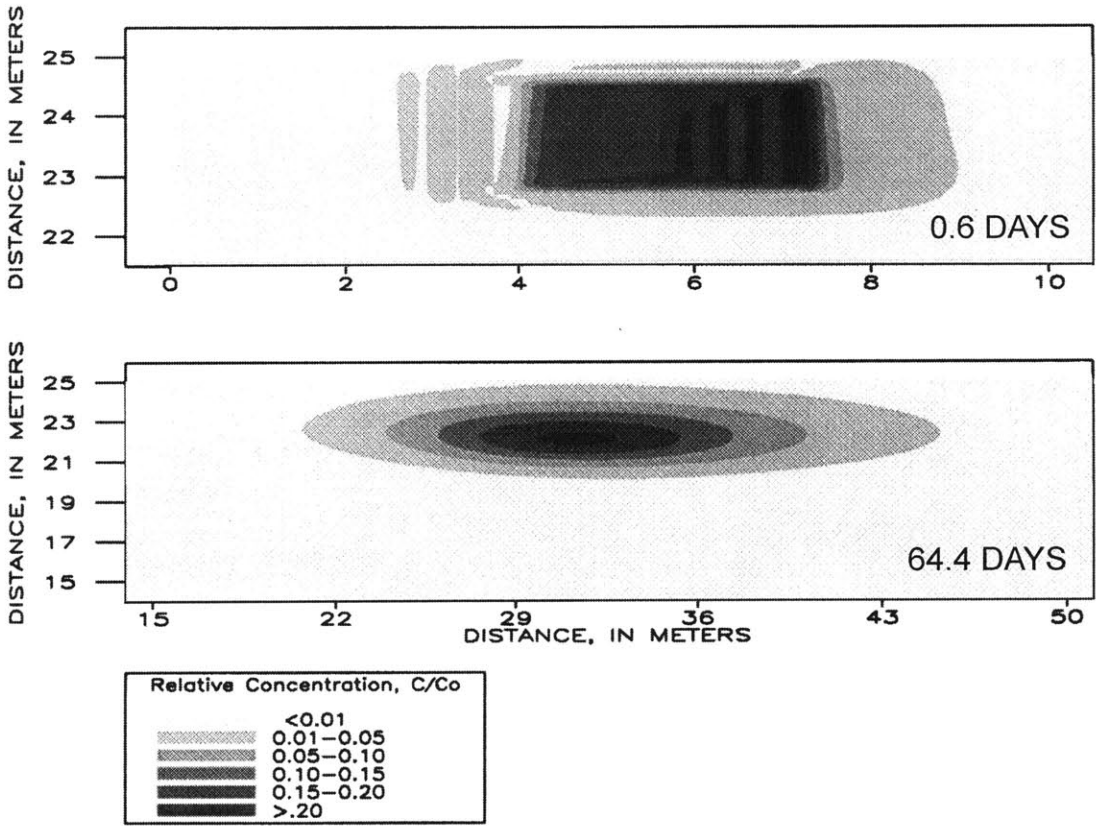

Figure 5-8. Distributions of the simulated solute mass fraction at 0.6 and 64.4 days since the start of the simulation period. Spatial scales and concentration-contour intervals differ to show features within the two clouds.

trailing edges of the tracer cloud. Note that small oscillations around a zero concentration value in the area behind and below the simulated cloud, which were also seen in run S2R4G, are not shown for clarity in Figure 5-8. At 64.4 days, the cloud had spread to a length of about 24 m and hasd developed the saddle shape described in the previous chapter. Concentrations were greater than 0.20 mass fraction units only in a small zone in the center of the tracer cloud.

Solute Mass

The length of the model grid was designed so that the simulated cloud remained in the modeled area during the 237-day-long simulation period. The zeroeth moment was used to track the total mass of the tracer cloud with time. Figure 5-9 shows that the total simulated mass was nearly constant at 2.3934 to 2.3947 solute mass fraction units (a variation of less than 0.1

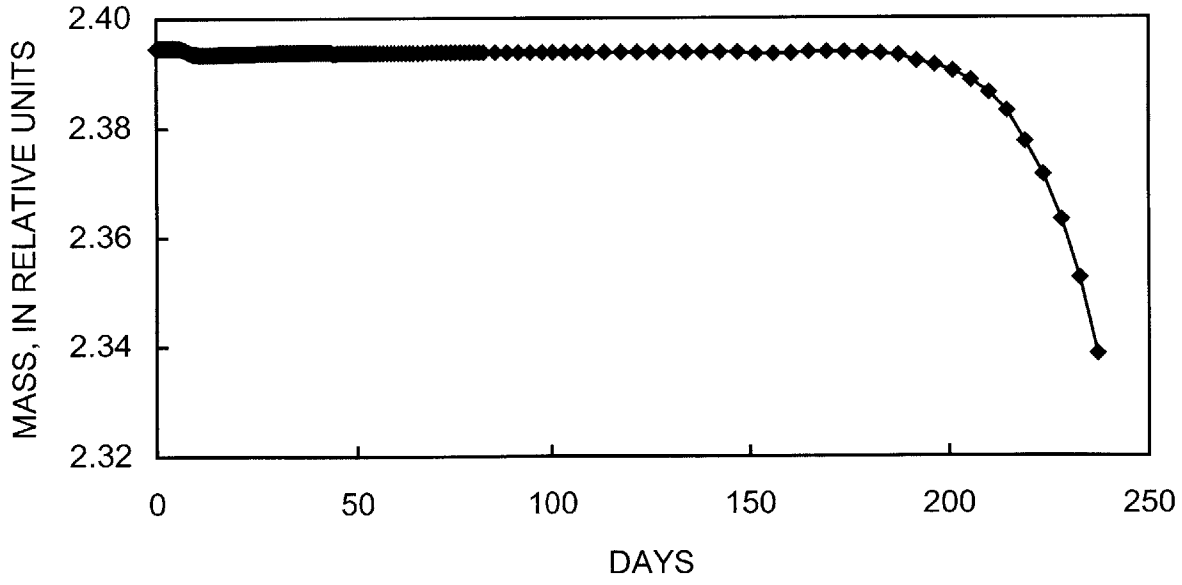

Figure 5-9. Total mass of the simulated tracer cloud during the 237-day-long simulation of the Cape Cod tracer test.

percent) until about 185 days into the simulated period. After 185 days, the total mass in the modeled area began to decrease until the end of the simulation, when it reached its lowest value of 2.3386 mass fraction units. This value represents about a 2 percent loss of the initial total solute mass in the tracer cloud. The small loss occurred as the leading edge of the tracer cloud (farther than $\bar{x}' \pm 2s_{x'}$ (Equation 5.2), or the volume defined by 95 percent of the mass) intersected the downgradient specified-pressure boundary, and mass was lost from the modeled area by advective transport across the boundary. The amount of mass loss was too small and too late in the simulation to affect the downward movement of the tracer cloud.

Horizontal Movement

Figure 5-10 shows the horizontal location of the center of mass of the simulated tracer cloud during the 237-day period. The location is plotted relative to the center of the initial cloud,

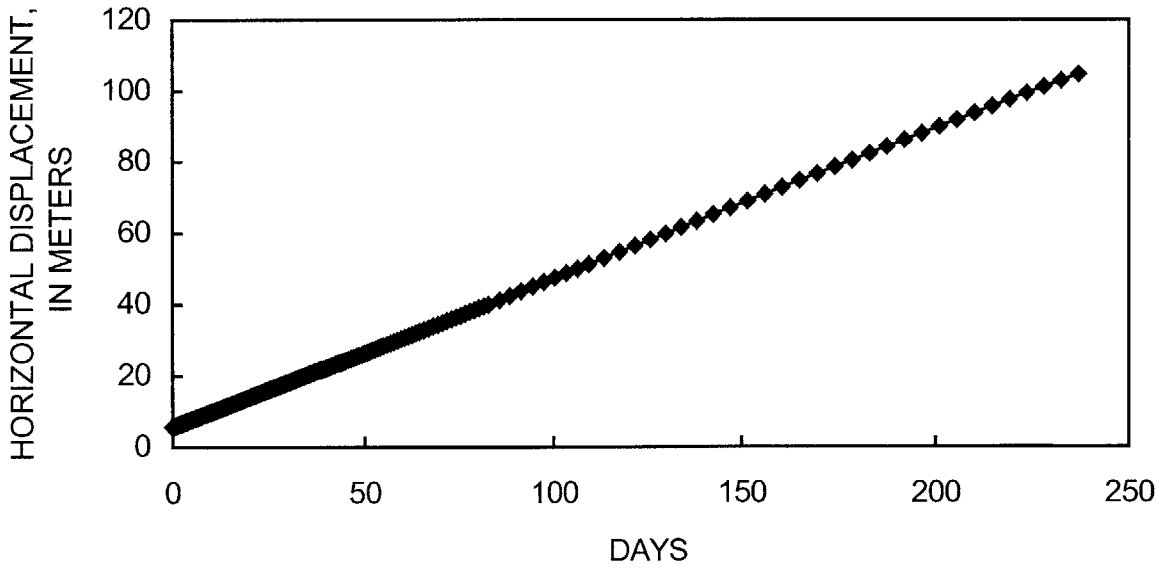

Figure 5-10. Horizontal location of the center of mass of the simulated tracer cloud during the 237-day-long simulation of the Cape Cod tracer test.

which was located 5.6 m from the left boundary of the model. The slope of the line shown in Figure 5-10 is about 0.42 m/day, which equals the horizontal velocity of the ambient ground water prior to the introduction of the tracer cloud. This velocity estimate does not account for the slight bias in the center of mass as solute began to exit the modeled area at the downstream specified-pressure boundary, but this bias is probably exceedingly small. The cloud also followed a slightly curved path (see below), but the true path was only about 0.1 percent longer than the horizontal distance traveled by the cloud. The results shown in Figure 5-10 indicate that the solute cloud was carried along by the predominantly horizontal flow; the small amount of downward movement because of density and areal recharge was superimposed on the dominant lateral regional flow.

Vertical Movement

The center of mass of the simulated tracer cloud moved downward about 2.13 m during the 237-day simulation period (Figure 5-11). The influence of density and areal recharge are both evident in the vertical trajectory. The simulated cloud moved downward about 0.94 feet during the first 37.9 days of the simulation period, or about 44 percent of the total simulated downward movement, when there was no areal recharge. During approximately the same period, the observed tracer cloud moved downward a similar distance (Figure 5-11). The simulated downward movement was caused entirely by the density difference between the ambient ground water and the tracer solution. The rate of downward movement decreased with time as dilution of the tracer cloud by dispersion decreased the density difference.

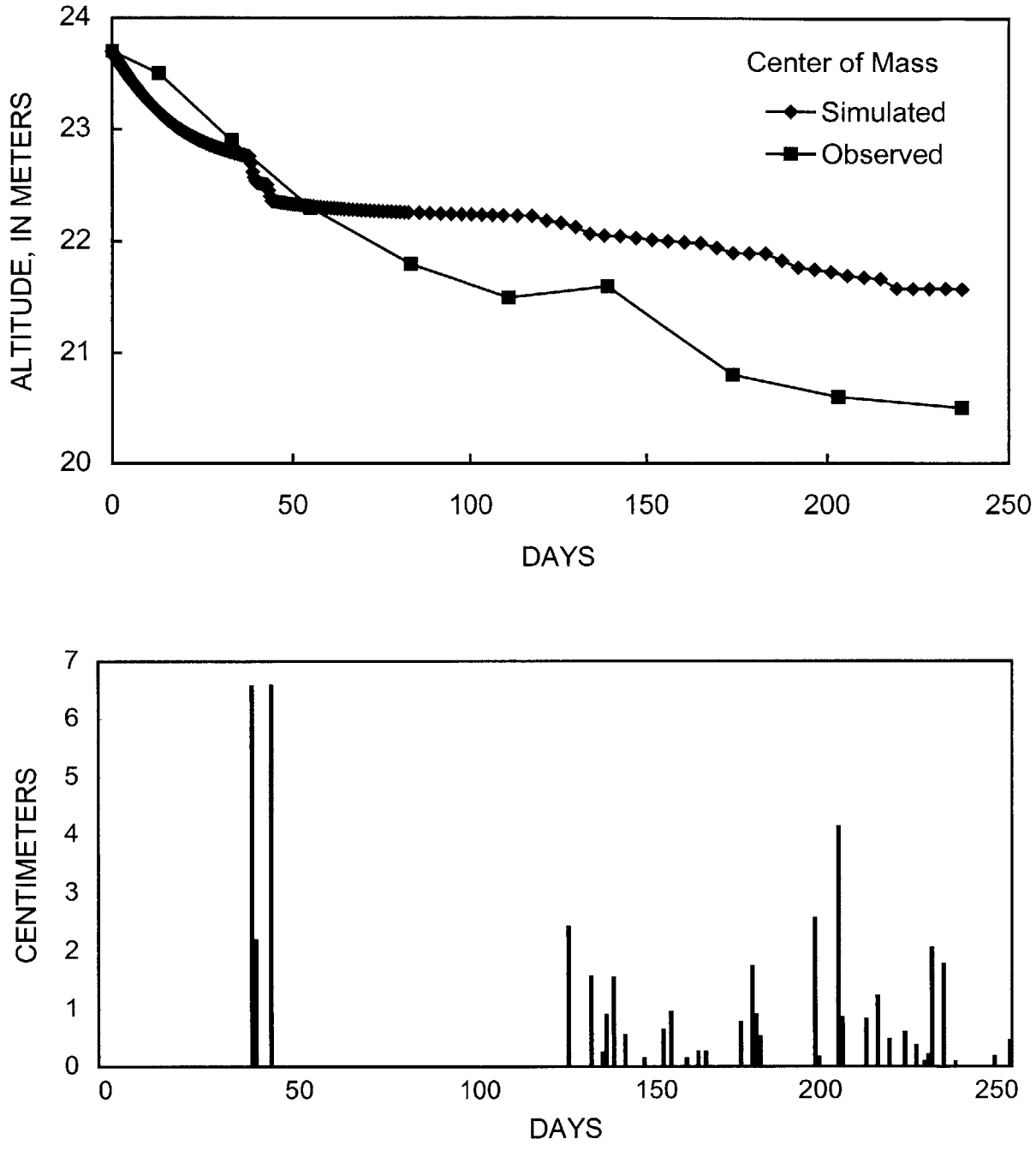

Figure 5-11. Vertical location of the center of mass of the simulated and observed tracer clouds, and the estimated daily recharge, during the 237-day-long simulation of the Cape Cod tracer test.

Downward movement because of density differences continued in a second period of no recharge between 44.2 and 117.6 days (Figure 5-11). The downward movement during this period was only 0.13 m, or about 6 percent of the total simulated downward movement of 2.13 m. However, the slightly curved trajectory typical of density-induced sinking of a tracer cloud that is being diluted by dispersion is still evident during this period.

The net simulated angle of downward movement from the horizontal during the first 33 days of the simulation period was about 3.7 degrees. The observed net angle of downward movement during the same period was about 2.7 degrees (LeBlanc and others, 1991, Table 3). In contrast, the method of Yih (1963) predicted that a circular fluid body with the same initial density in a similar two-dimensional flow field would move downward at an angle of about 17 degrees (Table 3-5). The prediction, however, assumed that the body does not mix with the ambient fluid (that is, the body is not diluted by dispersion), and there was no correction for the anisotropy of permeability.

The influence of areal recharge was particularly evident between days 37.9 and 44.2, when the simulated tracer cloud moved downward 0.40 m in two separate events. During this 6.3-day-long period, which occurred in late August 1985, about 15.4 cm of recharge was simulated in the model. Assuming a porosity of 0.39, the recharge equals 0.39 m of water in the aquifer, or about the amount of simulated downward movement.

A second period of intermittent recharge occurred between 118 and 237 days from the start of the simulation. The trajectory of the tracer cloud responded to the intermittent recharge in a series of short downward steps corresponding to each recharge event (Figure 5-11). The total recharge during this period was about 29 cm, which equals about 0.75 m of water in the aquifer. During the same period, the simulated tracer cloud moved downward about 0.66 m.

After about 55 days, the trajectory of the simulated tracer cloud became less steep compared to the trajectory of the observed cloud (Figure 5-11). Between 55 and 237 days, the simulated cloud moved downward about 0.7 m, whereas the observed tracer cloud moved downward about 1.8 m. Although the two trajectories have similar features, the actual cloud continued to move downward later in the test. Possible causes for the difference are discussed at the end of this chapter.

Variance and Dispersivity

The principal components of the variance measure the rate of spreading of the tracer cloud along its longitudinal and transverse axes and can be used to back-calculate the effective longitudinal and transverse dispersivities for the simulations. Figure 5-12 shows the longitudinal

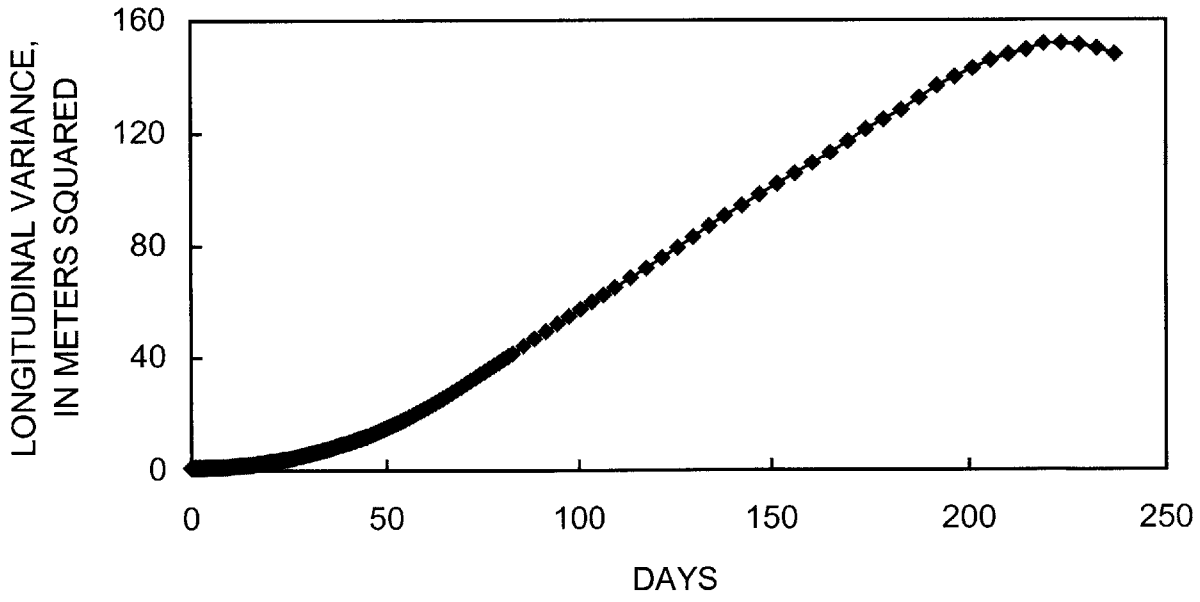

Figure 5-12. Longitudinal variance of the simulated tracer concentrations during the 237-day simulation of the Cape Cod tracer test.

variance of the simulated tracer cloud during the 237-day simulation period. The variance increased at a nonlinear rate during the first 65 days of the simulation, which corresponds to the early period in the tracer test when dispersivity was increasing with travel distance. Between about 65 and 210 days, the variance increased linearly with time, corresponding to the period when dispersivity had reached its asymptotic value of 0.96 m. After 210 days, the rate of increase dropped to zero, and the variance decreased slightly before the end of the simulation period. The decrease in the variance at the end of the simulation was caused when the leading edge of the tracer cloud intersected the downstream specified-pressure boundary. The loss of mass by advective transport across the boundary had the effect of cutting off the leading edge of the cloud and decreasing the apparent spreading of the cloud with time.

The change in longitudinal variance was used to calculate the effective longitudinal dispersivity during the simulation. Because the ground-water velocity was approximately constant and unidirectional, the dispersivity can be calculated from the change in variance with travel distance (Equation 4.19). The effective dispersivity α_L^{i+1} during a given time step Δt^{i+1} was obtained from the relationship,

$$\alpha_L^{i+1} = \frac{1}{2}\left[\frac{\sigma_{xx}^{2\,i+1} - \sigma_{xx}^{2\,i}}{\bar{x}^{i+1} - \bar{x}^{i}}\right], \tag{5.8}$$

where i and $i+1$ indicate two successive time steps and the other parameters are the same as those defined for Equation (4.19).

The time-step by time-step calculated longitudinal dispersivities (Figure 5-13) confirm that the dispersivity increased in a stepwise manner during the first 65 days of the simulation period, as was the intention of the simulation design outlined in Table 5-4 and Figure 5-2. The

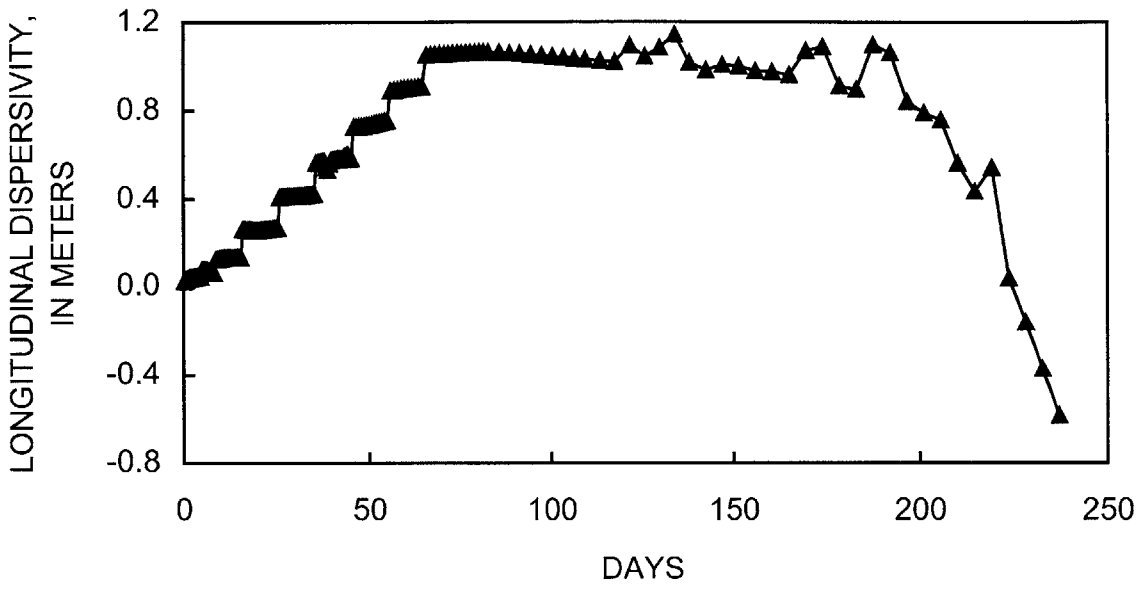

Figure 5-13. Estimated effective longitudinal dispersivity during the 237-day simulation of the Cape Cod tracer test.

calculated longitudinal dispersivities also show that an asymptotic value of about 1 m was reached after 65 days, as was intended. The decrease in dispersivity at the end of the simulation was caused by the boundary effect described above.

Figure 5-14 shows the transverse variance of the tracer cloud during the 237-day simulation. The abrupt increase in transverse variance at about 38 to 44 days corresponds to the 6-day period in late August 1985 when there was more than 15 cm of recharge. The transient vertical flow associated with the recharge caused the cloud to move downward about 0.4 m. The rapid downward movement was accompanied by increased spreading of the cloud in the vertical direction. There are two periods on either side of the abrupt increase during which the transverse

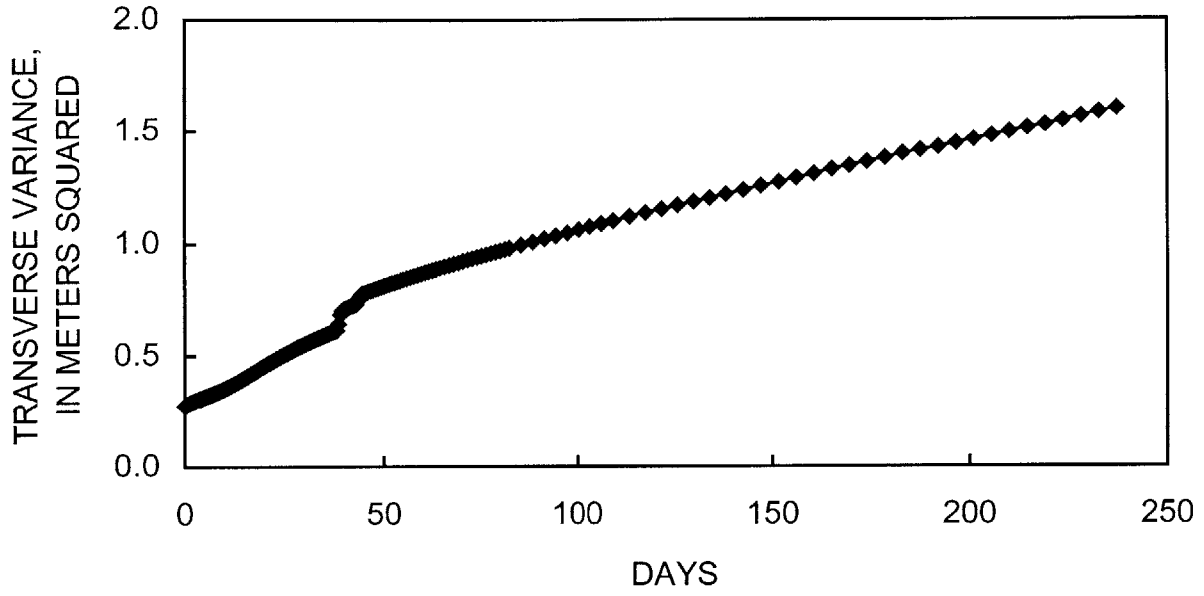

Figure 5-14. Transverse variance of the simulated tracer concentrations during the 237-day simulation of the Cape Cod tracer test.

variance increased linearly, but with different slopes (Figure 5-14). The greater slope early in the simulation period corresponds to the period of density-induced flow, during which there was more than 0.9 m of downward movement of the tracer cloud. The smaller slope later in the simulation period corresponds to the more flattened trajectory of the cloud, when density-induced sinking no longer was significant and downward movement was caused only by intermittent recharge. The transverse variance continued to increase linearly at the smaller slope, even when the longitudinal variance began to decrease, because the cloud remained approximately symmetrical in the vertical direction even as its leading edge intersected the downstream boundary.

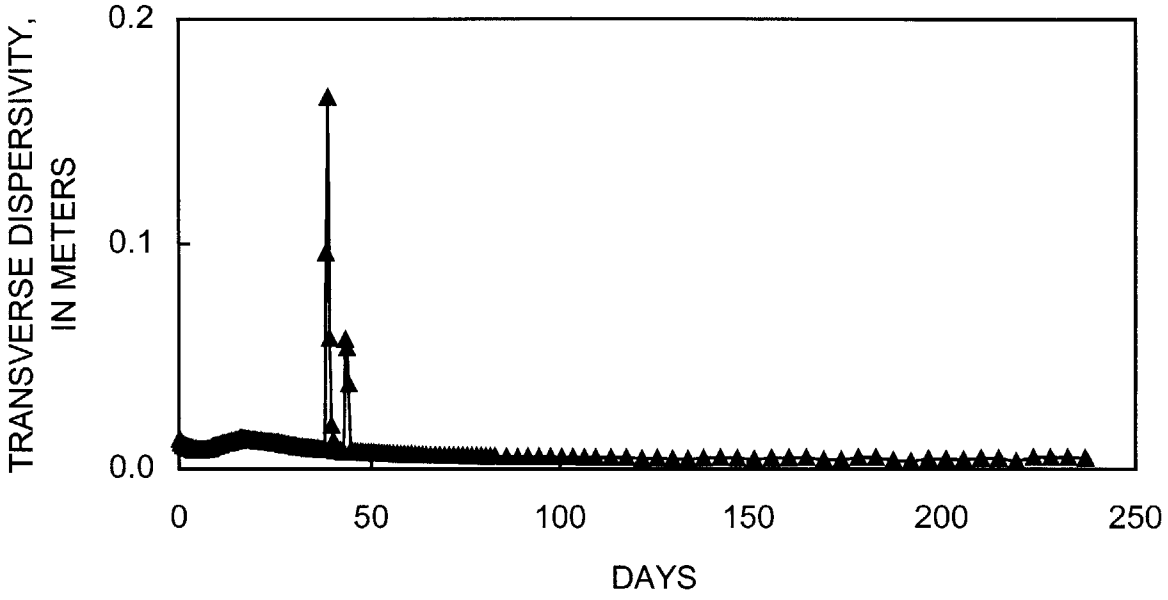

Figure 5-15. Estimated effective transverse dispersivity during the 237-day simulation of the Cape Cod tracer test.

The change in transverse variance was used to calculate the effective transverse dispersivity during the simulation. A relation similar to Equation (5.8) was used, but with α_T, $\bar{y}$, and σ_{yy}^2 instead of α_L, $\bar{x}$, and σ_{xx}^2. Figure 5-15 shows the calculated time-step by time-step transverse dispersivities. The August 1985 recharge events are reflected in two spikes in effective transverse dispersivity. Less obvious are the slightly elevated transverse dispersivity values early in the test that decreased over 90 days or so to about the input value of 0.005 m. The higher values reflect the downward components of flow associated with the period of density-induced flow.

The principal components of the variance from the simulated concentrations are compared to values reported by Garabedian and others (1991) in Table 5-9. The simulated longitudinal variances generally were smaller than the values obtained from the observed concentrations. The simulated transverse variances, however, generally were larger than the values obtained from the observed concentrations. LeBlanc and others (1991) reported that the tracer cloud developed an asymmetrical shape early in the field experiment, with a higher leading edge and a lower trailing edge. The simulated cloud, on the other hand, had a symmetrical shape that was maintained throughout the simulations. The differences between the simulated and observed variances may reflect the different shapes for the observed and simulated initial clouds that persisted during transport.

Discussion

The field-scale simulation provides compelling evidence that density-induced sinking contributed significantly to the downward movement of the tracer cloud during the Cape Cod tracer test. The simulated downward movement during the two periods with no recharge was 1.07 m, or 50 percent of the total simulated downward movement during the first 237 days of the test. Most of the downward movement caused by density differences occurred in the first 38 days of the simulation, although the downward trend was still evident during the second period of no recharge between 44 and 118 days from the start of the test.

The downward movement caused by density is somewhat surprising because the density difference between the tracer solution and the ambient ground water was very small – about 0.1 percent. However, this density contrast is sufficient to cause a component of downward force that results in downward movement in the predominantly horizontal flow regime. The angle of

Table 5-9. Principal components of the longitudinal and transverse vertical variances obtained from a spatial-moments analysis of the observed and simulated concentration distributions.

Days after start of field test	Principal component of longitudinal variance (m^2)		Principal component of transverse vertical variance (m^2)	
	Observed	Simulated	Observed	Simulated
0	--	0.98	--	.28
13	6.5	1.8	0.37	.38
33	20.2	6.9	0.46	.58
55	34.8	18.2	0.50	.84
83	52.4	41.4	0.72	.98
111	85.6	65.1	0.73	1.10
139	118	90.7	0.74	1.22
174	134	121	1.03	1.36
203	162	143[1]	1.02	1.46
237	189	148[1]	1.06	1.61

[1]Values reflect loss of mass by advective transport across downstream specified-pressure boundary.

downward movement below the horizontal depends in part on the horizontal ground-water velocity. In this system, where the ground-water velocity was 0.42 m/day, the initial angle of downward movement was almost 4 degrees. Over the 99 m traveled by the cloud in 237 days, the simulated density-related sinking was about 1.07 m, or a net angle of downward movement of about 0.6 degrees.

The persistence of the downward movement depends on the persistence of high solute concentrations in the center of the cloud. Any process that erodes the zone of highest

concentration diminishes the influence of the density difference. The simulation was designed to reproduce the increasing dispersivity reported by Garabedian and others (1991) during the first 70 days of the tracer test. The concave-upward shape of the trajectory of the cloud during the first 38 days, before the large recharge events, reflects this increasing dispersion and increasingly rapid erosion of the zone of highest concentrations in the center of the tracer cloud.

However, not all of the downward movement was caused by the density difference. About 44 cm of estimated recharge was simulated during the 237-day period. During the two periods encompassing all the recharge events, the tracer cloud moved downward 1.07 m. Given a porosity of 0.39, the recharge is equal to about 1.13 m of water in the aquifer. The remarkable equivalence of the two amounts is probably due to the proximity of the tracer cloud to the recharge boundary. The downward components of flow caused by recharge should decrease with depth as the bottom boundary of the flow system is approached. A tracer cloud injected farther below the water table would react in a more muted manner to recharge at the water table.

The effect of the two large recharge events in late August 1985 was particularly noticeable in the trajectory of the simulated tracer cloud. The effective dispersivities that were calculated from the variances of the simulated concentrations showed that the short bursts of rapid downward movement increased the rate of dispersion in the vertical direction. Rehfeldt (1988) demonstrated that short-term variations in horizontal flow direction during the Cape Cod field experiment increased the apparent transverse macrodispersion. A similar process clearly occurs in the vertical direction in response to specific recharge events. The effect on density-induced sinking of a tracer cloud would be greatest near the water table, where the transient downward movement would be largest.

The field-scale simulation predicted considerably less downward movement than was observed during the first 237 days of the tracer test. The predicted downward movement was about 2.1 m, or 33 percent less, than the observed downward movement. The agreement between simulated and observed downward movement was particularly good for the first 55 days of the simulation period, but the trajectory of the simulated cloud leveled off considerably after that time, while the observed cloud continued on a more or less steady downward trajectory.

It is possible that the good agreement between the simulated and observed trajectories during the first 55 days was fortuitous. According to LeBlanc and others (1991), local variations in hydraulic conductivity near the injection wells may have greatly influenced the behavior of the tracer cloud. These variations are not included in the simulation. Garabedian and others (1988) also noted that parts of the tracer cloud were not captured by the sampling array in the earliest snapshots of the experiment, so the true behavior of the cloud at early times may have been different than that shown by the spatial moments of the observed concentrations.

Many of the hydrologic and model-design considerations that were discussed in the previous chapter could have contributed to the under-prediction of the downward movement. In the simulation, a regularly shaped cloud was introduced instantaneously into the ambient flow system. However, the actual cloud was injected into the aquifer over a 16-hour period and likely had an initially irregular shape because of local variations in hydraulic conductivity near the injection wells. LeBlanc and others (1991) attribute the irregular shape observed later in the test to the imprinting of a shape during the injection of the tracer solution. The analysis in the previous chapter showed that the amount of downward movement was particularly sensitive to the horizontal cross-sectional area and aspect ratio of the initial cloud. It is possible that the

actual tracer cloud had a shape that was more conducive to density-induced sinking than the rectangular shape assumed for the simulations.

The analysis in the previous chapter also showed that the distance from the initial cloud to the top boundary of the modeled area affects the amount of simulated downward movement, particularly when the initial tracer cloud is located very close to the boundary. In the field-scale simulation, the top edge of the tracer cloud was only 0.4 m from the upper no-flow boundary. Both the small distance to the boundary and the no-flow specification could reduce the simulated downward movement by impeding the movement of water into the area being left by the sinking tracer cloud. The trajectories shown in Figure 4-15 suggest that a 50 percent increase in the distance to the upper boundary (for example, 0.6 m instead of 0.4 m) could increase the initial rate of downward movement by as much as 7 to 8 percent.

The water table is the upper boundary of the flow system at the field site. The representation of the water table as a no-flow boundary across which there is only intermittent recharge also probably reduced the amount of simulated downward movement. The pressure drop above the cloud as it began to move downward at the start of the field test probably caused a dimple to form in the water table above the cloud. The dimple, which is like a cone of depression, would induce additional flux from the unsaturated zone and, more importantly, the flow of water laterally into the area above the sinking cloud. This process would result in more vertical displacement of the cloud because of density-induced sinking than would be predicted with a fixed, no-flow upper boundary.

The correspondence between the amount of recharge and the downward movement of the tracer cloud during the recharge events shows that the simulated recharge rate directly affects the simulated trajectory of the tracer cloud. The recharge rate was estimated by the Thornthwaite

and Mather (1957) method, which was developed empirically from studies of agricultural lands in New Jersey. Application of the method to the bare sandy soils in the abandoned gravel pit is uncertain at best. The soil-moisture storage capacity may be even less than the assumed value of 5.08 cm (2 inches), which would increase the excess precipitation that would recharge the aquifer. In addition, recent regional ground-water modeling studies (Masterson and others, 1998) indicated that the Thornthwaite and Mather method may underestimate recharge rates on Cape Cod by as much as 25 percent. If the recharge values used in the simulation were increased by this amount, as much as 0.3 m of additional downward movement would have been simulated during the 237-day period.

The representation of the three-dimensional flow system as a two-dimensional vertical plane also could limit the predicted amount of downward movement. In Chapter 3, the models of Yih (1963, 1965) were used to show that the density-induced downward movement predicted by two-dimensional models may be about 25 percent smaller than that obtained from three-dimensional models. During the field test, water was able to move up and around the sinking cloud in all directions rather than being restricted to the two-dimensional plane. However, the additional dimension would also allow dispersion of the tracer cloud in the transverse, horizontal direction. The additional dispersion would reduce concentrations in the cloud and partly offset the additional sinking enabled by flow transverse to the longitudinal two-dimensional vertical section.

The simulation was designed to represent the processes that affect downward movement as accurately as possible within the restraints imposed by the two-dimensional, discretized model and the computational limitations at the time that the work was done. Equation (4.17) proved to be an accurate estimator of numerical dispersion, which allowed the input value of dispersivity to

be adjusted accordingly to produce the desired amount of effective longitudinal dispersivity at various travel distances. A three-dimensional simulation with a free-surface upper boundary and a statistically based representation of the hydraulic conductivity might be a more accurate representation of the flow system. The two-dimensional simulation appears to provide a sufficient examination of the density hypothesis, however, considering the uncertainties in recharge, local heterogeneity, and other factors that would affect any analysis of the field problem.

CHAPTER 6

DISCUSSION

The center of mass of the bromide tracer cloud moved downward about 3.2 m during the first 237 days of the Cape Cod tracer test. LeBlanc and others (1991) estimated that about half of this amount was caused by the accretion of recharge. They attributed the remainder to density-induced sinking, despite the relatively small density difference (about 0.1 percent) between the tracer solution and the ambient ground water. The preceding analysis provides compelling evidence that their hypothesis was correct. Although the predicted and observed amounts of downward movement differ, the general features of the observed trajectory were reproduced, and both modeling approaches demonstrated that even small density differences could result in significant sinking of a tracer cloud.

The analytical models over-predicted the amount of downward movement by several to tens of meters, mostly because the models do not account for the critical effect of dispersion. The analytical models also assume that the tracer cloud does not change shape with time; the observed cloud, however, had an irregular shape that became increasingly elongated with time, which would tend to reduce downward movement. The field-scale numerical model predicted about 2.1 m of downward movement, or about 33 percent less than the observed amount. Part of this difference may have been due to the two-dimensional representation of the three-dimensional flow system. Restriction of flow around the sinking cloud to the two-dimensional plane would reduce the rate of

downward movement. Other factors that could have contributed to the smaller than observed downward movement are the estimated recharge rate and transient dispersivity used in the numerical model. Recharge may have been greater through the sandy soil of the test site than was estimated by the Thornthwaite and Mather (1957) method. The stepwise increase in dispersivity may have overestimated the rate of dilution, particularly early in the test when the greatest rate of density-induced sinking is expected to occur. Finally, the representation of the free-surface water-table boundary as a no-flow boundary could have reduced the simulated amount of downward movement.

Many of these factors were discussed in the preceding chapters. As was noted at the end of the previous chapter, additional uncertainty in aquifer properties and the shape and size of the initial cloud would make it difficult to determine with greater confidence the contribution of density to the observed downward movement. However, many factors could be examined in more detail in additional simulations for their effects on density-induced sinking. Several of these factors are discussed in the next several sections.

Heterogeneity and Anisotropy

The analytical and numerical models treat the aquifer as a homogeneous porous medium. One value of permeability and one value of anisotropy were assumed to apply throughout the modeled domains. The effect of heterogeneity on the dispersion of the solute cloud was incorporated implicitly into the numerical model by using field-scale values of dispersivities, which are referred to as macrodispersivity, but the lenses and layers of the aquifer were not represented explicitly in the models.

A future study could represent the permeability fabric of the aquifer explicitly in a three-dimensional numerical model. Hess and others (1992) described the statistical properties of the aquifer at the field site from a variogram analysis of hydraulic-conductivity data obtained from permeameter measurements on cores and borehole flowmeter tests in long-screened wells. The incorporation of a statistically representative permeability fabric would allow the dispersion process to develop naturally with travel distance rather than approximately through the stepwise increase in dispersivity during the early part of the test. Zhang and others (1998) used this approach in their two-dimensional simulations of the Cape Cod experiment.

An equally important effect of heterogeneity may be on the shape of the injected tracer cloud. At the few-meter scale of the injected cloud, the local permeability distribution near the screened interval of the injection wells would control the initial shape and mixing of the tracer cloud. A few lenses of high-permeability material might dominate the shape and cause the cloud to have a highly irregular shape. The Cape Cod aquifer is composed of lenses and layers of sand and gravel that are longer than they are thick. Hess and others (1992) obtained correlation scales for hydraulic conductivity of 2.9 to 8 m in the horizontal direction and 0.18 to 0.38 m in the vertical direction. Therefore, the injected cloud is likely to have a very planar shape, which would reduce the amount of density-induced sinking.

The statistical analysis presented by Hess and others (1992) is based on data collected from boreholes that were located about 70 to 115 m from the injection wells. At best, a statistically based estimate of the local variations at the injection site is possible. One approach would be to create multiple realizations of the local permeability fabric at the injection site, inject the tracers into the system, and observe the rate of downward movement for each realization. The field experiment obviously is the one true, but unknowable, realization of the permeability

fabric. But this Monte Carlo style approach would allow an evaluation of the average rate of downward movement for the simulated systems.

LeBlanc and others (1991) noted that the bromide tracer cloud had two zones of elevated concentration, one near the leading edge of the cloud and just below the water table, and the other near the center of the cloud and deeper in the aquifer, which gave the cloud an asymmetrical shape. They hypothesized that this shape may have developed because of a zone of higher hydraulic conductivity near the water table. Part of the injected solution may have moved rapidly outward from the wells in a very permeable layer near the water table, while the remainder of the solution began sinking into the aquifer under the driving force of the density difference. They could only speculate about this process because the initial shape of the cloud and local variations in hydraulic conductivity at the injection site are unknown.

As the injected cloud moves away from the injection site and begins to pass through the various lenses and layers of the aquifer, the dispersion process develops as described by the stochastic models. However, the initial shape of the cloud that is the result of the local variations in permeability at the injection site would be imprinted on the cloud. This initial shape, although smoothed with time, would affect downward movement most significantly during the early times when density-induced sinking is greatest.

A similarly asymmetrical shape could develop in an aquifer with a trend of decreasing hydraulic conductivity with depth. Zhang and others (1998) produced an asymmetrical cloud in simulations of the Cape Cod tracer test by incorporation of three layers with different permeabilities at shallow depths across the entire modeled domain. There is some evidence for a decreasing hydraulic conductivity with depth at the field site, although the significant decrease in conductivity occurs below the path of the observed tracer cloud. LeBlanc and others (1991)

noted that local variations in permeability at the injection site might be sufficient to imprint the cloud with a shape that persists, without the added effect of a trending hydraulic conductivity, because of the limited vertical mixing.

A decreasing hydraulic conductivity with depth also could affect the response of the tracer cloud to recharge from precipitation. More flow would occur in the upper, more transmissive zone than in the lower, less transmissive zone. The result would be to limit the downward movement of the cloud in response to specific recharge events. The angle of downward movement would be reduced even more because the less than expected downward flux would be compensated for by an increased lateral flow.

An anisotropic permeability decreases the rate of downward movement in a flowing ground-water system because the direction of flow is biased toward the direction of greatest permeability. This effect would also be important in determining the shape of a tracer cloud during injection into the aquifer. In an anisotropic aquifer, the flow during the injection process would be biased toward the principal direction of the permeability tensor. The result, in most aquifers, would be a planar cloud that would be flatter than in an isotropic aquifer. Therefore, the limited sinking that results from anisotropy would be further reduced, indirectly, by the lateral spreading of the cloud during injection.

Dispersion

The stepwise method to approximate the period of increasing macrodispersivity was reasonably effective at matching the observed moments of the tracer cloud during the first 237 days of the field experiment. Much of the previous discussion about dispersion focused on the

dilution of the tracer cloud and the decrease in the rate of downward movement caused by decreasing density differences.

However, an equally important effect of dispersion may be the increase in the horizontal extent of the tracer cloud with time. The Yih (1963) analytical models provide an insight into this effect, even though the results are independent of the size of the tracer cloud. The bromide tracer cloud grew mostly in the longitudinal direction; vertical spreading was limited. This is analogous to an increasing length of the major axis of the two-dimensional ellipse in the Yih models. As was shown in Chapter 3, the downward movement of an elliptical cloud is greatly reduced as the length of the major ellipse is increased relative to that of the minor axis. Therefore, dispersion may decrease downward movement by increasing the aspect ratio of the cloud with time. Gelhar's model incorporated an approximation to the dilution effect, but it did not consider the additional effect on the cloud's shape.

Dispersion was represented in the numerical modeling as an isotropic parameter. The values for longitudinal and transverse dispersivity were defined relative to the direction of flow, not to the principal directions of the permeability tensor. Therefore, the dispersivities that controlled the dispersion of the tracer cloud did not vary with flow direction, even when the flow was at a downward angle and the cloud was moving across the layering of the sand and gravel. The stochastic theories of Gelhar and others indicate that macrodispersivity would vary with flow direction in a naturally layered system. Voss (1984) proposed an *ad hoc* method to incorporate an anisotropic dispersivity, but it was not used for this analysis.

The calculated incremental transverse dispersivities for the field-scale simulation clearly showed the effect of short periods of downward movement during the major recharge events of August 1985. However, the transient increase in the dispersion rate reflected the isotropic

representation of dispersivity. If the effective longitudinal and transverse dispersivities are different during vertical flow, the rate of dilution of the cloud and the predicted downward movement could be different. Transverse spreading would probably increase as the cloud moves downward across the lenses and layers of the aquifer. The result would be a decrease in the rate of downward movement. Significant downward movement when the density difference is large could produce a similar effect. Shincariol and Schwartz (1992) described this phenomenon in their sand-tank experiments with lenticular porous media. The Gelhar analytical model partly accounts for this situation by relating the downward movement to a mixing length and the amount of vertical displacement.

Recharge

The numerical simulation of the field-scale tracer test indicated that recharge from precipitation accounted for about half of the simulated downward movement during the first 237 days of the test. One possible cause for the greater observed downward movement during this period (3.2 m) is a greater amount of recharge than was estimated by use of the Thornthwaite and Mather (1957) water-balance method. Of course, the difference could also be due to any number of considerations related to the simulation of the density-induced sinking. The additional 1.2 m of downward movement during the next 274 days of the experiment (LeBlanc and others, 1991), when the influence of density should have been very small, suggest, however, that recharge was the major contributor to the total downward movement.

Therefore, simulations in which the vertical trajectory of the cloud may control the fate of reactive species should include as accurate a representation of the recharge flux as possible. Stollenwerk (1995) and Davis and others (2000) discussed this situation for the reactive species

included in the 1985-88 Cape Cod tracer test and in a later test conducted in 1993-95 with several reactive-metal species. The distance between the tracer cloud and the water table is expected to affect the amount of downward movement in response to a recharge event. The tracer cloud in the Cape Cod test was injected near the water table, where downward flow from recharge is expected to be greatest. Jacob (1950) derived a solution for the oblique angle to the water table of flow for particular recharge rates. LeBlanc and others (1991, p. 906) reported that 60 cm of recharge during 237 days would result in an angle of only 1 degree below the water table. However, the angle would be much larger for a short time during specific recharge events. The same model yields a downward angle of about 40° for the estimated 7.09 cm of recharge in 12 hours that occurred in late August 1985 (Table 4-7). The downward angle of movement would decrease with distance below the water table and be zero, by definition, at the no-flow bottom boundary of the flow system. Therefore, a cloud that is injected near the water table is expected to be more sensitive to specific recharge events than a cloud that is injected deeper in the flow system.

As mentioned above, the temporal pattern of recharge may also be important because it affects the dispersion rate in the vertical direction. A cloud that moves downward because of a continuous, but low, rate of recharge may disperse differently than a cloud that moves rapidly downward across many layers in the aquifer in a short period of time. The rapid downward movement may disperse the cloud more quickly and result in less density-induced vertical displacement than might have otherwise occurred.

The Water Table

The upper boundary in the field-scale simulation was represented as a no-flow boundary, and intermittent recharge was represented as a fluid flux to the top row of active nodes in the model. This representation was a compromise because the sensitivity simulations in Chapter 4 showed that the downward movement was greater when fluid flow was allowed across a specified-pressure boundary in response to the downward movement of the tracer cloud. The water table is a specified-pressure boundary, with the pressure equal to zero, but the water table also is a free surface and changes position in response to pressure changes on either side of the boundary.

For the field-scale simulation, the top of the tracer cloud was only 0.4 m below the no-flow boundary. It is possible that the predicted downward movement would be greater than was simulated if the water-table could be represented as a free surface. The pressure drop above the sinking cloud might not only cause the water table to move downward, but it might also induce additional flow from the unsaturated zone directly above the sinking cloud. Although the amount of effective inflow that would be generated might be small in the coarse sand and gravel, the effect might be to allow the cloud to "detach" itself from the no-flow boundary. In the extreme case where the top of the cloud abuts the boundary in the numerical simulations, the cloud is essentially "stuck" on the boundary and detaches itself only slowly as ambient ground water moves in laterally to fill in the area above the sinking cloud.

This phenomenon might be investigated by use of saturated-unsaturated density-dependent flow and transport models. The uncertainties associated with the model parameters

would not necessarily result in more accurate predictions, but the importance of the processes at the water table could be investigated quantitatively.

Internal Flow within the Tracer Cloud

The analytical models predicted more sinking than was observed during the tracer test, while the numerical model predicted less sinking than was observed. The analytical models of Yih (1963, 1965) account for the flow of the tracer fluid; the Laplace equation is solved for both the ambient and tracer fluids. But the tracer cloud is assumed to move as a rigid body that is not distorted with time. The numerical simulations showed, however, that there are patterns of flow that develop within the tracer cloud that cause it to become asymmetrical with time. As the cloud becomes diluted, the concentration distribution changes in the cloud. The concentration of solutes decreases near the cloud's boundaries, the edges sink less than the central core, and the cloud develops a saddle shape.

This pattern of flow reflects an internal circulation that develops within the cloud itself. Even within the cloud, fluid with low concentrations around the edges moves up into the area left by the denser, sinking core. The analytical models do not capture these internal dynamics and, therefore, may result in too energy-efficient a sinking process. This may contribute to the over-prediction of the amount of downward movement.

Injection of the Tracer Cloud

In all of the simulations described in this report, the tracer cloud was assumed to appear instantaneously with a rectangular shape in the ambient flow field. During the 1985-88 field

experiment, the cloud was injected over a 16-hour-long period at a rate of about 7.6 L/min (LeBlanc and others, 1991). This rate of injection was much greater than the ambient flow, and it is reasonable to approximate the injection as one that occurred into a static ambient flow. However, as has been discussed above and in other chapters of this report, it is unlikely that the cloud assumed the regular shape used in the simulations.

The explicit representation of the injection process in the simulations could shed light on how the actual test began. As mentioned above, however, the initial shape of the tracer cloud would be dominated by the local variations in permeability around the well screens, and this variability is essentially unknowable for most practical situations. Simulation of the effect of the heterogeneity on the initial cloud would have to include algorithms that apportion the injected flow among the various permeability units intersected by the well screens. Simulation of the injection process in two dimensions is also problematic because the flow around the line sources that represent the screens is inherently three-dimensional. A decision would need to be made *a priori* about the width of the cloud transverse to the plane of the section so that the amount of injected fluid could be scaled accordingly.

The injection process could also bring other factors into play. For example, injection close to the water table could create a temporary mound in the free surface. During the injection, when the fluid enters the aquifer at its maximum density, downward flow could begin immediately and proceed throughout the injection period. If the tracer solution was sufficiently dense, the initial cloud could have spread significantly in the vertical direction even before the ambient flow was once again allowed to dominate, and the cloud began to be translated laterally. As was shown by the elliptical cloud in the Yih models and by the sensitivity analysis of source configuration with the numerical models, a cloud that is longer in the vertical direction than in

the horizontal direction would sink more rapidly than a cloud that presents a larger area perpendicular to the gravitational force.

Reactive Tracers

The movement of the tracer cloud during the 1985-88 Cape Cod experiments was described in terms of the spatial moments of bromide, a conservative anionic tracer. The tracer solution also contained lithium, a cation; molybdate, an oxyanion; and fluoride, another anion, that were expected to react with the porous medium and move nonconservatively in the ground water (LeBlanc and others, 1991; Garabedian and others, 1988; Stollenwerk, 1995). Therefore, the chemical composition of the tracer solution was expected to change with time, although bromide comprised about 75 percent of total mass added (LeBlanc and others, 1991, Table 2).

It was beyond the scope of this effort to account for the changing fluid composition as the tracer cloud was transported through the aquifer. Zhang and others (1998) used the work described in this thesis and two preliminary proceedings papers (LeBlanc and Celia, 1991, 1996) as the basis for simulations of variable-density flow for the bromide and lithium tracer clouds. They demonstrated that the lithium cloud, which was retarded relative to the bromide cloud, moved downward less as it separated from the dense, sinking bromide cloud. Stollenwerk (1995) reported a similar observation for the molybdate tracer, which was also retarded relative to the bromide.

In a tracer test in which the reactive tracers are a major source of the dissolved mass, the reactions that change the concentrations of the added tracers, or add other species from the sediments, would have to be considered. The downward movement of a tracer cloud defined by

one of the tracers would depend on the concentrations of the other tracers in the same volume of water at various points along the flow path.

CHAPTER 7

SUMMARY

Many contaminant plumes in shallow, unconsolidated aquifers sink downward below the water table and are overlain by a zone of contaminant-free ground water (Kimmel and Braids, 1980; MacFarlane and others, 1983; LeBlanc, 1984; Ryan and Kipp, 1997). The downward movement is usually attributed to areal recharge and density-induced sinking. The density effect arises because the difference in density between the ambient ground water and the plume water creates vertically oriented driving forces that result in a downward component of velocity (Hubbert, 1953; Bear, 1972).

Downward movement of solutes has also been observed in several large-scale natural-gradient tracer experiments in which the relative density differences were small (less than 0.5 percent). These experiments generally have involved the injection of a finite volume of tracer solution into a shallow aquifer, and monitoring of the solute cloud as it moved through an array of multilevel wells (Sudicky and others, 1983; Mackay and others, 1986; LeBlanc and others, 1991; Boggs and others, 1992; Jensen and others, 1993; Davis and others, 2000). In a 1985-88 tracer test conducted in the Cape Cod sand and gravel aquifer, LeBlanc and others (1991) observed that the bromide tracer cloud moved downward 3.2 m below the water table in 237 days of transport. They estimated that about 60 cm of recharge occurred during this period, which accounted for only about half of the observed vertical displacement. They hypothesized that the downward movement was also due to density-induced sinking of the tracer cloud, which

was about 0.1 percent denser than the ambient ground water. The purpose of this report was to examine this hypothesis.

The first step in this effort was the use of analytical and numerical models to examine the hydrologic factors that affect the rate of downward movement caused by density differences. The analytical model of Hubbert (1953) assumes that the tracer fluid is dispersed in the ambient fluid, and both fluids move in response to their own potential fields. The potential field of the tracer fluid is related to the potential field of the ambient fluid by the relative density difference. The analytical models of Yih (1963, 1965) consider tracer clouds of various regular shapes in an ambient flow field. The models solve the Laplace equation with appropriate pressure and continuity conditions at the boundary between the two fluids. The solutions described by Yih are independent of cloud size, and the fluid body does not change shape or orientation as it moves through the aquifer. The Hubbert and Yih models also do not consider the effects of dispersion and dilution. A modification of the Yih models to approximate the effects of dispersion (Lynn Gelhar, written communication, 1983) was also considered.

The analytical models demonstrate that the relative density difference ($\Delta\rho/\rho$) directly affects the rate of downward movement. The vertical driving force associated with the density difference causes a vertically downward velocity component that is added to the ambient ground-water velocity, which is approximately horizontal in most field situations. Therefore, the trajectory of the tracer cloud is at an oblique angle to the water table that depends on the magnitudes of the relative density difference and the horizontal ground-water velocity. The effect of anisotropy of permeability is to reduce the amount of downward movement in the typical case where the greatest permeability is in the horizontal direction.

The Yih (1963) models also show that the shape and orientation of the fluid body affect the rate of downward movement. In a two-dimensional flow system, an elliptical body with its major axis oriented horizontally sinks at a slower rate than an elliptical body with its major axis oriented vertically. The rate of downward movement of a circular body is intermediate between the two cases for the elliptical body. As the tracer cloud sinks because of density, the ambient ground water is displaced and moves up and around the body to fill the area being left by the sinking body. A body that presents a large dimension broadside to the density-induced downward movement sinks more slowly than a body that presents a relatively narrow profile to the direction of movement. In essence, a streamlined body cuts more readily through the ambient ground water.

A comparison of the Yih models for a circular body in a two-dimensional system and a sphere in a three-dimensional system indicates that the restriction of flow to the two-dimensional plane reduces the amount of downward movement. In the three-dimensional system, the ambient ground water can move up and around the sinking body in all directions, while the circulation is restricted in the two-dimensional system. The result is a less energy-efficient circulation in the two-dimensional system and about 25 percent less downward movement than for the three-dimensional case.

Gelhar (written communication, 1983) derived a modification of the Yih model for a two-dimensional circular body that includes the effect of dispersion as the body moves vertically through the ambient fluid. The model indicates that the rate of downward movement decreases as the body is diluted and the relative density difference decreases with travel distance. The trajectory of a dense tracer cloud undergoing dispersion in a horizontal ambient flow field is concave upward. The rate at which the downward movement decreases is strongly dependent on

initial size of the tracer cloud. The maximum solute concentration in a small cloud will decrease more rapidly because of dispersion than the maximum concentration in a large cloud.

The analytical models were applied using aquifer and test parameters from the 1985-88 Cape Cod tracer test. All the models greatly over-predicted the amount of downward movement, especially considering that the observed vertical displacement of 3.2 m was caused by both recharge and density differences, while the models only considered the density effects. The closest agreement was obtained when the effects of dispersion were estimated using the Gelhar modification of the Yih model. The representation of the tracer cloud as an ideal body that does not disperse or change shape as it moves in an aquifer clearly does not capture important processes that affect the rate of downward movement.

The factors affecting density-induced sinking were also examined with the two-dimensional finite-element model SUTRA (Voss, 1984), which can simulate density-dependent flow and solute transport. The density was assumed to be linearly dependent on the solute concentration. Simulations were run for a 5-day period using a grid that was 20 m long and 12 m high. The grid spacing was designed to minimize the effects of numerical dispersion and oscillations. Spatial moments were used to characterize the simulated tracer cloud as it moved and dispersed in the ground-water system. The initial tracer cloud, which was 3.2 m long and 1.8 m high, was assumed to appear instantaneously in the ambient flow field, rather than being injected into the aquifer over a finite time period.

The numerical model demonstrated that the trajectory of a sinking tracer cloud is concave upward because of decreasing density differences with travel distance. The simulated cloud developed a saddle shape as the cloud dispersed because the region with persistent high concentrations in the center moves downward more rapidly than the region with low

concentrations near the boundary of the cloud. The downward component of ground-water velocity is greatest near the center of the cloud, and the upward component of velocity is greatest behind and slightly above the cloud, where ambient ground water is moving into the area left by the sinking cloud.

The rate of downward movement simulated using the numerical model increased as the initial density difference increased. The downward movement is particularly sensitive to dispersivity, which affects how quickly solute concentrations and the associated density-driving force decrease. The size and shape of the initial tracer cloud also affect the rate of downward movement. For clouds of similar shape, a large cloud moves downward farther than a small cloud because solute concentrations persist longer in the large cloud than in the small cloud. The horizontal length of the cloud also significantly affects the rate of downward movement. A large, horizontally oriented planar cloud resists downward movement because a large perturbation in the ambient flow system is required for the ambient ground water to move up and around the broad, sinking cloud. Horizontal spreading of the tracer cloud because of dispersion probably increases the significance of this effect with travel distance.

The numerical modeling also demonstrated that areal recharge causes the simulated tracer cloud to move downward below the water table. The effect is greatest when the initial tracer cloud is located near the water table. In this situation, the amount of downward movement is nearly equal to the equivalent thickness of the zone of recharged water in the aquifer. The effect of recharge on downward movement probably decreases if the cloud is farther below the water table.

The location of the initial tracer cloud relative to the top boundary of the flow system, and the type of top boundary, also affected the simulated rate of downward movement. The

downward movement is greater for a specified-pressure top boundary than for a no-flow top boundary. With the specified-pressure representation of the water table, water can enter the model domain across the boundary to fill the area left by the sinking cloud, while the water must flow in laterally from the ground-water system in the no-flow representation. Because the ease with which the lateral inflow occurs can affect the rate of downward movement in the no-flow case, a tracer cloud that is located close to the boundary moves downward less rapidly than a cloud that is located farther below the boundary.

The results of the analytical and numerical simulations were used to guide the design of a field-scale SUTRA numerical simulation of the Cape Cod tracer test. The movement of the tracer cloud was simulated for the first 237 days of the experiment, when 70 percent of the total downward movement during the 511-day test occurred, and when the density effects would have been greatest. The modeled area was 136 m long and 25 m high. The top boundary was represented as a no-flow boundary across which there was intermittent recharge from precipitation. The total recharge during the simulation period was about 44 cm, which was estimated using the Thornthwaite and Mather (1957) water-balance method. An ambient horizontal ground-water velocity of 0.42 m/d was established by appropriate specification of boundary conditions on the upstream and downstream sides of the model. The tracer cloud, which was 3.4 m long and 1.8 m high, was assumed to appear instantaneously in the aquifer; the top edge of the cloud initially was 0.4 m below the top boundary of the model. The initial relative density difference between the tracer solution and the ambient ground water was about 0.1 percent.

The grid was designed to insure that the tracer cloud remained within the modeled area during the 237-day simulation. The spatial and temporal discretization was chosen to minimize

numerical oscillations and to insure that the tracer cloud experienced the appropriate amount of longitudinal dispersion as it traveled about 99 m across the modeled area. Based on observations during the field experiment (Garabedian and others, 1991), the longitudinal dispersivity was assumed to increase linearly during the first 70 days to an asymptotic value of 0.96 m. The time discretization was chosen so that the sum of the estimated numerical longitudinal dispersivity and the model-input dispersivity matched the trend observed in the field experiment.

The simulated tracer cloud moved downward 2.13 m and laterally about 99 m during the 237-day period. The cloud moved downward about 0.94 m in the first 38 days, during which time there was no recharge. The estimated total downward movement caused by the density difference was about 1.07 m, or about half of the total vertical displacement. The net simulated angle of downward movement below the horizontal during the first 33 days of the simulation period was about 3.7 degrees. The observed net angle during the same period was about 2.7 degrees.

The tracer cloud also moved downward because of areal recharge from precipitation. Recharge occurred in two periods, one from about 38 to 44 days from the start of the test, when there was an estimated 15 cm of recharge, and the other from about 118 to 237 days, when there was about 29 cm of recharge. The total downward movement during these two periods was about 1.07 m, which agrees closely with the estimated thickness occupied in the aquifer by the recharged water (assuming a porosity of 0.39).

The field-scale simulation provides compelling evidence that density-induced sinking contributed significantly to the downward movement of the tracer cloud during the Cape Cod field experiment. Although the simulated downward displacement (2.1 m) was about 33 percent less than the observed downward displacement (3.2 m), the general features of the observed

trajectory were reproduced. Despite the small initial density difference (0.1 percent), the simulated downward movement during the first 38 days was about one third of the observed downward movement during the entire 237-day period. It is clear that even small density differences can result in significant sinking of a tracer cloud.

A number of factors could have contributed to the under-prediction of the downward movement. Part of the difference may have been due to the two-dimensional representation of the three-dimensional flow system. Other factors include the estimated recharge rate and transient dispersivity. Recharge may have been greater through the sandy soil of the test site than was estimated by the water-balance method. The stepwise increase in longitudinal dispersivity may have overestimated the rate of dilution, particularly early in the test when the greatest rate of density-induced sinking would occur. The representation of the water table as a no-flow boundary also could have reduced the simulated amount of downward movement.

Several other factors that were not considered in this analysis could influence downward movement caused by density differences. The numerical model represented the aquifer as a homogeneous, anisotropic porous medium, and the tracer solution was assumed to appear instantaneously in the aquifer rather than being injected over a period of time. Local heterogeneity near the injection wells would likely result in an irregularly shaped cloud. Because the aquifer is comprised of horizontal lenses and layers of sand and gravel, the initial cloud probably had an irregular, planar shape that would have tended to reduce the rate of density-induced sinking. During the injection, downward flow could begin immediately and proceed throughout the injection period. The result would be an initial cloud that would have spread in the vertical direction even before the cloud began to move laterally with the ambient flow.

These factors could be examined in three-dimensional simulations that include the water table as an upper boundary, better estimates of recharge, a statistically based representation of heterogeneity, and simulated injection of the tracer solution. However, further analysis of the problem would still have to face uncertainties in recharge, local heterogeneity, and other factors. The two-dimensional numerical simulation provides convincing evidence of density-induced sinking of the bromide tracer cloud during the 1985-88 Cape Cod tracer test.

REFERENCES

Adams, E.E., and Gelhar, L.W., 1992, Field study of dispersion in a heterogeneous aquifer, 1. Spatial moments analysis: Water Resources Research, v. 28, no. 12, p. 3293-3307.

Bear, Jacob, 1972, Dynamics of fluids in porous media: New York, Elsevier, 764 p.

Boggs, J.M., Young, S.C., Beard, L.M., Gelhar, L.W., Rehfeldt, K.R., and Adams, E.E., 1992, Field study of dispersion in a heterogeneous aquifer, 1. Overview and site description: Water Resources Research, v. 28, no. 12, p. 3281-3291.

Dagan, Gedeon, 1982, Stochastic modeling of groundwater flow by unconditional and conditional probabilities, 2. The solute transport: Water Resources Research, v. 18, no. 4, p. 835-848.

Dagan, Gedeon, 1984, Solute transport in heterogeneous porous formations: Journal of Fluid Mechanics, v. 145, p. 151-177.

Dagan, Gedeon, 1988, Time-dependent macrodispersion for solute transport in anisotropic heterogeneous aquifers: Water Resources Research, v. 24, no. 9, p. 1491-1500.

Davis, J.A., Kent, D.B., Coston, J.A., Hess, K.M., and Joye, J.L., 2000, Multispecies reactive tracer test in an aquifer with spatially variable chemical conditions: Water Resources Research, v. 36, no. 1, p. 119-134.

Freeze, R.A., and Cherry, J.A., 1979, Groundwater: Englewood Cliffs, N.J., Prentice-Hall, 604 p.

Freyberg, D.L., 1986, A natural gradient experiment on solute transport in a sand aquifer, 2. Spatial moments and the advection and dispersion of nonreactive tracers: Water Resources Research, v. 22, no. 13, p. 2031-2046.

Frind, E.O, 1982, Simulation of long-term transient density-dependent transport in groundwater: Advances in Water Resources, v. 5, no. 2, p. 73-78.

Garabedian, S.P., Gelhar, L.W., and Celia, M.A., 1988, Large-scale dispersive transport in aquifers: Field experiments and reactive transport theory: Cambridge, Mass., Massachusetts Institute of Technology, Dept. of Civil Engineering, Ralph M. Parsons Laboratory, Hydrology and Water Resources Systems Report No. 315, 290 p.

Garabedian, S.P., LeBlanc, D.R., Gelhar, L.W., and Celia, M.A., 1991, Large-scale natural-gradient tracer test in sand and gravel, Cape Cod, Massachusetts: 2. Analysis of spatial moments for a nonreactive tracer: Water Resources Research, v. 27, no. 5, p. 911-924.

Gelhar, L.W., and Axness, C.L, 1983, Three-dimensional stochastic analysis of macrodispersion in aquifers: Water Resources Research, v. 19, no. 1, p. 161-180.

Gelhar, L.W., Gutjahr, A.L., and Naff, R.L., 1979, Stochastic analysis of macrodispersion in a stratified aquifer: Water Resources Research, v. 15, no. 6, p. 1387-1397.

Hess, K.M., 1989, Use of a borehole flowmeter to determine spatial heterogeneity of hydraulic conductivity and macrodispersion in a sand and gravel aquifer, Cape Cod, Massachusetts, *in* Molz, F.J., Melville, J.G., and Guven, Oktay, eds., Proceedings of the Conference on New Field Techniques for Quantifying the Physical and Chemical Properties of Heterogeneous Aquifers, Dallas, Texas, March 20-23, 1989: Dublin, Ohio, National Water Well Association, p. 497-508.

Hess, K.M., Wolf, S.H., and Celia, M.A., 1992, Large-scale natural gradient tracer test in sand and gravel, Cape Cod, Massachusetts: 3. Hydraulic-conductivity variability and calculated macrodispersivities: Water Resources Research, v. 28, no. 8, p. 2011-2027.

Hubbert, M.K., 1940, The theory of ground-water motion: Journal of Geology, v. 48, no. 8, p. 785-944.

Hubbert, M.K., 1953, Entrapment of petroleum under hydrodynamic conditions: Bulletin of the American Association of Petroleum Geologists, v. 37, no. 8, p. 1954-2026.

Istok, J.D., and Humphrey, M.D., 1993, Buoyancy-induced flow at small relative densities: Implications for tracer test interpretation and contaminant transport: EOS, Transactions of the American Geophysical Union, p. 268.

Jacob, C.E., 1950, Flow of ground water, *in* Rouse, H., ed., Engineering Hydraulics: New York, John Wiley, p. 321-386

Jalbert, Marc, Dane, J.H., Abriola, L.M., and Pennell, K.D., 2000, A nondimensional evaluation of tracer sensitivity to density effects: Ground Water, v. 38, no. 2, p. 226-233.

Jensen K.H., Bitsch, K., and Bjerg, P.L., 1993, Large-scale dispersion experiment in a sandy aquifer in Denmark: Observed tracer movements and numerical analysis: Water Resources Research, v. 29, no. 3, p. 673-696.

Kimmel, G.E., and Braids, O.C., 1980, Leachate plumes in ground water from Babylon and Islip landfills, Long Island, New York: U.S. Geological Survey Professional Paper 1085, 38 p.

Kipp, K.L., Jr., 1987, HST3D, A computer code for simulation of heat and solute transport in three-dimensional ground-water flow systems: U.S. Geological Survey Water-Resources Investigations Report 86-4905, 517 p.

Koch, Manfred, and Zhang, Gangpeng, 1992, Numerical simulation of the effects of variable density in a contaminant plume: Ground Water, v. 30, no. 5, p. 731-742.

LeBlanc, D.R., 1984, Sewage plume in a sand and gravel aquifer, Cape Cod, Massachusetts: U.S. Geological Survey Water-Supply Paper 2218, 28 p.

LeBlanc, D.R., Guswa, J.H., Frimpter, M.H., and Londquist, C.J., 1986, Ground-water resources of Cape Cod, Massachusetts: U.S. Geological Survey Hydrologic-Investigations Atlas HA-692, 4 sheets.

LeBlanc, D.R., and Celia, M.A., 1991, Density-induced downward movement of solutes during a natural-gradient tracer test, Cape Cod, Massachusetts, *in* Mallard, G.E., and Aronson, D.A., eds., U.S. Geological Survey Toxic Substances Hydrology Program--Proceedings of the technical meeting, Monterey, California, March 11-15, 1991: U.S. Geological Survey Water-Resources Investigations Report 91-4034, p. 10-14.

LeBlanc, D.R., and Celia, M.A., 1996, Numerical simulation of downward movement of solutes during a natural-gradient tracer test in sand and gravel, Cape Cod, Massachusetts, *in* Morganwalp, D.W., and Aronson, D.A., eds., U.S. Geological Survey Toxic Substances Hydrology Program--Proceedings of the technical meeting, Colorado Springs, Colorado, September 20-24, 1993: U.S. Geological Survey Water-Resources Investigations Report 94-4015, v. 1, p. 283-287.

LeBlanc, D.R., Garabedian, S.P., Hess, K.M., Gelhar, L.W., Quadri, R.D., Stollenwerk, K.G., and Wood, W.W., 1991, Large-scale natural-gradient tracer test in sand and gravel, Cape Cod, Massachusetts: 1. Experimental design and observed tracer movement: Water Resources Research, v. 27, no. 5, p. 895-910.

LeBlanc, D.R., Hess, K.M., Kent, D.B., Smith, R.L., Barber, L.B., Stollenwerk, K.G., and Campo, K.W., 1999, Natural restoration of a sewage plume in a sand and gravel aquifer, Cape Cod, Massachusetts, *in* Morganwalp, D.W., and Buxton, H.T., eds., U.S. Geological Survey Toxic Substances Hydrology Program--Proceedings of the Technical Meeting, Charleston, South Carolina, March 8-12, 1999--Volume 3 of 3--Subsurface Contamination from Point Sources: U.S. Geological Survey Water-Resources Investigations Report 99-4018C, p. 245-259.

MacFarlane, D.S., Cherry, J.A., Gillham, R.W., and Sudicky, E.A., 1983, Migration of contaminants in groundwater at a landfill: A case study, 1. Groundwater flow and plume delineation: Journal of Hydrology, v. 63, p. 1-29.

Mackay, D.M., Freyberg, D.L., Roberts, P.V., and Cherry, J.A., 1986, A natural gradient experiment on solute transport in a sand aquifer, 1. Approach and overview of tracer movement: Water Resources Research, v. 22, no. 13, p. 2017-2029.

Masterson, J.P., Stone, B.D., Walter, D.A., and Savoie, Jennifer, 1997a, Hydrogeologic framework of western Cape Cod, Massachusetts: U. S. Geological Survey Hydrologic-Investigations Atlas HA-741, 1 plate.

Masterson, J.P., Walter, D.A., and LeBlanc, D.R., 1998, Delineation of contributing areas to selected public-supply wells, western Cape Cod, Massachusetts: U.S. Geological Survey Water-Resources Investigations Report 98-4237, 45 p.

Masterson, J.P, Walter, D.A., and Savoie, Jennifer, 1997b, Use of particle tracking to improve numerical model calibration and to analyze ground-water flow and contaminant migration, Massachusetts Military Reservation, Cape Cod, Massachusetts: U.S. Geological Survey Water-Supply Paper 2482, 50 p.

Mendoza, C.A., and Frind, E.O, 1990a, Advective-dispersive transport of dense organic vapors in the unsaturated zone, 1. Model development: Water Resources Research, v. 26, no. 3, p. 379-387.

Mendoza, C.A., and Frind, E.O., 1990b, Advective-dispersive transport of dense organic vapors in the unsaturated zone, 2. Sensitivity analysis: Water Resources Research, v. 26, no. 3, p. 388-398.

Neuman, S.P., Winter, C.L., and Newman, C.M., 1987, Stochastic theory of field-scale Fickian dispersion in anisotropic porous media: Water Resources Research, v. 23, no. 3, p. 453-466.

Oostrom, M., Hayworth, J.S., Dane, J.H., and Guven, O., 1992, Behavior of dense aqueous leachate plumes in homogeneous porous media: Water Resources Research, v. 28, no. 8, p. 2123-2134.

Paschke, N.W., and Hoopes, J.A., 1984, Buoyant contaminant plumes in groundwater: Water Resources Research, v. 20, no. 9, p. 1183-1192.

Rehfeldt, K.R., 1988, Prediction of macrodispersivity in heterogeneous aquifers: Cambridge, Mass., Massachusetts Institute of Technology, Dept. of Civil Engineering, unpublished Ph.D. thesis, 233 p.

Rivett, M.O., Feenstra, S., and Cherry, J.A., 1994, Transport of a dissolved-phase plume from a residual solvent source in a sand aquifer: Journal of Hydrology, v. 159, no. 1-4, p. 27-41.

Ryan, B.J., and Kipp, K.L., Jr., 1997, Ground-water flow and contaminant transport at a radioactive-materials processing site, Wood River Junction, Rhode Island: U.S. Geological Survey Professional Paper 1571, 89 p.

Sanford, W.E., and Konikow, L.F., 1985, A two-constituent solute-transport model for ground water having variable density: U.S. Geological Survey Water-Resources Investigations Report 85-4279.

Schincariol, R.A., and Schwartz, F.W., 1990, An experimental investigation of variable density flow and mixing in homogeneous and heterogeneous media: Water Resources Research, v. 26, no. 10, p. 2317-2329.

Stollenwerk, K.G., 1995, Modeling the effects of variable groundwater chemistry on adsorption of molybdate: Water Resources Research, v. 31, no. 2, p. 347-357.

Sudicky, E.A, Cherry, J.A., and Frind, E.O., 1983, Migration of contaminants in groundwater at a landfill: A case study, 4. A natural gradient dispersion test: Journal of Hydrology, v. 63, p. 81-109.

Thorthwaite, C.W., 1944, A contribution to the Report of the Committee on Transpiration and Evaporation, 1943-33: Transactions of the American Geophysical Union, v. 25, p. 686-693.

Thornthwaite, C.W., and Mather, J.R., 1957, Instructions and tables for computing potential evapotranspiration and the water balance: Centerton, N.J., Drexel Institute of Technology, Publications in Climatology, v. 10, no. 3, 311 p.

Van der Mollen, W.H., and Van Ommen, H.C., 1988, Transport of solutes in soils and aquifers: Journal of Hydrology, v. 100, p. 433-451.

Van Walsun, Nell, 1987, An alternating direction Galerkin technique for simulation of transient density-dependent flow in groundwater transport: Waterloo, Ontario, M.S. thesis, Dept. of Earth Sciences, University of Waterloo, 101 p.

Voss, C.I., 1984, A finite-element model for saturated-unsaturated, fluid-density-dependent ground-water flow with energy transport or chemically-reactive single-species solute transport: U.S. Geological Survey Water-Resources Investigations Report 84-4369, 409 p.

Walter, D.A., Rea, B. A., Stollenwerk, K.G., and Savoie, Jennifer, 1996, Geochemical and hydrologic controls on phosphorus transport in a sewage-contaminated sand

and gravel aquifer near Ashumet Pond, Cape Cod, Massachusetts: U.S. Geological Survey Water-Supply Paper 2463, 89 p.

Weast, R.C., ed., 1987, CRC Handbook of Chemistry and Physics, 68th Edition: Boca Raton, Florida, CRC Press, various pagination.

Wolf, S.H., 1988, Spatial variability of hydraulic conductivity in a sand and gravel aquifer: Cambridge, Mass., Massachusetts Institute of Technology, Dept. of Civil Engineering, unpublished Engineers thesis, 118 p.

Wolf, S.H., Celia, M.A., and Hess, K.M., 1991, Evaluation of hydraulic conductivities calculated from multi-port permeameter measurements: Ground Water, v. 29, no. 4, p. 516-525.

Wood, W.W., Kraemer, T.F., and Hearn, P.P., Jr., 1990, Intragranular diffusion: An important mechanism influencing solute transport in clastic aquifers?: Science, v. 247 (March 30, 1990), p. 1569-1572.

Yih, Chia-Shun, 1963, Velocity of a fluid mass imbedded in another fluid flowing in a porous medium: The Physics of Fluids, v. 6, no. 10, p. 1403-1407.

Yih, Chia-Shun, 1965, Dynamics of nonhomogeneous fluids: New York, MacMillan, 301 p.

Zhang, Hubao, 1995, Simulations of multi-species contaminant transport in variable-density flow systems: Columbus, Ohio, Ph.D. thesis, Ohio State University.

Zhang, Hubao, and Schwartz, F.W., 1995, Multispecies contaminant plumes in variable density flow systems: Water Resources Research, v. 31, no. 4, p. 837-847.

Zhang, Hubao, Schwartz, F.W., and Sudicky, E.A., 1994, On the vectorization of finite element codes for high performance computers: Water Resources Research, v. 30, p. 3553-3559.

Zhang, Hubao, Schwartz, F.W., Wood, W.W., Garabedian, S.P., and LeBlanc, D.R., 1998, Simulation of variable-density flow and transport of reactive and nonreactive solutes during a tracer test at Cape Cod, Massachusetts: Water Resources Research, v. 34, no. 1, p. 67-82.